NASA Contractor Report 4102

A Simulation Study of the Flight Dynamics of Elastic Aircraft

Volume One—Experiment, Results and Analysis

Martin R. Waszak, John B. Davidson,
and David K. Schmidt
School of Aeronautics and Astronautics
Purdue University
West Lafayette, Indiana

Prepared for
Langley Research Center
under Grant NAG1-254

National Aeronautics
and Space Administration

Scientific and Technical
Information Division

1987

ACKNOWLEDGMENTS

This research was supported by the NASA Langley Research Center under grant number NAG-1-254. Thanks go to Mr. William Grantham and Mr. Jerry Elliott who have served as technical monitors.

TABLE OF CONTENTS

Page

LIST OF TABLES

LIST OF FIGURES

Figure Page

LIST OF SYMBOLS

Symbol	Meaning
$C_{(\cdot)}$	aerodynamic coefficient for the parameter $(\cdot)$
F_{pitch}, F_{roll}, F_s	stick input forces, lbs
I_{xx}, I_{yy}, etc.	mass moments of inertia, slug-ft^2
$K_{(\cdot)}$	control gains
$\underline{L}$	aerodynamic rolling moment in body axes, ft-lbs
M	Mach number and vehicle mass, slugs
$\underline{M}$	aerodynamic pitching moment in body axes, ft-lbs
M_y	generalized modal mass for antisymmetric mode, slug-ft^2
M_z	generalized modal mass for symmetric modes, slug-ft^2
$\underline{N}$	aerodynamic yawing moment in body axes, ft-lbs
P_ε	longitudinal tracking error, degrees
Q_{η_y}	generalized force for antisymmetric mode, ft-lbs
Q_{η_z}	generalized force for symmetric mode, ft-lbs
R_ε	lateral tracking error, degrees
S	wing planform area, ft^2
T	total vehicle thrust force, lbs
U, V, W	velocity components of vehicle body axes, ft/sec
$\underline{W}$	vehicle weight, lbs
V_{TOT}	total velocity, ft/sec
V_0	trim velocity, ft/sec
X, Y, Z	aerodynamic force components in body axes, lbs
$a_{n_{(\cdot)}}$, $a_{y_{(\cdot)}}$	normal and lateral accelerations, g's
b	wing span, ft
$\bar{c}$	mean aerodynamic chord, ft
g	gravitational acceleration, ft/sec^2
h	altitude, ft
l_{cp}	distance from cg to cockpit in x-direction, ft
$n_{z_{(\cdot)}}$, $n_{y_{(\cdot)}}$	normal and lateral accelerations, g's

Symbol	Meaning
p	roll rate of vehicle body axes, rad/sec
q	pitch rate of vehicle body axes, rad/sec
q_M	pitch rate of the ideal body-reference (mean) axes, rad/sec
q_T	total pitch rate measured at cockpit location, rad/sec
r	yaw rate of vehicle body axes, rad/sec
s	Laplace variable
t	time, sec
x, y, z	coordinate directions of the vehicle body axes
z_{cp}	distance from cg to cockpit in negative z-direction, ft
Λ	wing sweep, degrees
Φ_{cp}^{y}	modal displacement at cockpit in y-direction, ft
Φ_{cp}^{z}	modal displacement at cockpit in z-direction, ft
Φ_{cp}^{ϕ}	fuselage torsional displacement mode shape at cockpit, rad
α	angle of attack, degrees
β	sideslip angle, degrees
γ	flight path angle, degrees
δ_{cv}	forward control vane deflection, degrees
$\delta_{long}, \delta_{lat}$	longitudinal and lateral stick deflections, inches
δ_p	pilot stick input, inches
δ_{ped}	rudder pedal deflection, inches
δ_{RL}, δ_{RU}	lower and upper split rudder deflections, degrees
δ_{DH}	differential horizontal tail deflection, degrees
δ_t	symmetric horizontal tail deflection, degrees
δ_S	spoiler deflection, degrees (right spoiler positive)
$\varepsilon_{(\cdot)}$	tracking errors
ζ_y, ζ_z	antisymmetric and symmetric modal damping ratios
η_y	antisymmetric generalized modal coordinate, ft
η_z	symmetric generalized modal coordinate, ft
η_1, η_2	random variables to drive command signals
ρ	atmospheric density, slug/ft^3

Symbol	Meaning
$\sigma_{(\cdot)}^2$	variance of parameter $(\cdot)$
$\tau_{(\cdot)}$	time delay and time constant, sec
ϕ, θ, ψ	standard Euler angles
ω	frequency, rad/sec
ω_y	invacuo vibration frequency of antisymmetric mode, rad/sec
ω_z	invacuo vibration frequency of symmetric mode, rad/sec
ω_θ, ω_ϕ	corner frequencies of tracking command filter, rad/sec

subscripts

C	commanded
D	displayed
ERROR	error
TOT	total
TRIM	trim
c, cmd, com	commanded
cg	center of gravity
cp	cockpit
n	normal
p	pitch
r	roll
y	antisymmetric mode and lateral direction
z	symmetric mode

γ	flight path
ε	error
θ	pitch
ϕ	roll
ψ	yaw

Symbol Meaning

operations

$\hat{(\cdot)}$ .....measured response of $(\cdot)$
$\dot{(\cdot)}$ .....time derivative of $(\cdot)$
$|\cdot|$ .....magnitude of $(\cdot)$

abbreviations

AGT .....Adage Graphics Terminal
A/D.....Analogue-to-Digital Converter
CRT.....Cathode Ray Tube
D/A.....Digital-to-Analogue Converter
ESC .....Eigenspace Assignment Controller
ETAY.....lateral axis structural mode status
ETAZ .....longitudinal axis structural mode status
FNE.....engine thrust parameter
KQ.....gain on pitch-rate feedback in SCAS
OMEGAY .....antisymmetric mode frequency
OMEGAZ .....symmetric mode frequency
PLA .....Power Lever Angle
RMS .....Root-Mean-Square
SCAS.....Stability and Control Augmentation System
SPDH .....Speed Hold (Phugoid Augmentation Controller)
THCINC.....thrust increment
THCDEC.....thrust decrement
VMS.....Langley Visual/Motion Simulator

ABSTRACT

The simulation experiment described herein addresses the effects of structural flexibility on the dynamic characteristics of a generic family of aircraft. The simulation was performed using the NASA Langley Visual/Motion Simulator facility. The vehicle models were obtained as part of this research project. The simulation results include complete response data and subjective pilot ratings and comments and so allow a variety of analyses. The subjective ratings and analysis of the time histories indicate that increased flexibility can lead to increased tracking errors, degraded handling qualities, and changes in the frequency content of the pilot inputs. These results, furthermore, are significantly affected by the visual cues available to the pilot.

CHAPTER 1
INTRODUCTION

With the advent of larger aircraft and the ever-present desire for lighter structures for improved fuel economy, there is increased potential for significant contributions from aeroelastic effects in the dynamic response of flight vehicles of the future to pilot inputs and/or atmospheric turbulence. Earlier results[1,2,3] from the present research program indicate how aeroelastic effects can be significant and that, as stiffness is reduced, these effects become magnified. Not only can the dynamic response due to the aeroelastic modes themselves become significant, but coupling between the aeroelastic and the rigid-body degrees of freedom can noticeably alter the "rigid-body" dynamics of the vehicle.[2,3]

One of the few generic experiments in the literature studying aeroelastic effects on pilot-vehicle performance was conducted by Yen.[4] Yen's experiment, using a very low bandwidth longitudinal task, exposed the potential for significant degradation in performance due to dynamic aeroelastic effects. This experiment was conducted in a fixed-base simulation, treated the longitudinal axis only and used a pursuit display in which the effects of elastic deformation were clearly indicated.

In the experiment described herein, both the pitch and roll vehicle axes are being controlled and the effects of motion cues and display dynamics are specifically addressed. The experiment addresses these effects in a generic way for a representative flexible aircraft. It is intended that the results help further identify important factors in determining overall aeroelastic effects.

The experimental results include complete response data, as well as subjective data, to allow a variety of analyses. The data was recorded in several forms to facilitate subsequent analyses. These include vehicle responses recorded on magnetic tape, and pilot comments and subjective ratings with complete cross-referencing of all the data. Simulator frequency response data was also collected to more completely document the simulation facility and provide a database that may be used later to address simulation fidelity issues.

The simulation facility that was used is the NASA Langley Visual/Motion Simulator (VMS). This simulator has programmable displays and control manipulators along with motion capability. The elastic aircraft model that was used was developed by modifying an

CHAPTER 2
THE EXPERIMENT

The documentation of the experiment involves descriptions of - 1) the simulation facility; 2) the vehicle math model; and 3) the tasks, displays and configurations.

Facility

The NASA Langley Visual/Motion Simulator (VMS) Facility was used for the experiment and is described in the functional block diagram shown in Figure 1. Each of the blocks represent dynamic elements in the simulation. This structure is useful, not only for visualizing the various functions of the simulator, but also for understanding the dynamics of the simulator itself.

The VMS is a general purpose simulation facility consisting of a two-man fully instrumented cockpit mounted on a six-degree-of-freedom synergistic motion base.[5,6,7] The computational functions of the simulator are accomplished by means of a CYBER 175 computer.[8] The visual display and conventional cockpit instrumentation are capable of accepting inputs from several sources.

The control manipulators that were used include a center stick for pitch and roll control, rudder pedals for yaw control, and a throttle. The instrumentation included the standard aircraft instruments; airspeed indicator, turn indicator, artificial horizon, vertical speed indicator, etc. The command display was implemented with a head-up type of display using a CRT.

The control stick and pedals effect command inputs through a programmable hydraulic control loading system. This system provides control of the force/feel feedback to the pilot and was used to simulate realistic stick and pedal forces and travel distances. The control loader was adjusted to provide good force/feel feedback for the baseline vehicle and was not varied among the configurations. The values that were used are presented in Table 1.

The display of the VMS is driven by the Graphics Display System which consists of two Adage Graphics Terminals (AGT's). Each AGT has three display generators which are interfaced with television cameras to provide cockpit displays. Each AGT is also digitally

existing NASA Langley simulation model of a rigid vehicle and was implemented to allow on-line variation of several configuration parameters. Among these were, for example, invacuo-vibration frequencies allowing the experimenter to quickly alter the effective stiffness of the vehicle. The tasks and configurations were designed to provide a challenging environment for the pilots.

This report is organized to systematically present the description, documentation and results of the simulation experiment described above. First, the simulation facility, vehicle model and experimental set-up are discussed. Next, the basic results are presented and discussed. In addition, some preliminary analysis of the data is presented along with some discussion and interpretation of the results. The report then concludes with a general summary and suggestions for future applications and analyses of the data.

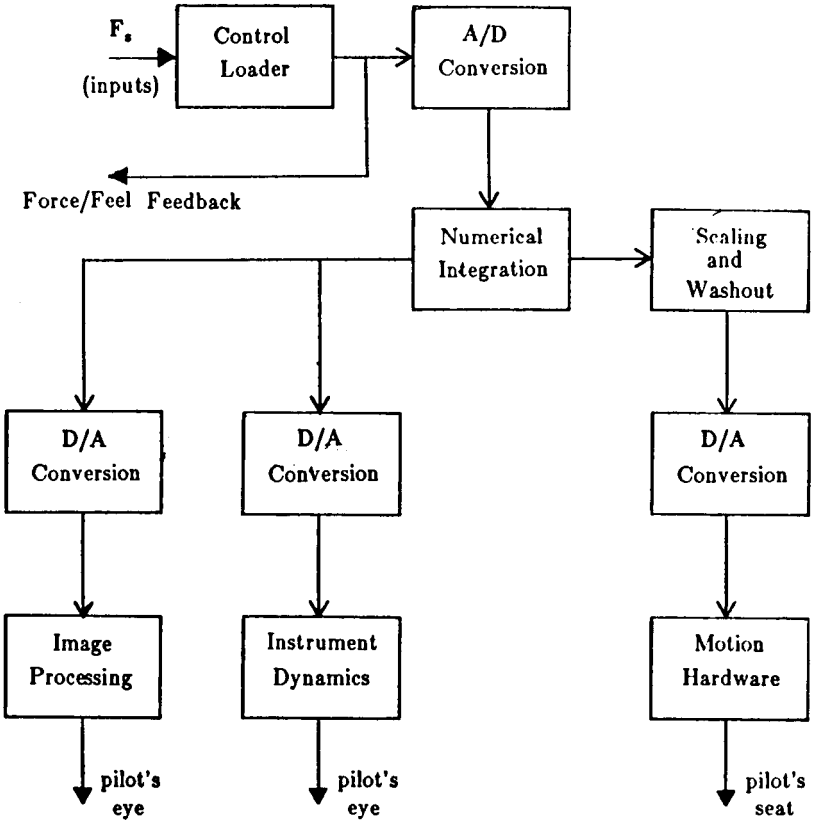

Figure 1 - Simulator Functional Block Diagram

Table 1 - Force/Feel System Parameters

	Travel (± in.)	Breakout Force (lbs.)	Preload (lbs.)	Friction Force (lbs.)	Force Gradient (lbs/in)	Trim Limits	
						Position	Rate
Pitch Stick	6 aft 4 fwd	3.3	1.8	1.5	10	2.7" fwd stick 5.3" aft stick	0.5 $\frac{in}{sec}$
Roll Stick	± 5	3.0	1.4	1.6	6.5	±20° of tail deflection	2.0 $\frac{deg}{sec}$
Pedal	±3.25	14.0	6.5	7.5	40.0	±1.3" pedal	0.3 $\frac{in}{sec}$

interfaced with the CYBER 175 to provide the capability to drive the displays with simulation variables during real-time simulation.

Vehicle Model

The vehicle that was modeled (shown in Figure 2) is similar to an early version of the Rockwell B-1 and is considered to be typical of advanced transport-type aircraft. This vehicle was chosen also because of the availability of structural data and of a nonlinear rigid-body simulation model that was used in a previous NASA study.

Airframe

The rigid vehicle model consists of the rigid-body equations of motion, tabulated nonlinear aerodynamic coefficients, control system and engine models, auxiliary and kinematic equations, and force/feel feedback (i.e. control loader) parameter values. The rigid model was then appended with structural dynamics which are coupled to the rigid-body degrees-of-freedom via the aerodynamic forces.

The equations of motion for the rigid model are written in a body-fixed reference frame. They consist of the traditional six rigid-body degrees-of-freedom, three translational and three rotational. The structural dynamics that were added to the model consist of two structural degrees-of-freedom which correspond to a symmetric and antisymmetric free vibration mode of the structure.

The integration of the rigid-body degrees-of-freedom with the aeroelastic degrees-of-freedom was accomplished according to the modeling method discussed in Reference 9. The equations which result describe the overall motion of the vehicle relative to a mean-axes coordinate system, with origin at the instantaneous center of mass. The structural displacements are assumed to be small so that variations in the moments of inertia are negligible.

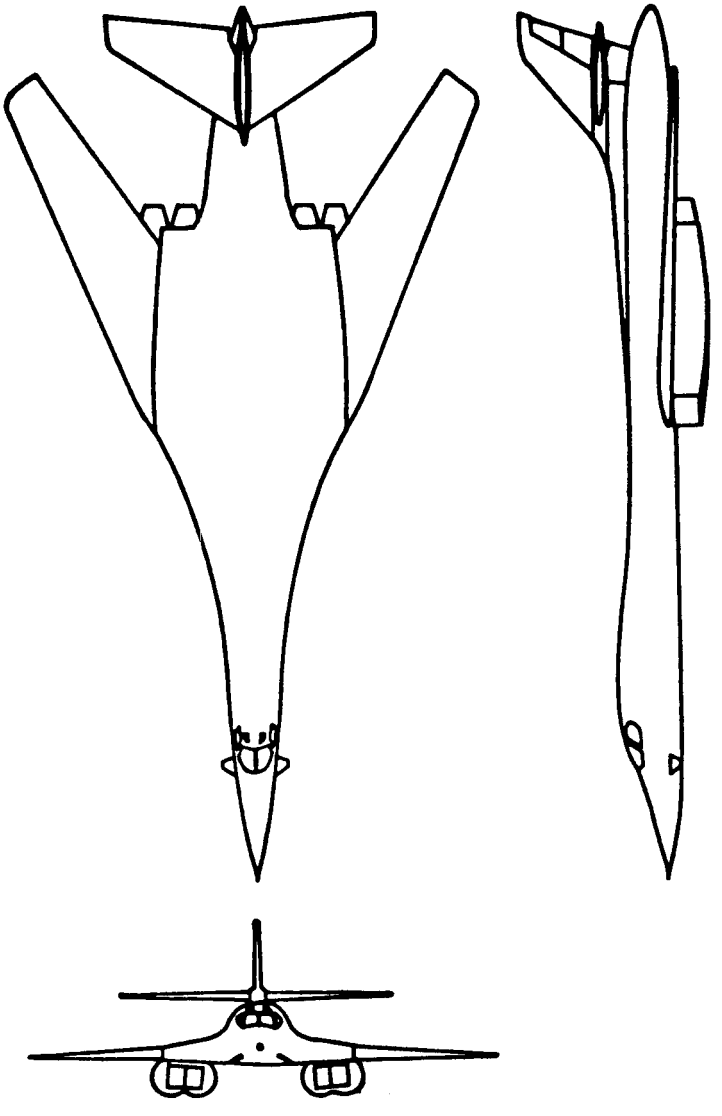

Figure 2 - Geometry of Study Vehicle

The equations of motion for the simulation model of the flexible vehicle are presented in Table 2. Notice that the form of the equations is very similar to that of a rigid aircraft[10] but with the addition of equations associated with structural degrees-of-freedom. This allows the rigid vehicle model data to be used with very little alteration. The primary difference between the rigid model and the elastic model, beside the additional equations, is in the aerodynamic forces and moments (viz. X, Y, Z, $\underline{L}$, $\underline{M}$, and $\underline{N}$). The coupling between the rigid-body degrees-of-freedom and the aeroelastic degrees-of-freedom occurs via the aerodynamic forces and moments.

Consider, as an example, a flexible vehicle model for the longitudinal degrees-of-freedom with one structural mode in straight, horizontal flight. The equations of motion for this model are,

$$\dot{U} = -qW - g\sin\theta + X \tag{1a}$$

$$\dot{W} = Uq + g\cos\phi\cos\theta + Z \tag{1b}$$

$$\dot{q} = \underline{M} \tag{1c}$$

$$\ddot{\eta} = -2\zeta\omega\dot{\eta} - \omega^2\eta + Q_\eta \tag{1d}$$

where U and W are the surge and plunge velocities in the body-reference axes, respectively; q is the pitch rate; ϕ and θ are the Euler angles of the vehicle; η, ζ, and ω are the generalized coordinate, damping and frequency for the structural mode, respectively; and X, Z, $\underline{M}$ and Q_η are the aerodynamic forces, moment and generalized force, respectively. Assuming the vehicle has elevator deflection as the only control variable, the aerodynamic force, Z, for example, might be expressed as

$$Z = \frac{\rho V_0^2 S}{2M}\left[C_{Z_0} + C_{Z_\alpha}\alpha + C_{Z_\delta}\delta + C_{Z_\eta}\eta\right]$$

$$+ \frac{\rho V_0 S\bar{c}}{4M}\left[C_{Z_q}q + C_{Z_{\dot{\eta}}}\dot{\eta} + C_{Z_{\ddot{\eta}}}\ddot{\eta}\right] \tag{2}$$

where $C_{Z_{(\cdot)}}$ is the aerodynamic stability derivative associated with the variable $(\cdot)$, ρ is the air density, V_0 is the vehicle velocity, S is the planform area, $\bar{c}$ is the mean aerodynamic chord, and M is the mass of the vehicle. The coupling between the aeroelastic degree-of-freedom

Table 2 - Vehicle Equations of Motion

$$\dot{U} = r V - q W - g \sin\theta + X$$

$$\dot{V} = pW - r U + g \sin\phi \cos\theta + Y$$

$$\dot{W} = U q - V p + g \cos\phi \cos\theta + Z$$

$$\dot{p} = \frac{1}{I_{xx}} \{(I_{yy} - I_{zz})\, q r + I_{xz}(\dot{r} + pq)\} + \underline{L}$$

$$\dot{q} = \frac{1}{I_{yy}} \{(I_{zz} - I_{xx}) p r + I_{xz}(r^2 - p^2)\} + \underline{M}$$

$$\dot{r} = \frac{1}{I_{zz}} \{(I_{xx} - I_{yy}) p q + I_{xz}(\dot{p} - q r)\} + \underline{N}$$

$$\ddot{\eta}_y = -2\zeta_y \omega_y \dot{\eta}_y - \omega_y^2 \eta_y + Q_{\eta_y}$$

$$\ddot{\eta}_z = -2\zeta_z \omega_z \dot{\eta}_z - \omega_z^2 \eta_z + Q_{\eta_z}$$

and rigid-body vertical translation occurs through the coefficients C_{Z_η}, $C_{Z_{\dot{\eta}}}$ and $C_{Z_{\ddot{\eta}}}$. Similar coupling terms arise in the (generalized) forces for each degree-of-freedom, rigid and elastic, in the model. Some of these terms, furthermore, depend on the vibration mode shapes (see Reference 7).

The original, rigid vehicle model has several control effectors. These include horizontal tail deflection, δ_t, differential horizontal tail deflection, δ_{DH}, wing spoiler deflection, δ_S, upper split-rudder deflection, δ_{RU}, lower split-rudder deflection, δ_{RL}, and thrust, T (via power lever angle, PLA). Additionally, estimates for the control power available from the forward control vane, δ_{cv}, were included in this study.

The expressions for the aerodynamic forces and moments and generalized forces are shown in Table 3. The numerical values for the aerodynamic force coefficients are presented in Appendix 1. This tabular data was used with a ''table look-up scheme'' in the simulation to determine the aerodynamic forces and moments.

The geometry, mass and inertia, and flight condition for the simulation model are shown in Table 4. The shapes of the two structural modes included in the model are shown in Figure 3. More complete modal data for the baseline vehicle is presented in Appendix 2. This includes finite element control point locations and control point displacements for the two modeled structural modes.

Additional information needed to drive the displays, instrumentation and motion base of the simulator are given in Table 5.

Augmentation

The simulation model includes actuator dynamics and stability and control augmentation system (SCAS) dynamics as well. These were necessary to assure good handling qualities for the baseline vehicle. Block diagrams of the SCAS systems for the pitch, roll, and yaw axes are shown in Figures 4 through 6. The actuator/servo elements that are modeled consist of lags, limiters, and gearing effects. The control laws include both constant and variable gains, scheduled with altitude and Mach number. The constant gain values are tabulated in Table 6 and the scheduled gains are presented in Appendix 3. The limiters and gearing effects are also

Table 3 - Aerodynamic Forces and Moments

$$X = \frac{\rho V_o^2 S}{2M}[C_X + C_{X\delta_t}\delta_t + C_{X\delta_s}|\delta_s| + C_{X\delta_{cv}}\delta_{cv}] + \frac{\rho V_o S\bar{c}}{4M}[C_{Xq}q] + \frac{T}{M}$$

$$Y = \frac{\rho V_o^2 S}{2M}[C_{Y\beta} + C_{Y\delta_{RU}}\delta_{RN} + C_{Y\delta_{RL}}\delta_{RL} + C_{Y\delta_s}\delta_s + C_{Y\delta_{DH}}\delta_{DH} + C_{Y\eta_y}\eta_y]$$

$$+ \frac{\rho V_o Sb}{4M}[C_{Y\dot{\eta}_y}\dot{\eta}_y]$$

$$Z = \frac{\rho V_o^2 S}{2M}[C_Z + C_{Z\delta_t}\delta_t + C_{Z\delta_s}|\delta_s| + C_{Z\delta_{cv}}\delta_{cv} + C_{Z\eta_z}\eta_z] + \frac{\rho V_o S\bar{c}}{4M}[C_{Zq}q + C_{Z\dot{\eta}_z}\dot{\eta}_z]$$

$$\underline{L} = \frac{\rho V_o^2 Sb}{2I_{xx}}[C_{l\beta}\beta + C_{l\delta_{RU}}\delta_{RU} + C_{l\delta_{RL}}\delta_{RL} + C_{l\delta_s}\delta_s + C_{l\delta_{DH}}\delta_{DH} + C_{l\eta_y}\eta_y]$$

$$+ \frac{\rho V_o Sb^2}{4I_{xx}}[C_{lp}p + C_{lr}r + C_{l\dot{\eta}_y}\dot{\eta}_y]$$

$$\underline{M} = \frac{\rho V_o^2 S\bar{c}}{2I_{yy}}[C_m + C_{m\delta_t}\delta_t + C_{m\delta_s}|\delta_s| + C_{m\delta_{cv}}\delta_{cv} + C_{m\eta_z}\eta_z]$$

$$+ \frac{\rho V_o S\bar{c}^2}{4I_{yy}}[C_{mq}q + C_{m\dot{\alpha}}\dot{\alpha} + C_{m\dot{\eta}_z}\dot{\eta}_z] + \frac{4.29}{I_{yy}}T$$

$$\underline{N} = \frac{\rho V_o^2 Sb}{2I_{zz}}[C_{\eta\beta}\beta + C_{n\delta_{RU}}\delta_{RU} + C_{n\delta_{RL}}\delta_{RL} + C_{n\delta_s}\delta_s + C_{n\delta_{DH}}\delta_{DH} + C_{n\eta_y}\eta_y]$$

$$+ \frac{\rho V_o Sb^2}{4I_{zz}}[C_{np}p + C_{nr}r + C_{n\dot{\beta}}\dot{\beta} + C_{n\dot{\eta}_y}\dot{\eta}_y]$$

$$Q_{\eta_y} = \frac{\rho V_o^2 S}{2M_y}[C_{\eta_y} + C_{\eta_y\beta}\beta + C_{\eta_y\delta_{RU}}\delta_{RU} + C_{\eta_y\delta_{RL}}\delta_{RL} + C_{\eta_y\delta_s}\delta_s + C_{\eta_y\delta_{DH}}\delta_{DH}$$

$$+ C_{\eta_y\delta_{cv}}\delta_{cv} + C_{\eta_y\eta_y}\eta_y] + \frac{\rho V_o Sb}{2M_y}[C_{\eta_y p}p + C_{\eta_y r}r + C_{\eta_y\dot{\eta}_y}\dot{\eta}_y]$$

$$Q_{\eta_z} = \frac{\rho V_o^2 S}{2M_z}[C_{\eta_z} + C_{\eta_z\alpha}\alpha + C_{\eta_z\delta_t}\delta_t + C_{\eta_z\delta_{cv}}\delta_{cv} + C_{\eta_z\delta_s}|\delta_s| + C_{\eta_z\eta_z}\eta_z]$$

$$+ \frac{\rho V_o S\bar{c}}{4M_z}[C_{\eta_z q}q + C_{\eta_z\dot{\alpha}}\dot{\alpha} + C_{\eta_z\dot{\eta}_z}\dot{\eta}_z]$$

Table 4 - Geometry, Inertia and Flight Condition of Study Vehicle

Geometry	$\bar{c}$	1.34 ft. (mean chord)
	b	136.7 ft. (wing span)
	S	1946 ft^2 (planform area)
	Λ	65° (sweep angle)
Weight	$\underline{W}$	288,000 lbs (gross weight)
Inertia	I_{xx}	950,000 slug–ft^2
	I_{yy}	6,400,000 slug–ft^2
	I_{zz}	7,100,000 slug–ft^2
	I_{xz}	-52,700 slug–ft^2
Modal Generalized Mass	M_y	28,991 slug–ft^2 (antisymmetric model)
	M_z	183.6 slug–ft^2 (symmetric mode)
Flight Condition	ρ	$0.002055 \frac{slug}{ft^3}$ (air density)
	V_0	$657.5 \frac{ft}{sec}$ (cruise velocity)

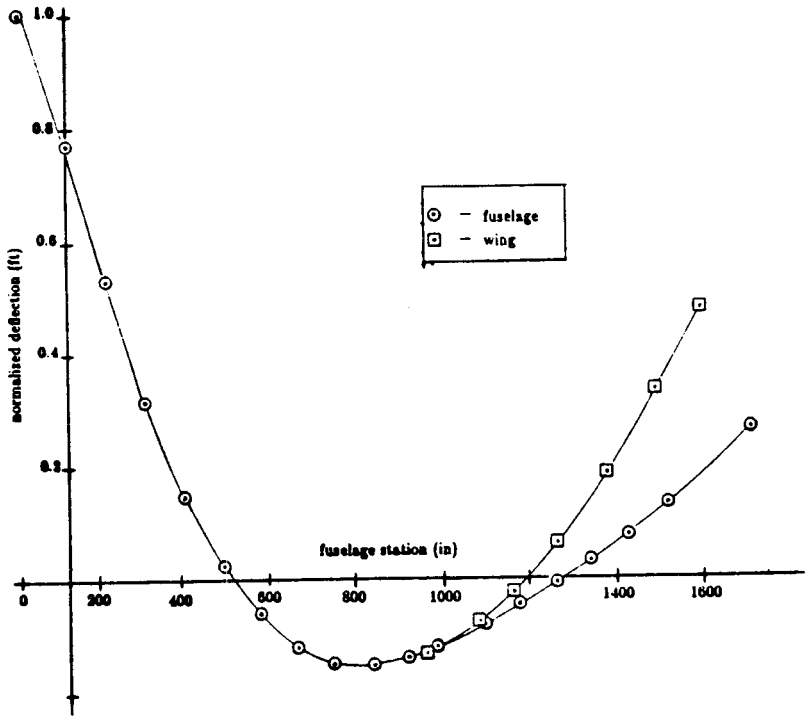

(a) Symmetric Mode

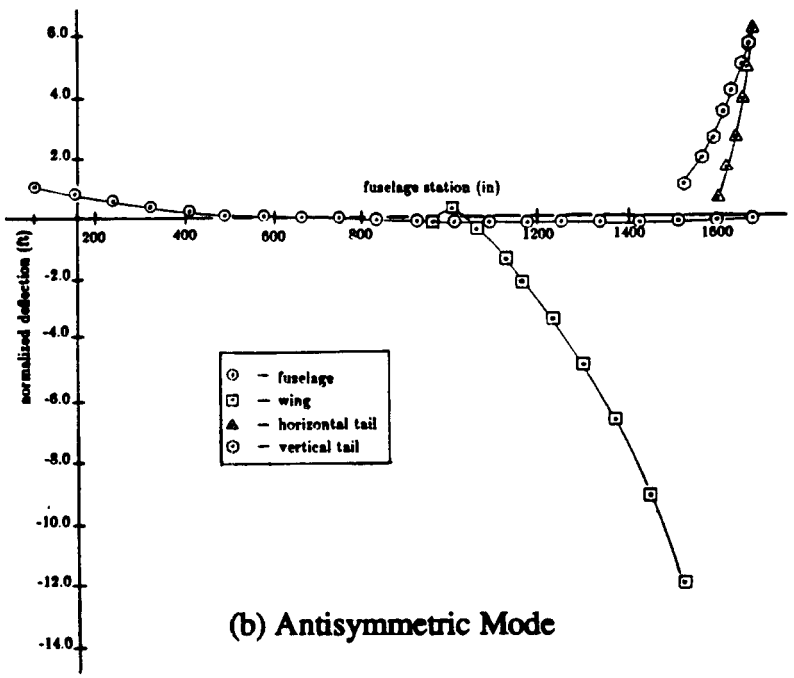

(b) Antisymmetric Mode

Figure 3 - Shapes of Modeled Structural Modes

Table 5 - Additional Vehicle Equations

Euler Angles and Auxillary Equations

$$\dot{\theta} = q \cos\phi - r \sin\phi$$

$$\dot{\phi} = p + q \tan\theta \sin\phi + r \tan\theta \cos\phi$$

$$\dot{\psi} = r \cos\phi \sec\theta + q \sin\phi \sec\theta$$

$$V_o \triangleq [U^2+V^2+W^2]^{1/2} \quad \text{(velocity)}$$

$$\alpha \triangleq \text{Tan}^{-1}\left(\frac{W}{U}\right) \quad \text{(angle of attack)}$$

$$\beta \triangleq \text{Tan}^{-1}\left(\frac{V}{V_o}\right) \quad \text{(side slip)}$$

$$\dot{h} \triangleq U \sin\theta - V \cos\theta \sin\phi - W \cos\theta \cos\phi \quad \text{(rate of climb)}$$

Acclerations at Center of Mass (g's)

$$a_{x_{cg}} = \frac{1}{g}(\dot{U} - Vr + Wq + g \sin\theta)$$

$$a_{y_{cg}} = \frac{1}{g}(\dot{V} - Wp + Ur - g \cos\theta \sin\phi)$$

$$a_{z_{cg}} = \frac{1}{g}(g \cos\theta \cos\phi - \dot{W} + Uq + Vr) = -a_{n_{cg}}$$

Accelerations at Cockpit (g's)

$$a_{x_{cp}} = a_{x_{cg}} - (\dot{q} + pr)\frac{z_{cp}}{g} - (r^2 + q^2)\frac{l_{cp}}{g}$$

$$a_{y_{cp}} = a_{y_{cg}} + (\dot{r} + pq)\frac{l_{cp}}{g} + (\dot{p} - rq + \Phi^{\phi}_{cp}\ddot{\eta}_y)\frac{z_{cp}}{g} + \frac{\Phi^{y}_{cp}}{g}\ddot{\eta}_y$$

$$a_{n_{cp}} = a_{n_{cg}} + (\dot{q} - pr)\frac{l_{cp}}{g} - (q^2 + p^2)\frac{z_{cp}}{g} - \frac{\Phi^{z}_{cp}}{g}\ddot{\eta}_z$$

Numerical Values at Cockpit

$\Phi^{y}_{cp} = 0.45$ (ft) $\qquad z_{cp} = 0.0$ (ft)

$\Phi^{z}_{cp} = 0.39$ (ft) $\qquad l_{cp} = 63.4$ (ft)

$\Phi^{\phi}_{cp} = -0.0027$ (rad)

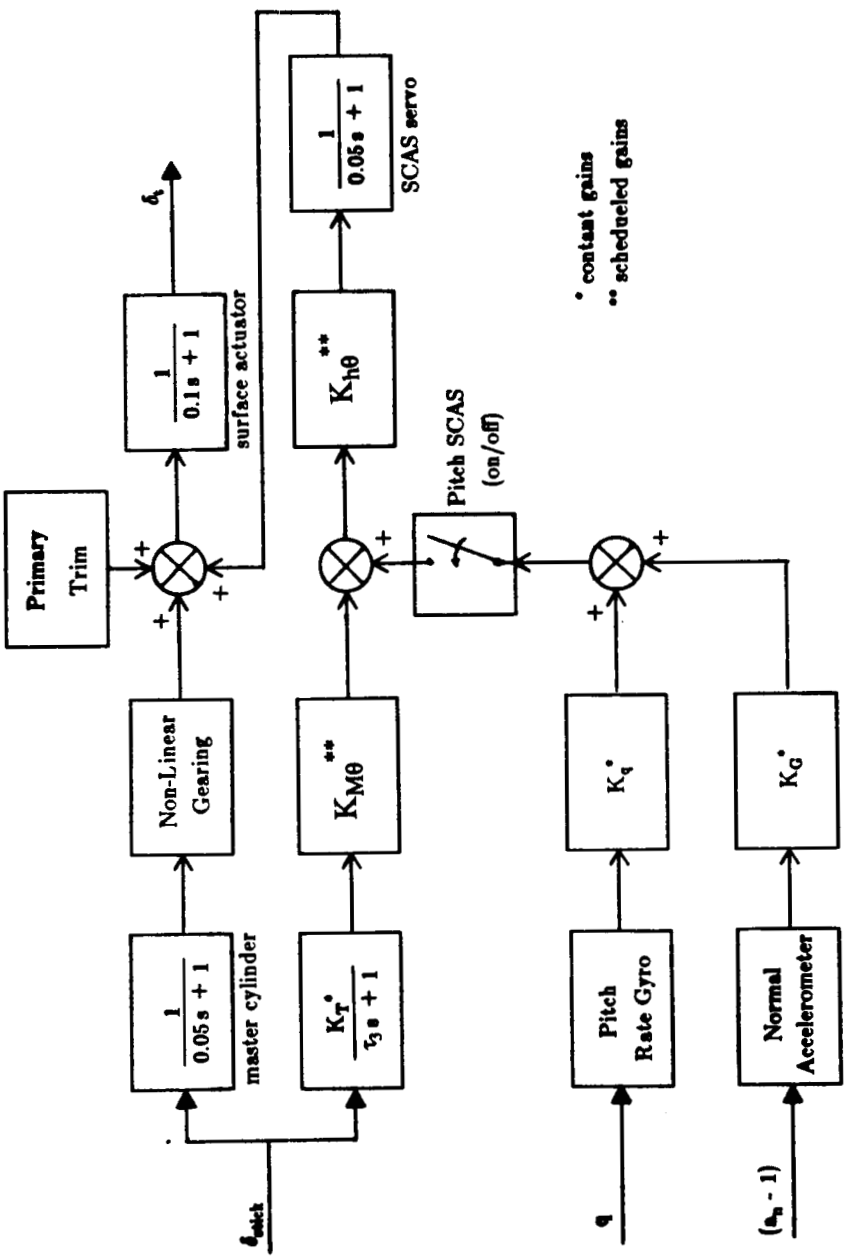

Figure 4 - Pitch SCAS Block Diagram

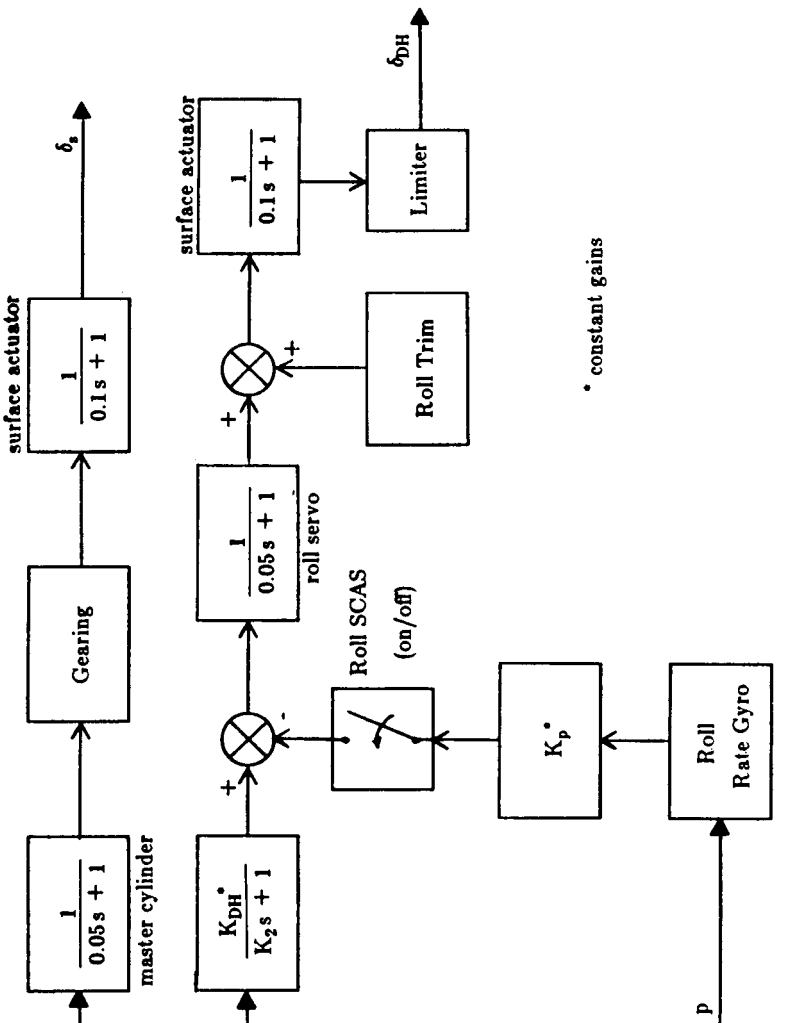

Figure 5 - Roll SCAS Block Diagram

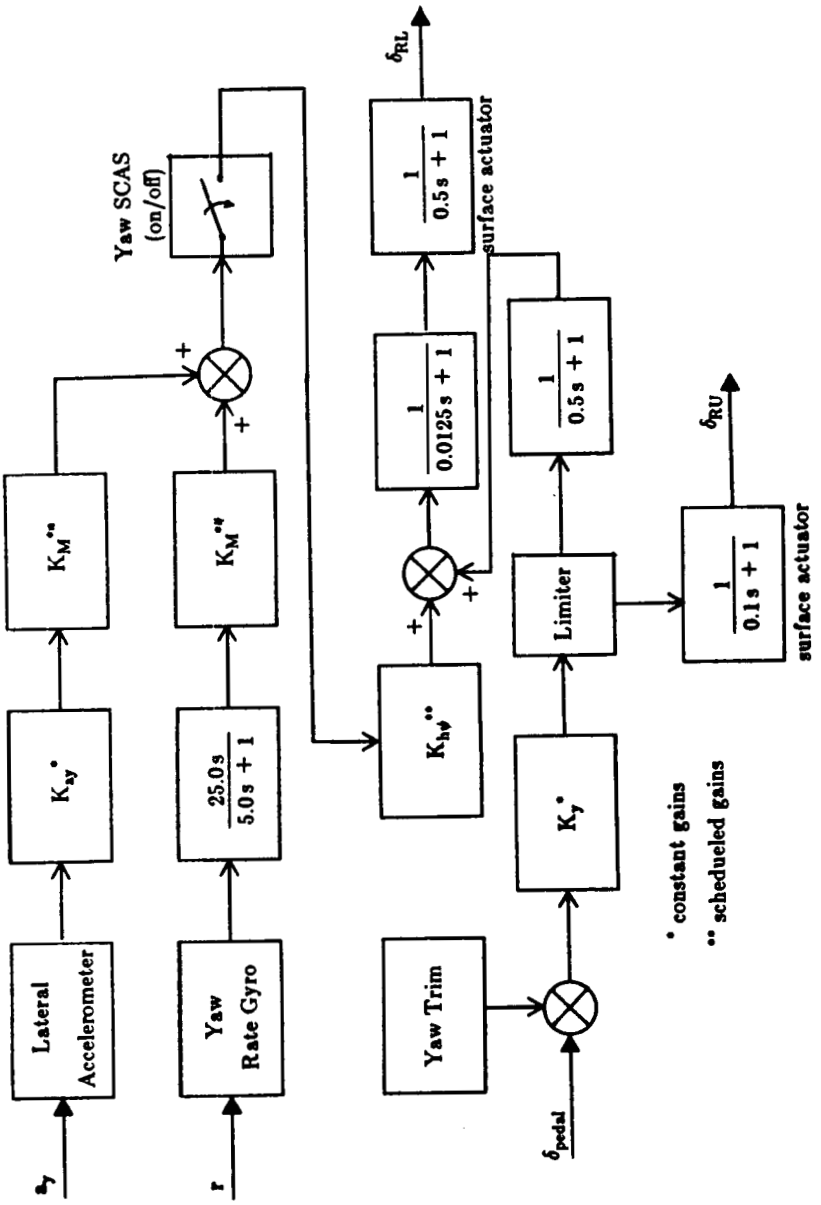

Figure 6 - Yaw SCAS Block Diagram

Table 6 - Constant Control Gains

Pitch SCAS	$K_T = 5.5 \frac{DEG}{IN}$ $\tau_3 = 0.02$ sec $K_q = 1.6$ or 2.0 sec (configuration dependent) $K_G = 4.58 \frac{DEG}{g}$
Roll SCAS	$K_{DH} = 9.0 \frac{DEG}{IN}$ $K_2 = 0.02$ sec $K_p = 0.57 \frac{deg}{deg/sec}$
Yaw SCAS	$K_{ay} = 200.0 \frac{deg}{g}$ $K_y = -7.7 \frac{deg}{in.}$
Phugoid Augmentation	$K_{PA} = 250 \frac{lb-sec}{ft}$

presented in Appendix 3. It is important to note that for the most part, the control system gains were not variables of the experiment. The control gains were altered on very few configurations and are so noted.

An additional controller was added to the flexible aircraft model to increase the damping of the phugoid mode for the baseline configuration. This was done to improve the handling qualities of the baseline configuration and reduce the need for the pilot to monitor speed. The phugoid augmentation controller consists of a velocity error signal and gain, as shown in the block diagram in Figure 7. The value of the gain, K_{PA}, is shown in Table 6 with the other controller gains. Note that, in the simulation data this phugoid augmentation is referred to as a "speed hold" controller.

To illustrate the effects of varying the structural stiffness (i.e. changing the invacuo vibration frequencies) on the vehicle dynamics, pitch-rate-to-stick-deflection transfer functions are shown in Table 7, both for total pitch rate measured at the cockpit location, q_T, and for the pitch rate of the ideal body-reference (mean) axes, q_M. These transfer functions were obtained from the longitudinal degrees-of-freedom of the baseline nonlinear simulation model, linearized in level flight at the flight conditions summarized in Table 4. The transfer functions include the effect of the baseline pitch SCAS, phugoid augmentation and a first-order approximation for the actuator lag, with a time constant of 0.1 seconds. Engine dynamic effects, however, are not included.

Two of the modes roughly correspond to the standard dynamic modes of aircraft dynamics. These include a phugoid-like mode and a short-period-like mode. In addition, an aeroelastic-structural mode and an (augmented) actuator mode are present. The poles associated with these modes are listed in Table 7 in the following order; phugoid mode, short period mode, aeroelastic mode and augmented actuator mode. These dynamic modes are readily identified for the stiffer configurations, that is those with a symmetric mode frequency of 1.5 or 2.0 Hertz. However, as the symmetric mode frequency is reduced the dynamics change from these "standard" modes. In particular, the "short period" mode and "structural" mode become highly coupled. Note also that the phugoid poles begin as a well damped complex conjugate pair but migrate to become two real poles as the vibration frequency is reduced. In fact, one phugoid pole becomes slightly unstable in the most flexible configuration.

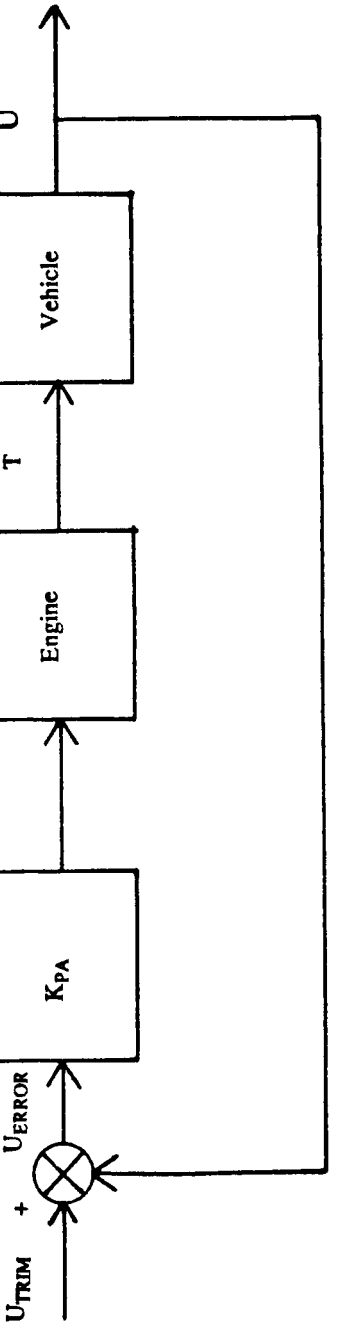

Figure 7 - Phugoid Augmentation Controller Block Diagram

Table 7 - $\frac{q(s)}{\delta(s)}$ Transfer Function Data for Simulation Model

	Invacuo Symmetric Mode Frequency (Hz)			
	2.0	1.5	1.0	0.8
T.F. Gain	4.764	4.764	4.782	4.782
$\frac{q_T}{\delta_p}$ Zeros*	0.0 -0.0647 -0.440 -5.1205 4.499	0.0 -0.0666 -0.491 -3.569 2.985	0.0 -0.0511 -0.795 -1.619 1.347	0.00 -0.0652 (1.211,0.744) 0.578
T.F. Gain	-0.858	-0.858	-0.839	-0.839
$\frac{q_M}{\delta_p}$ Zeros*	0.0 -0.0624 -0.402 (11.86,0.008)	0.0 -0.0620 -0.408 (8.45,0.003)	0.0 -0.0361 -0.422 (4.77,-0.013)	0.0 -0.0365 -0.509 (2.77,-0.047)
Poles*	(0.0397,0.675) (6.054,0.820) (12.57,0.0544) -1.733	(0.037,0.748) (5.615,0.825) (9.46,0.081) -1.857	-0.0010 -0.0229 (4.03,0.795) (6.523,0.281) -2.322	-0.0495 0.0363 (2.14,0.453) (6.359,0.460) -4.123

*complex conjugate poles and zeros written: (ω (rad/sec), ζ)

The transfer functions for total pitch rate, q_T, are all nonminimum phase due to the mode shape of the vibration mode, that is, structural deflections cause initial pitch displacements to be opposite in direction to the final pitch attitude. The location of the nonminimum phase zero varies considerably as a function of symmetric mode frequency. In addition, the migration of the other zeros due to changes in the structural mode frequency also affect the vehicle dynamics, especially the two negative real zeros which merge and break off into two well damped oscillatory zeros when the symmetric mode frequency is reduced to 0.8 Hertz.

The set of transfer functions for mean-axis pitch rate, q_M, are fundamentally different. They are minimum phase and have a pair of lightly damped oscillatory zeros that for the stiffer configurations are located close to the complex poles associated with the aeroelastic mode. As the frequency of the symmetric mode is reduced, the oscillatory zeros migrate until, for the more flexible configuration, they are closer to the two low-frequency complex poles. This clearly reflects fundamentally different dynamics, compared to the stiffer configurations.

An additional exploratory control system was briefly implemented in the simulation as a demonstration. The structure of the simulation model, both in the structure of the equations of motion and in the structure of the SCAS implementation allows the model to be readily altered by appending additional system dynamics. This demonstration controller was synthesized using eigenspace assignment methods[11] and implemented in place of the pitch SCAS controller. Although the performance of such a control law was investigated briefly, handling qualities assessments were not obtained.

The implementation of the eigenspace assignment controller was accomplished as shown in Figure 8. The controller requires feedback of the velocities, U and W, pitch attitude and pitch attitude rate, θ and q, plunge acceleration and plunge acceleration rate, n_z and $\dot{n}_z$, tail deflection, δ_t, and control vane deflection, δ_{cv}. The command signals for this controller are determined from Equations (3) and (4). The control gains for each of the parameters, given in these equations, are presented in Table 8.

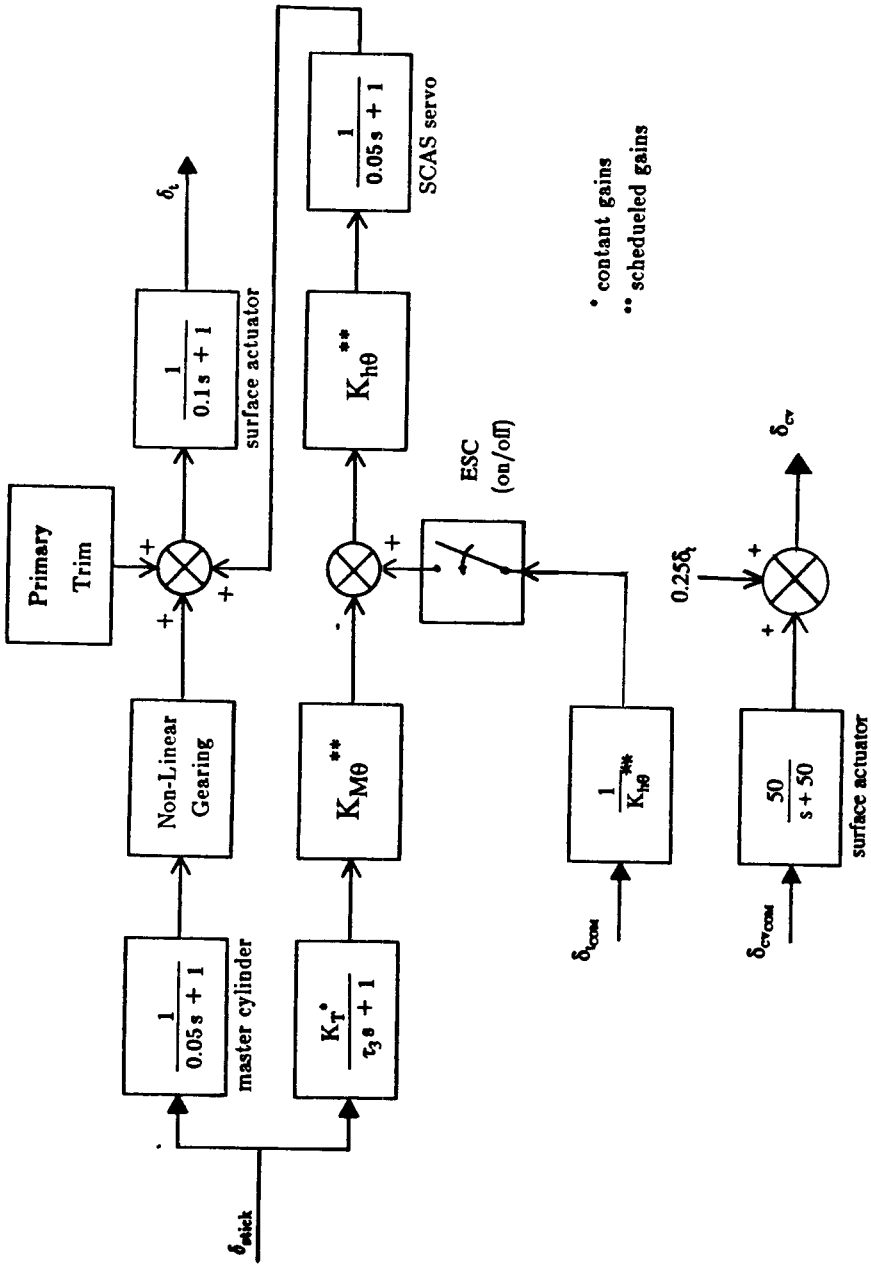

Figure 8 - Eigenspace Assignment Controller Block Diagram

Table 8 - Eigenspace Assignment Controller Gains

Tail Command Gains		Vane Command Gains	
K_u^t	-0.51172	K_u^{cv}	-1.2567
K_w^t	0.07557	K_w^{cv}	0.1498
K_q^t	1.5044	K_q^{cv}	-61.693
K_θ^t	-85.842	K_θ^{cv}	-192.59
$K_{n_z}^t$	0.4197	$K_{n_z}^{cv}$	4.1918
$K_{\dot{n}_z}^t$	0.1336	$K_{\dot{n}_z}^{cv}$	0.3579
$K_{\delta_t}^t$	-0.1575	$K_{\delta_t}^{cv}$	0.4970
$K_{\delta_{cv}}^t$	-0.02579	$K_{\delta_{cv}}^{cv}$	-0.09404

(note: all δ's in degrees; u, w in ft/sec; $\dot{\theta},\dot{\eta}$ in $\frac{\text{rad}}{\text{sec}}$; θ, η in rad)

$$\delta_{t_{COM}} = \delta_{t_{TRIM}} - K^{t}_{u}\left[U - U_{TRIM}\right] + K^{t}_{w}\left[W - W_{TRIM}\right] + K^{t}_{q}\left[q - q_{TRIM}\right] + K^{t}_{\theta}\left[\theta - \theta_{TRIM}\right] + K^{t}_{n_z}\left[n_z - n_{z_{TRIM}}\right] + K^{t}_{\dot{n}_z}\left[\dot{n}_z - \dot{n}_{zTRIM}\right] + K^{t}_{\delta_t}\left[\delta_t - \delta_{t_{TRIM}}\right] + K^{t}_{\delta_{cv}}\left[\delta_{cv} - \delta_{cv_{TRIM}}\right] \quad (3)$$

$$\delta_{cv_{COM}} = \delta_{cv_{TRIM}} - K^{cv}_{u}\left[U - U_{TRIM}\right] + K^{cv}_{w}\left[W - W_{TRIM}\right] + K^{cv}_{q}\left[q - q_{TRIM}\right] + K^{cv}_{\theta}\left[\theta - \theta_{TRIM}\right] + K^{cv}_{n_z}\left[n_z - n_{z_{TRIM}}\right] + K^{cv}_{\dot{n}_z}\left[\dot{n}_z - \dot{n}_{zTRIM}\right] + K^{cv}_{\delta_t}\left[\delta_t - \delta_{t_{TRIM}}\right] + K^{cv}_{\delta_{cv}}\left[\delta_{cv} - \delta_{cv_{TRIM}}\right] \quad (4)$$

Engine

The simulation model also includes engine dynamics. This model was present in the original, rigid model and was retained in the flexible model. A block diagram is shown in Figure 9. The functional elements (e.g. f(PLA,h,M) and f(h,M)) which appear in the model are expressed in the tabular forms presented in Tables 9 through 11. It should be noted that the effect of the engine dynamics on the simulation results are most likely very small, and the throttle was utilized little by the pilots during the experiment.

Tasks and Displays

The multi-axis piloting tasks used in the simulation experiment were developed to require the pilot to fully utilize his entire dynamic range, to provide an indication of the pilot's ability to excite the aeroelastic modes. The tasks designed were generic, but intended to be representative of activities experienced in actual flight. The intent is to allow the results of the simulation to be better interpreted in terms of actual vehicle requirements and to allow the pilot to relate the results to his previous experiences.

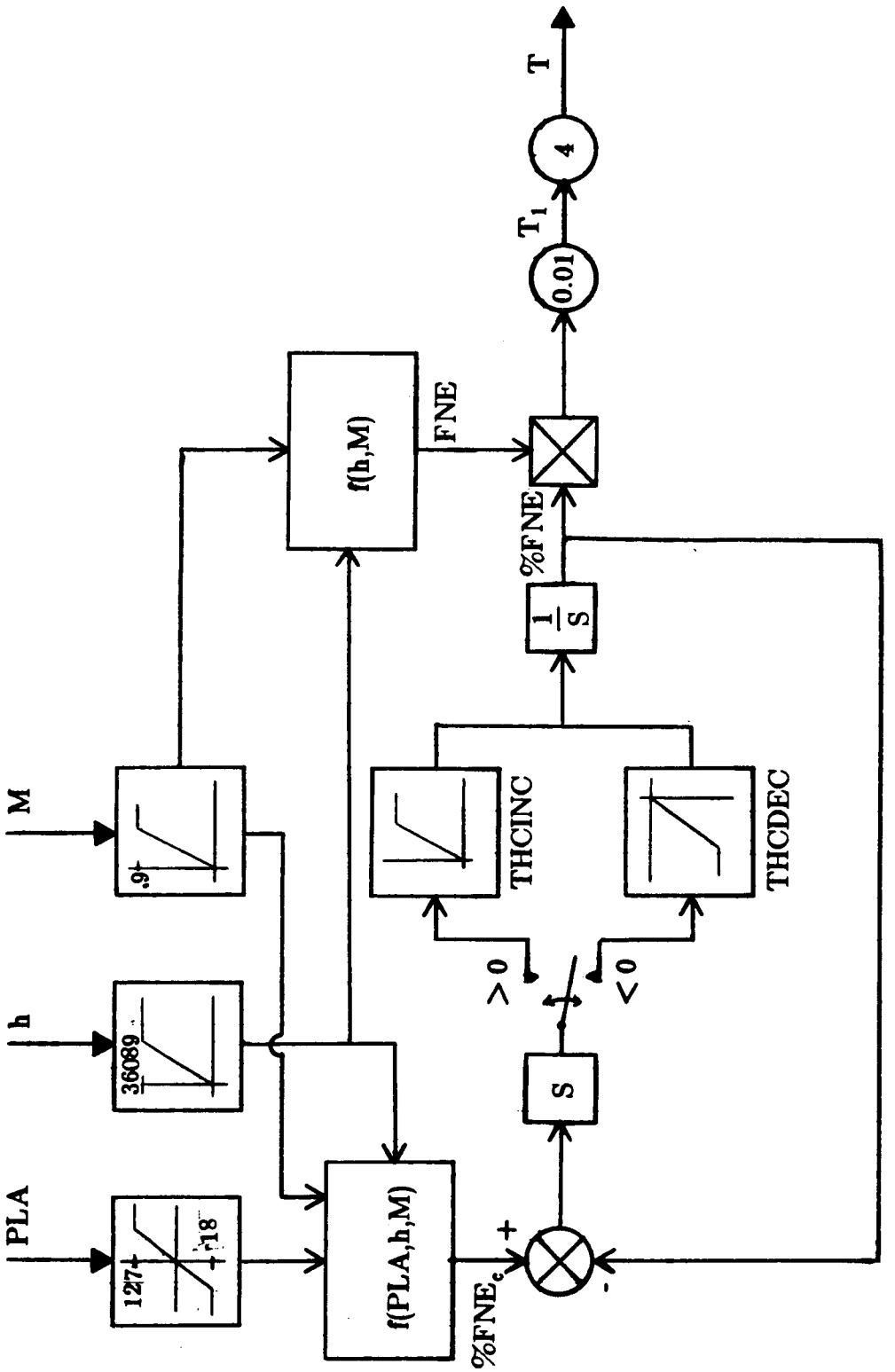

Figure 9 - Engine Model Block Diagram

Table 9 - Engine Data : FNE

h \ M	0	.3	.4	.5	.6	.7	.8	.9
0	26000	28400	29300	30500	31700	32150	32200	31900
20000	13800	13800	13800	15300	16800	18500	20300	22200
36089	7900	7900	7900	7900	7900	8900	10000	11100

Table 10 - Engine Data : %FNE / sec

%FNE	THCINC	%FNE	THCDEC
-8	2	-8.2	-1.3
-3	2.63	-5.5	-1.8
1.5	7.5	.5	-12
11.5	10.53	10	-19
14	2.38	16.5	-6.5
19.5	5.5	36.5	-20
31	11.5	58	-43
100	19.71	90	-60
200	.01	95	-33.33
300	.01	100	-14.29

Table 11 - Engine Data : %FNE_c

						IDLE								MIL (110)		A.B.
M	PLA / h	18	29	43	50	54	61	66	75	79.98	80.02	84	95	106	115	127
0	0 to 36089	3	12.5	24	30.5	34	40	44	52	52	56	56	68	78.3	86	100
.4	0 to 36089	-5	3	9	16.2	20	27	39	44	44	49	49	65	76.2	86	100
.8	0	-15	-7	4	9	12	20	26.8	38	38	43	43	61	74.2	86	100
	20000	-11	-4	6	9	13.8	22	27	37	37	39	39	54.5	67.5	83.5	100
	36089	-11	-4	5	10	15.5	24.5	34	40	40	43	43	59	72	84	100

The two generic tasks developed to fulfill these objectives are

(1) a pitch and roll attitude pursuit tracking task, and

(2) a flight-path elevation and heading tracking task.

These tasks are representative of the critical loop closures in the pilot/vehicle system for many aircraft operations.[12] The pitch/roll task was chosen to evaluate characteristics of the ''inner-loop'' dynamics and the flight-path/heading task was chosen to evaluate characteristics of the overall, ''outer-loop'' dynamics of the vehicle. The complement of piloting tasks that were utilized during the simulation experiment primarily included these two dual-axis tasks, along with some single-axis variants of these tasks.

The visual displays that were used in the tasks were designed to provide the pilot with the necessary information in a way that was complete yet made use of simple symbology. In addition, the displays had to be acceptable to the pilot and provide the information in a consistent, ''realistic'' manner.

In order to accomplish these objectives, the displays were chosen to be of the inside-out and ''fly-to'' format. That is, the own-ship symbol is fixed on the display, the horizon is driven by the aircraft pitch attitude and bank angle, and the target is driven by the tracking errors. The pilot attempts to fly to the target.

The symbology that was used in the displays is similar to that depicted in Figure 10. This symbology was implemented via the AGT and displayed to the pilot by means of a CRT in the simulator cockpit. The display parameters that determine the display motion scaling, target range, field of view, etc. were chosen to provide sufficient resolution of attitude and error information for the task. The display scaling used is presented in Table 12.

The pitch/roll tasks are pursuit tasks. That is, both pitch and/or roll attitude errors and the pitch and/or roll attitudes of the aircraft is displayed to the pilot. The horizon is driven by the displayed pitch and roll attitude responses, θ_D and ϕ_D, but the vehicle responses used were varied. A discussion of these variations will be presented later. The target aircraft relative roll attitude and position are described by the pitch and/or roll tracking errors, ε_θ and ε_ϕ, where

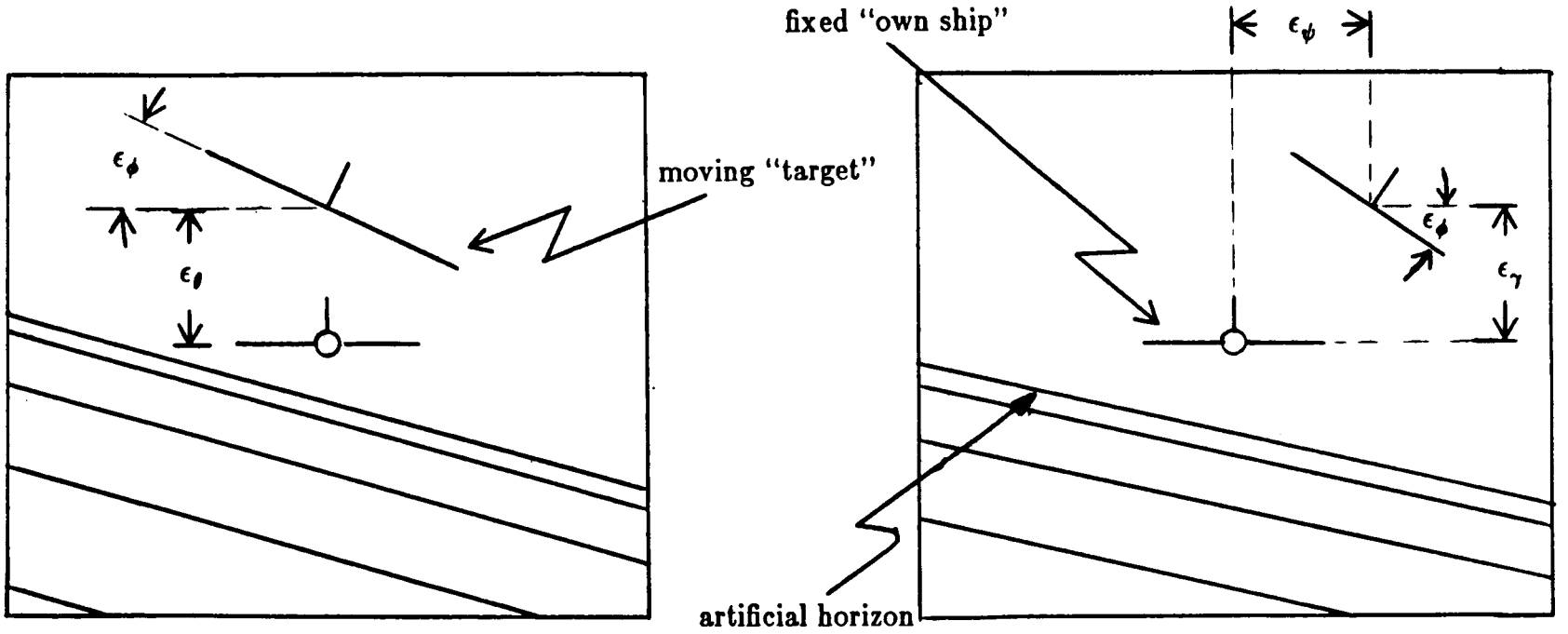

Figure 10 - Tracking Task Display Symbology

Table 12 - Display Scaling Parameters

Parameter	Scaling
θ_D, ε_θ, ε_γ, ε_ψ	Displacement of horizon and target yields one-to-one angular deflection at pilot's eye
ϕ_D	Angular rotation of horizon on display is one-to-one
ε_ϕ	Angular rotation of target on display is two-to-one

Table 13 - Command Parameters

	Tracking Task	
Parameter	Pitch/Roll	Flight-Path/Heading
η_1 (mean)	0 rad	0 rad
η_2 (mean)	0 rad	0 rad
$\sigma^2_{\eta_1}$ (variance)	0.4/32 rad^2	0.3/32 rad^2
$\sigma^2_{\eta_2}$ (variance)	0.77/32 rad^2	1.5/32 rad^2
ω_θ	0.5 rad/sec	0.3 rad/sec
ω_ϕ	0.5 rad/sec	0.3 rad/sec
τ_c	0.5 sec	0.5 sec
σ_{θ_c}	2.7 deg	1.8 deg
σ_{ϕ_c}	3.8 deg	4.1 deg

$$\varepsilon_\theta = \theta_C - \theta_D \tag{5a}$$

$$\varepsilon_\phi = \phi_C - \phi_D \tag{5b}$$

and where θ_C and ϕ_C are the command signals.

The command signals that were used in the task were chosen to provide the pilot with a challenging task, with the potential to result in excitation of the aeroelastic modes. They were driven by two independent random signals, governed by the following relations.

$$\ddot{\theta}_C + 1.4\,\omega_\theta \dot{\theta}_C + \omega_\theta^2 \theta_C = \omega_\theta^2 \eta_1 \tag{6a}$$

$$\ddot{\phi}_C + 1.4\,\omega_\phi \dot{\phi}_C + \omega_\phi^2 \phi_C = \omega_\phi^2 \eta_2 \tag{6b}$$

The statistics for the random signals, η_1 and η_2, were chosen to obtain command signals with the desired statistics. The appropriate statistical parameters and filter frequencies are presented in Table 13.

The flight-path and heading tracking tasks also provided the pilot with the aircraft attitude situation as well as the flight-path tracking errors. The displayed attitudes (horizon) for the pilot's vehicle in these tasks are once again θ_D and ϕ_D. But, the target aircraft relative positions are described by flight-path and heading errors, ε_γ and ε_ψ, where

$$\varepsilon_\gamma = \left[\gamma_C - \gamma \right] \cos\phi_D + \left[\psi_C - \bar{\psi} \right] \sin\phi_D \tag{7a}$$

$$\varepsilon_\psi = \left[\left[\psi_C - \bar{\psi} \right] - \varepsilon_\gamma \sin\psi_D \right] / \cos\phi_D \tag{7b}$$

and where,

$$\gamma = \theta_D - \alpha \tag{8a}$$

$$\bar{\psi} = \psi - \psi_0 \tag{8b}$$

where ψ_0 is a reference heading. The command signals for flight-path and heading, γ_C and ψ_C, are related to the pitch and roll commands through the kinematic relations shown below.

$$\dot{\gamma} = -\frac{1}{\tau_C}\gamma + \frac{1}{\tau_C}\theta_C \tag{9a}$$

$$\dot{\gamma}_C = \dot{\gamma}\cos\phi_C \tag{9b}$$

$$\dot{\psi}_C = \dot{\gamma}\sin\phi_C \tag{9c}$$

The appropriate values for τ_C are also given in Table 13.

The displayed attitudes of the aircraft, θ_D and ϕ_D, were variable as part of the experiment, leading to two different types of display dynamics. The first represents an "out-of-the-window" display, that is the displayed attitudes correspond to those of the aircraft at the cockpit location, including the effects of structural displacements. In this case,

$$\theta_D = \theta + K_\theta \eta_z \tag{10a}$$

$$\phi_D = \phi + K_\phi \eta_y \tag{10b}$$

where θ and ϕ are the rigid-body (mean-axis) Euler angles of the aircraft, K_θ and K_ϕ are the slopes of the two modeled structural modes evaluated at the cockpit location, (i.e. $K_\theta = -0.03$ rad, and $K_\phi = -0.0027$ rad), and η_y and η_z are the generalized coordinates of the two modeled structural modes.

The second variation can be thought of as a filtered display. In this case,

$$\theta_D = \theta \tag{11a}$$

$$\phi_D = \phi \tag{11b}$$

or the dynamic structural effects are filtered out. In subsequent discussions regarding the two display variations described above, the former (Equation 10) will be referred to as the "flexible display" and the later (Equation 11) will be referred to the "rigid display."

Configurations

The experimental configurations that were used in the simulation study were developed to address variations in structural stiffness, simulator motion effects, display dynamics effects, and consequences of multi-axis versus single-axis tasks. As mentioned previously, the variation in structural stiffness was accomplished by changing the invacuo free vibration frequencies of the two modeled structural modes. The baseline vehicle had invacuo vibration frequencies of 2.0 Hertz for each mode. These values were varied between 0.8 and 2.0 Hertz for the symmetric mode and between 1.0 and 2.0 Hertz for the antisymmetric mode. The simulator motion effects were examined by conducting some simulation runs with the same model dynamics, both with the motion enabled and disabled. Similarly, the effects of display dynamics were addressed by conducting runs with the same model dynamics, but with both display variations. The multi-axis/single-axis task effects were examined by simulating the same dynamics in both single-axis and dual-axis tasks.

The configuration variations described above can be categorized by the choice of several parameters. Some of these parameters are associated with the experimental "set-up" (e.g. simulator motion, pilot task, etc.) and others are related to the "dynamic properties" of the vehicle (e.g. invacuo vibration frequencies). Case numbers were assigned to each configuration to provide a systematic way to differentiate between various combinations of parameters.

The set-up parameters are reflected in the first four entries in the case number. These "identifiers" are defined in Table 14. An example is also included to demonstrate the numbering system. Notice that the last entry in the case number is called a "dynamic parameters identifier." This identifier is used to indicate the combination of dynamic parameters chosen for each configuration. Figure 11 is an excerpt of the list of configurations tested, the entire list is presented in Appendix 4. The combination of dynamic parameters for each configuration is defined in this list.

Notice that in addition to the frequencies of the invacuo vibration modes, the dynamic information includes structural mode status (e.g. ETAY OFF implies the dynamics were that of the rigid aircraft in the lateral axis), SCAS status, and speed hold (i.e. phugoid

Table 14 - Case Number Definition

NL - XY - Z ← Dynamic Parameters Identifier (see Figure 11 and Appendix 4)		
	Display Identifier	1 - flexible display 2 - rigid display
	Motion Identifier	1 - motion on 2 - motion off
	Task Identifier (letter)	A - longitudinal B - lateral-directional axis only C - two axes (both long. & lat.-dir.)
	Task Identifier (number)	1 - pitch/roll tracking 2 - heading/flight path tracking
Example: Case No. 1C-12-5		
	task properties	-pitch/roll tracking task -long. (pitch) axis and lat. (roll) axis enabled -motion on -standard display in use (flexible display)
	dynamic properties	-ω_y = 2.0 Hz (antisymmetric mode freq.) -ω_z = 1.0 Hz (symmetric mode freq.) -SCAS-on (Kq = 2.0) -Speed Hold-on

CASE NO.	ETAY	ETAZ	OMEGY	OMEGZ	SCAS	KQ	SPDH	OLD CASE
1A-11-1	OFF	OFF	-	-	ON	2.0	OFF	4
1A-11-2	OFF	ON	2.0	2.0	ON	2.0	OFF	10
1A-11-3	OFF	ON	2.0	1.75	ON	2.0	OFF	16
1A-11-4	OFF	ON	2.0	1.5	ON	2.0	ON	22
1A-21-1	OFF	OFF	-	-	ON	1.6	OFF	1*
1A-21-2	OFF	OFF	-	-	ON	2.0	OFF	1
1A-21-3	OFF	ON	2.0	2.0	ON	2.0	OFF	7
1A-21-4	OFF	ON	2.0	1.5	ON	2.0	ON	21
1B-11-1	OFF	OFF	-	-	ON	2.0	OFF	5
1B-11-2	ON	OFF	2.0	2.0	ON	2.0	OFF	11
1B-11-3	ON	OFF	1.5	2.0	ON	2.0	ON	32
1B-21-1	OFF	OFF	-	-	ON	1.6	OFF	2*
1B-21-2	OFF	OFF	-	-	ON	2.0	OFF	2
1B-21-3	ON	OFF	2.0	2.0	ON	2.0	OFF	8
1B-21-4	ON	OFF	1.5	2.0	ON	2.0	ON	31

Figure 11 - Configuration Listing (excerpt)

DATE	RUN	CASE	COMMENT
4/30	1	1A-21-1	no taped data, limited strips
	2	1B-21-1	"
	3	1C-21-1	"
	4	1A-21-2	"
	5	1A-21-2	"
5/2	1	1A-21-1	
	2	1B-21-2	
	3	1C-21-2	
	4	1A-11-1	
	5	1B-11-1	
	6	1C-11-1	
5/3	1	1C-11-1	tau(3) = 0
	2	1C-11-1	
	3	1A-21-3	
	4	1B-21-3	
	5	1C-21-3	
	6	1A-11-2	
	7	1B-11-2	
	8	1C-11-2	

Figure 12 - Chronological Listing of Runs (excerpt)

augmentation) controller status. Notice also that the gain on pitch-rate feedback in the pitch SCAS, KQ, is indicated. This parameter was varied as part of the tuning process which will be discussed in the next chapter. The entry for pitch SCAS gain was also used to indicate when the eigenspace assignment controller was used. When this is the case, ESC appears rather than a numerical value for KQ. The next item is the the entry entitled "SPDH" (for speed hold) and is used to indicate the status of the phugoid augmentation controller. Finally, the parameter called "old case" is tabulated. This number corresponds to the case number originally assigned to the configuration during the study. It is included in this list since it is useful in cross-referencing the experimental data, for example in relating the data recorded on the strip charts and the pilot comments made during the simulation sessions.

To further facilitate cross-referencing of the experimental data, a chronological listing of the simulation runs and case numbers has been developed as well. This list presents the case number corresponding to each simulation run, it also includes comments regarding the availability of data associated with particular runs. An excerpt of this list is shown in Figure 12 and the entire chronological listing is presented in Appendix 4.

The baseline vehicle configuration corresponds approximately to the dynamics of an early B-1 aircraft. In terms of the parameters described above, this chosen baseline configuration includes the dynamics of the two structural modes with frequencies of 2.0 Hertz, simulator motion disabled, and the flexible display. A more complete specification of the baseline configuration is shown in Table 15.

Table 15 - Baseline Configuration Parameters

Flight Condition	$\Lambda = 65^{\circ}$ (swing sweep) h = 5000 ft (altitude) M = 0.6 (Mach number)
Vehicle Dynamics	Flexible modes - enabled $\omega_y = 2.0$ Hz (vibration $\omega_z = 2.0$ Hz frequencies) SCAS - enabled $K_q = 2.0$ sec (pitch rate gain) Phugoid Augmentation - enabled
Motion and Display	Motion - disabled Display - flexible ("out-of-window")
Task and Commands	Task - pitch/roll tracking $\sigma_\theta^2 = 0.4$ (command $\sigma_\phi^2 = 0.77$ variances) $\tau_c = 0.5$ (sec)

CHAPTER 3
RESULTS AND ANALYSIS

Conduct of the Experiment

The vehicle configurations were evaluated in the order specified in the chronological listing shown in Appendix 4. Three pilots participated in evaluating the experimental configurations, although pilot B was the primary test pilot. The background and experience of each pilot is summarized in Table 16. Their backgrounds reflect a wide range of piloting experience and this should be considered when the simulation results are reviewed.

Each pilot was briefed on the experimental structure and task objectives. They were required to keep the center of the target (i.e. the intersection of the wing-line and the tail-line) inside the circle (or dot) at the center of the own-ship symbol. See Figure 10 for an illustration of the display symbology. The pilots were encouraged to use whatever technique they considered useful in minimizing the displayed error and were allowed to practice with a configuration until they felt they were ready to attempt an evaluation run. When an evaluation run was completed, the pilot was asked to comment on any aspect of the run he felt was noteworthy. For example, he might note his preferences relative to the vehicle responses, performance, and the techniques he employed to perform the task. Then he was requested to rate the configuration using the Cooper-Harper rating scale.

Early in the experiment, the simulation was tuned to improve the "feel" of the simulation of the baseline configuration. Several model parameters were varied to obtain a baseline configuration which had acceptable and "realistic" responses, when evaluated by the pilots. This tuning process resulted in the baseline parameters noted in Table 15. During the tuning process small variations in some simulation model parameters occurred. When these parameters differ from those of the baseline configuration it is noted in the data records.

Three types of data were collected during each simulation run: (1) pilot comments and subjective ratings (Cooper-Harper), (2) strip chart recordings, and (3) vehicle response time-series data (i.e. recorded on magnetic tape). The pilot comments and ratings for each simulation run were documented using a summary sheet. Figure 13 depicts a typical summary sheet and the entire collection of summary sheets is presented in Appendix 5. The sheets are

Table 16 - Test Pilot Profiles

Pilot	Background
A	Student general aviation pilot. Limited experience in piloting aircraft, no experience with large aircraft. Familiar with experimental set-up, model characteristics and project goals and expectations. No previous experience in rating aircraft handling qualities.
B	Experienced test pilot. Extensive background in flying large aircraft. Basic (general) understanding of experimental set-up and objectives. Substantial background in rating aircraft handling qualities using the Cooper-Harper scale.
C	Experienced general aviation pilot. No experience with large aircraft or with rating handling qualities. Basic understanding of experimental set-up and objectives.

CASE NO.	SPECS :		
1C-11-3	η_y : ON $\omega_y = 2.0$ SCAS : ON $K_q = 2.0$ η_z : ON $\omega_z = 2.0$ SPEED HOLD ; ON OLD CASE NO. : 13		
RUN/PILOT	SCORES :		COOPER-HARPER RATING
5-10-2 / B	$\varepsilon_{long} = .079$	$\sigma_{long} = 1.17$	
	$\varepsilon_{lat} = -.10$	$\sigma_{lat} = 1.14$	5

COMMENTS :

- PILOT CAN CONTROL THE SITUATION AND RIDE IS MUCH SMOOTHER

- VISUAL CUES AID IN CONTROL OF THE SITUATION

- QUALITATIVELY DISCONCERTING THAT SCORES ARE NOT HIGHER (WORSE) SINCE NOTED MORE ERROR

- THE PILOT PERCIEVED WORSE PERFORMANCE AND HIGH WORK LOAD

- NOTE : NO DIGITAL DATA

Figure 13 - Sample Summary Sheet

ordered by case number to make comparisons between and among various cases easier. Each sheet is cross-referenced with the strip charts and time response data by means of the run number. The run number indicates both the day and order in which the run was made. For example, RUN 5-10-3 is the third run completed on May tenth. Other information found on the summary sheets are the dynamic parameters described in the previous chapter and are included to facilitate later analysis. The pilot identifier is also included to indicate which of the evaluation pilots participated in each run. These summary sheets are also used to indicate variations from the baseline configuration due to the tuning process described earlier.

During the simulation runs, the strip charts provided a real-time graphical record of twenty-four different responses of interest. Table 17 lists the twenty-four parameters that were plotted on three recorders. The strip charts are organized chronologically by run number to facilitate cross-referencing with the other data. Figure 14 depicts a sample strip chart plot, notice that the parameter names, scales and units are noted directly on each response.

The time histories recorded on magnetic tape consists of the twenty-six responses listed in Table 18. The sampling period was 3/32 second and the average run length was about 120 seconds. A header/title for each data file on the magnetic tapes indicates the run number (i.e. date and chronological order) of each simulation run. This header allows the contents of any data file to be readily located, identified and accessed, and facilitates cross-referencing with the other forms of data.

The subjective pilot ratings, of course, provide a measure of the handling qualities of the various experimental configurations. In addition, several of the recorded responses provide other indications of vehicle performance. For instance, the pitch (or flight-path) and roll (or heading) tracking errors provide a measure of tracking performance. Stick displacements and rates provide measures of pilot activity and workload. Normal and lateral accelerations provide an indication of the ride quality and the pilot induced vibration environment. Root mean squared (RMS) values for these vehicle responses were calculated for each simulation run.

The pilot ratings and RMS values of the responses discussed above were summarized graphically to allow direct interpretation of the experimental results, and these results are grouped by configuration class. A configuration "class" is made up of the experimental configurations which possess a specified set of characteristics. These include the task definition, motion status, display dynamics, and varying degrees of structural flexibility. The

Table 17 - Strip Chart Response Parameters

Strip Chart Recorder #1 - (Longitudinal Responses)							
α	θ	q	V_{TOT}	γ	h	$a_{n_{cp}}$	P_{ϵ}
angle of attack (deg)	pitch altitude (deg)	pitch rate ($\frac{deg}{sec}$)	total velocity ($\frac{ft}{sec}$)	flight path angle (deg)	altitude (ft)	normal acceleration (at cockpit) (g's)	long. tracking error (deg)
Strip Chart Recorder #2 - (Lateral-Directional Responses)							
β	ϕ	p	r	ψ	$a_{y_{cp}}$	T	R_{ϵ}
sideslip angle (deg)	bank angle (deg)	roll rate ($\frac{deg}{sec}$)	yaw rate ($\frac{deg}{sec}$)	heading angle (deg)	lateral acceleration (at cockpit) (g's)	thrust (total) (lbs)	lateral tracking error (deg)
Strip Chart Recorder #3 - (Control Input Responses)							
δ_{long}	δ_{lat}	δ_{ped}	δ_{tail}	δ_{DH}	δ_S	η_z	η_y
long. stick deflection (in)	lateral stick deflection (in)	pedal deflection (in)	elevator deflection (deg)	differential horizontal tail deflection (deg)	spoiler deflection (deg)	generalized displacement of symmetric mode	generalized displacement of antisymm. mode

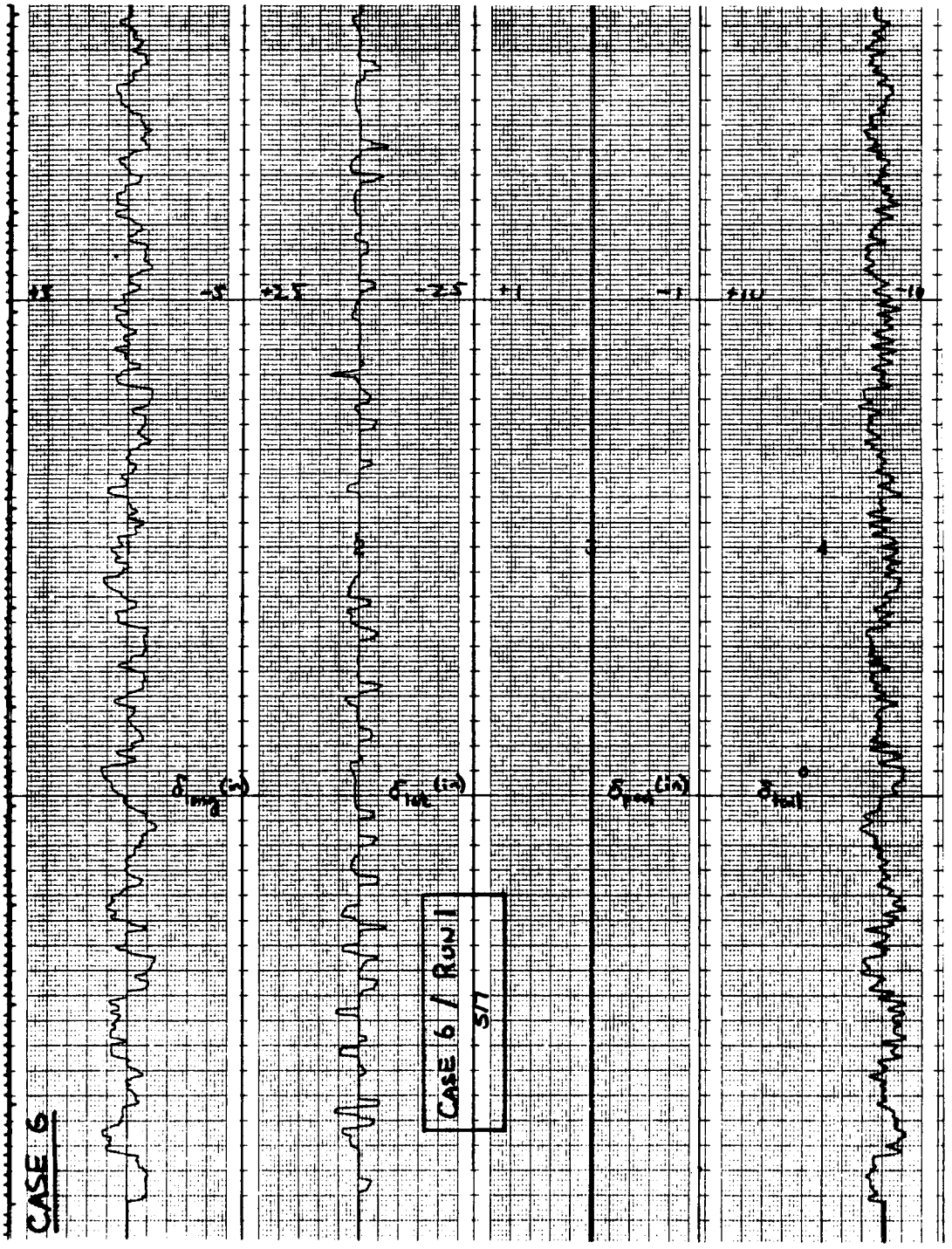

Figure 14 - Sample Strip Chart Plot

Table 18 - Tabulated Response Parameters

parameter	description	parameter	description	parameter	description
t	time [seconds]	η_2	random sequence (for roll command)	ϕ_D	displayed bank [degrees]
η_1	random sequence (for pitch command)	ϕ_c	roll command [degrees]	$\delta_{long.}$	long. stick displacement [inches]
θ_c	pitch command [degrees]	R_ε	lateral error [degrees]	δ_{lat}	lateral stick displacement [inches]
P_ε	long. error [degrees]	p	roll rate [rad/sec]	δ_{ped}	pedal displacement [inches]
θ	pitch attitude [degrees]	q	pitch rate [rad/sec]	$\dot{\delta}_{long}$	long. stick rate [inches/sec]
ϕ	bank angle [degrees]	r	yaw rate [rad/sec]	$\dot{\delta}_{lat}$	lateral stick rate [inches/sec]
ψ	heading angle [degrees]	$a_{n_{cp}}$	normal acceleration [g's]	$\dot{\delta}_{ped}$	pedal rate [inches/sec]
α	angle of attack [degrees]	$a_{y_{cp}}$	lateral acceleration [g's]	V_{TOT}	total velocity [ft/sec]
β	sideslip angle [degrees]	θ_D	displayed pitch [degrees]		

specific characteristics associated with each configuration class are indicated by the configuration numbers defined in Table 14 and the configuration listings in Appendix 4.

Experimental Results

An illustration of the simulation results is shown in Figure 15. This plot represents the Cooper-Harper pilot ratings that were given to each configuration in the class 1C-11 with the level of flexibility characterized by variations in the symmetric mode frequency (i.e. the antisymmetric mode frequency is fixed at 2.0 Hertz). Configuration class 1C-11 consists of experimental configurations in which the dual-axis pitch/roll pursuit tracking task was performed with the simulator motion enabled and the flexible display dynamics utilized. Each plot indicates which configuration class is being considered and which of the two structural modes is used to characterize variations in structural flexibility. Plotted along the axis labeled "Level of Flexibility" is simply the invacuo free vibration frequency of the mode which is varied. When multiple data points are available for a given level of flexibility, all points associated with that frequency are connected by a line.

The effects of variations in structural flexibility can be addressed by evaluating the trends or variations which appear on each individual plot. The effects of variations in the other experimental variables, (e.g. task definition, motion status and display status), can be addressed by comparing and contrasting the plots for the appropriate configuration classes. For example, to compare the effects of motion on the dual-axis pitch/roll tracking task one might compare the results for configuration classes 1C-11 and 1C-21 (i.e. those utilizing the flexible display dynamics) or configuration classes 1C-12 and 1C-22 (i.e. those utilizing the rigid display).

The complete graphical results are presented in Figures 16 through 26. Figures 16 through 18 depict the plots of the pilot ratings that were collected during the experiment. Figure 16 depicts the pilot ratings associated with the pitch/roll pursuit tracking task with the symmetric mode frequency varied. Figure 17 depicts the ratings associated with the same task, but with the frequency of the antisymmetric mode varied. Figure 18 depicts the ratings associated with the flight-path/heading task where the symmetric mode frequency is varied.

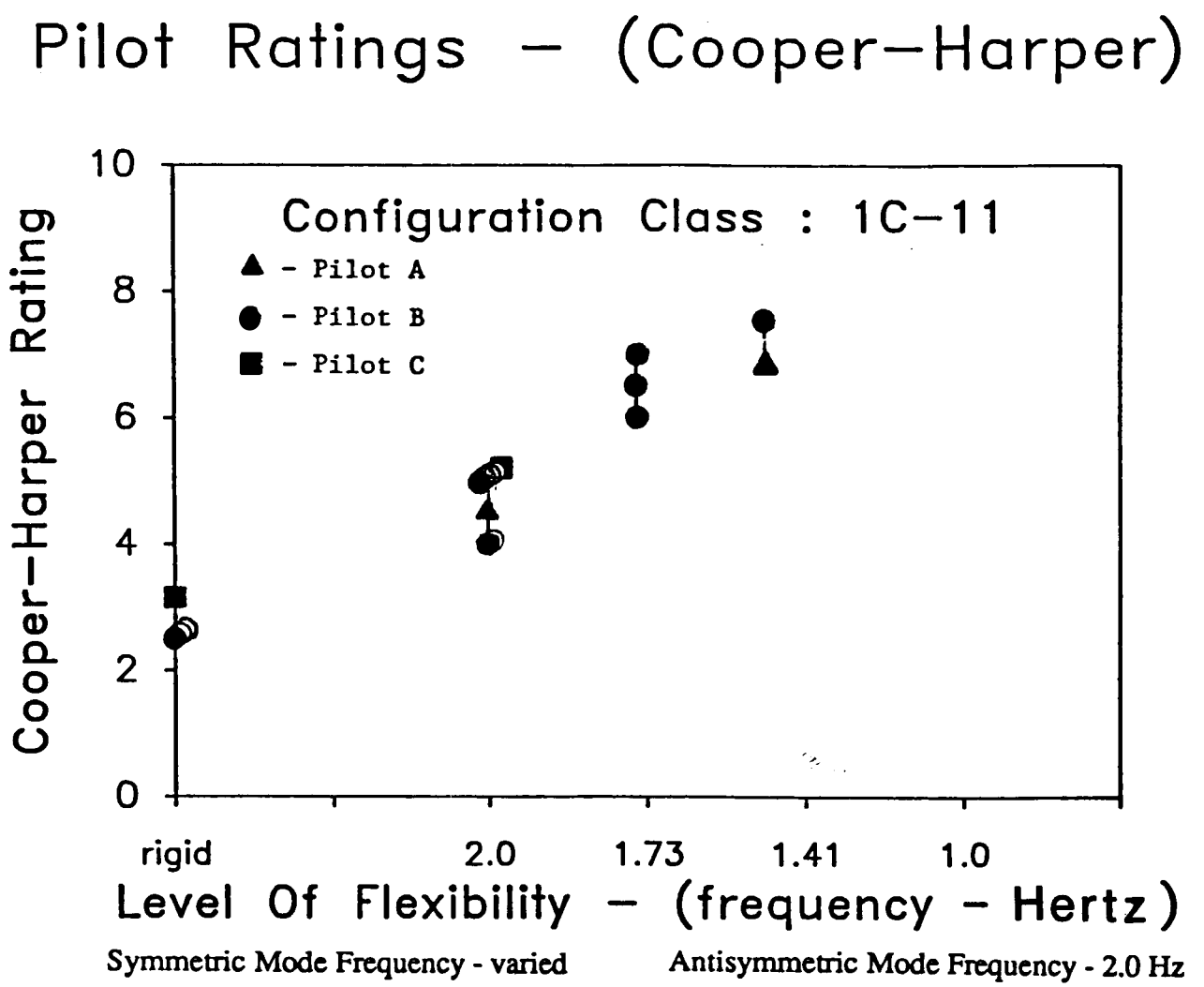

Figure 15 - Cooper-Harper Rating : 1C-11

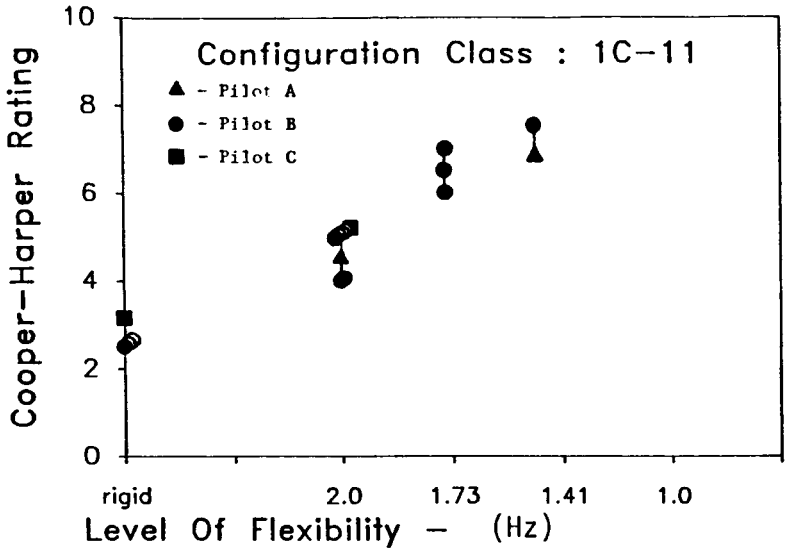

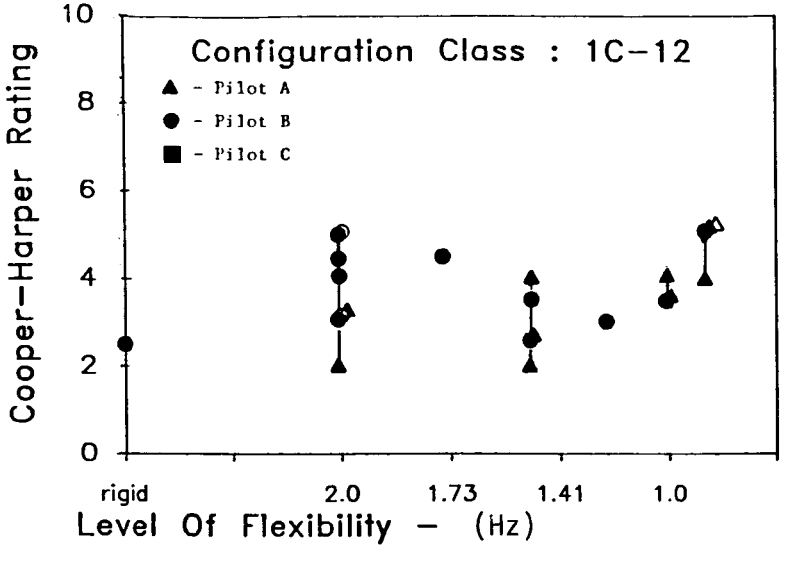

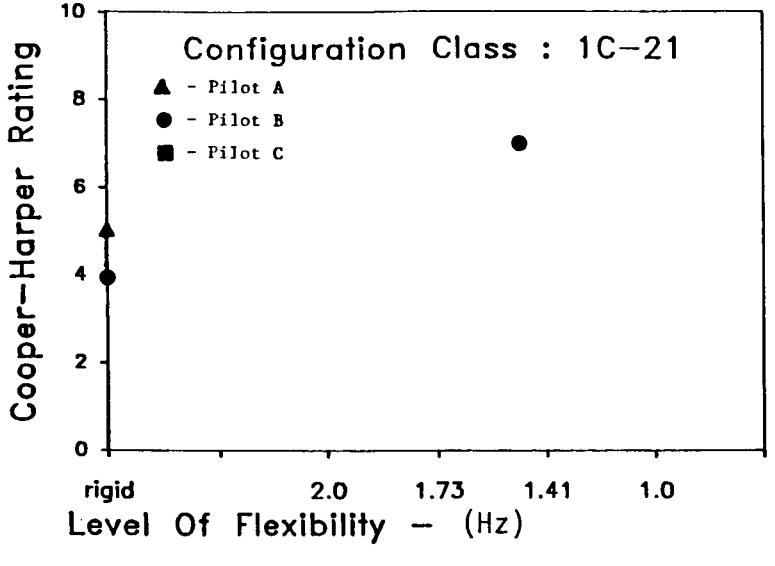

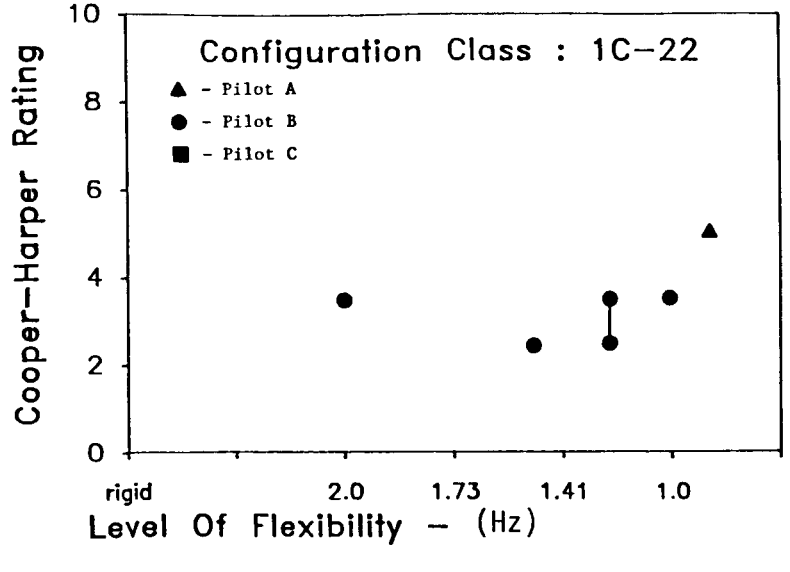

Symmetric Mode Frequency - varied

Antisymmetric Mode Frequency - 2.0 Hz

Figure 16 - Cooper-Harper Rating : 1C-11, 1C-12, 1C-21 and 1C-22 (Symmetric Mode Varied)

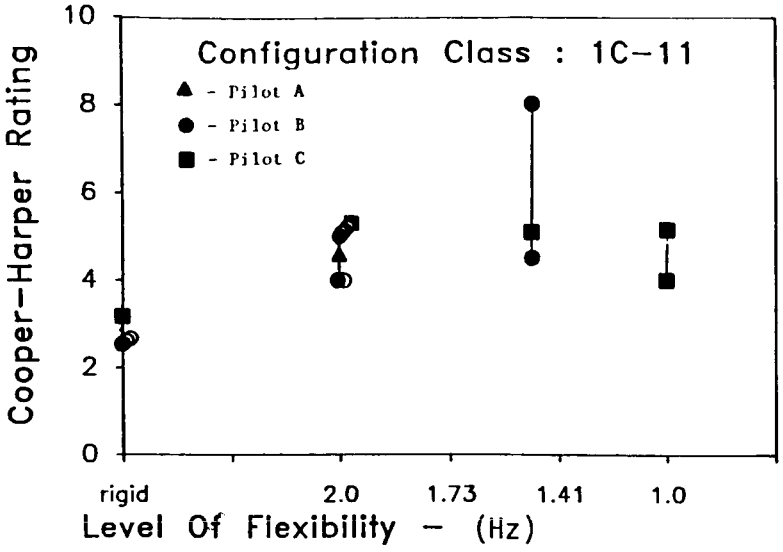

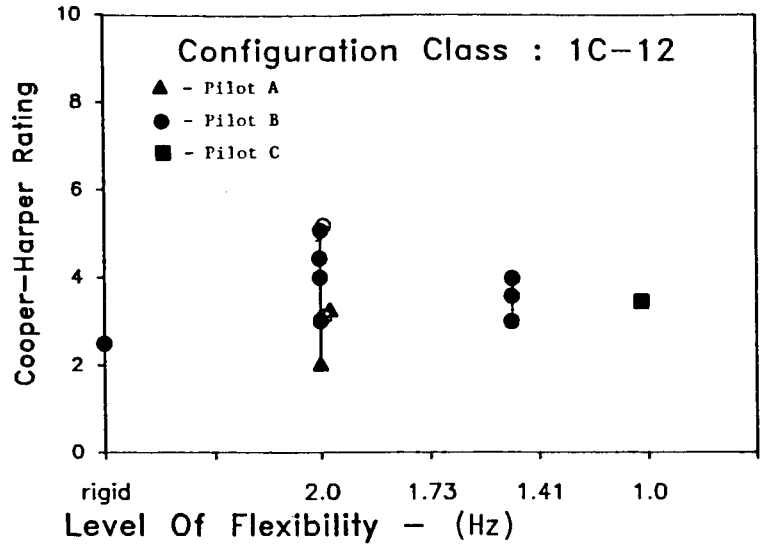

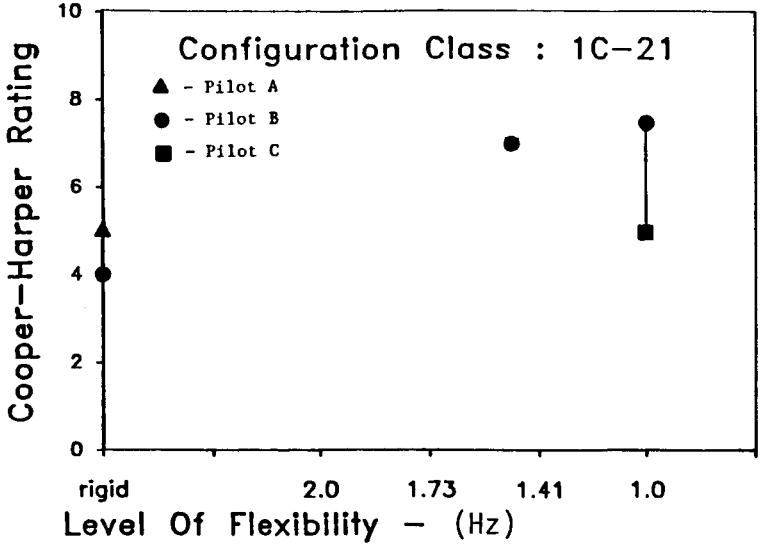

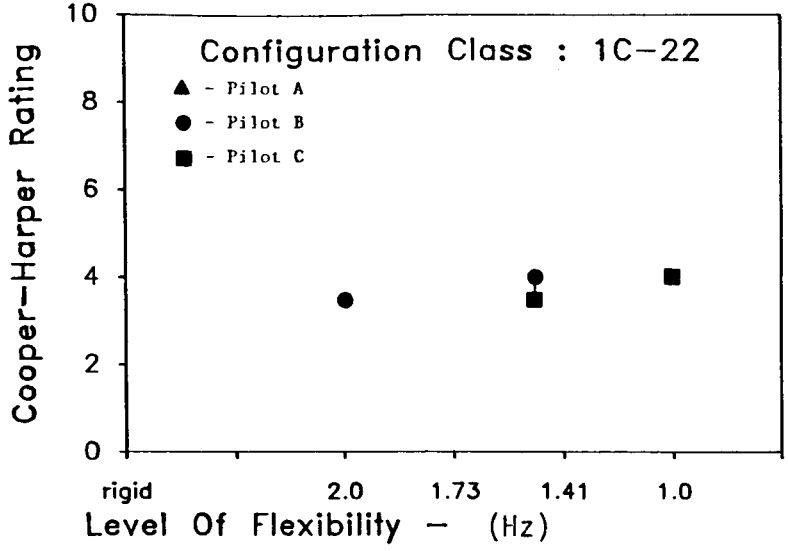

Symmetric Mode Frequency - 2.0 Hz Antisymmetric Mode Frequency - varied

Figure 17 - Cooper-Harper Rating : 1C-11, 1C-12, 1C-21 and 1C-22 (Antisymmetric Mode Varied)

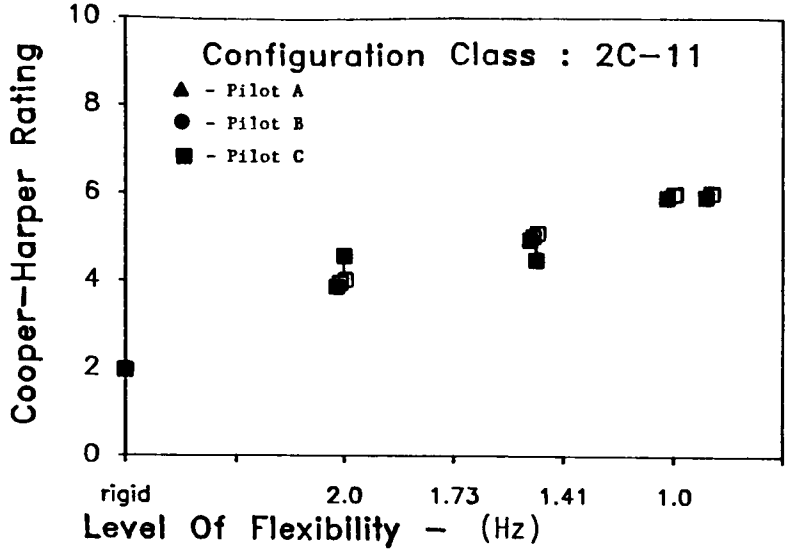

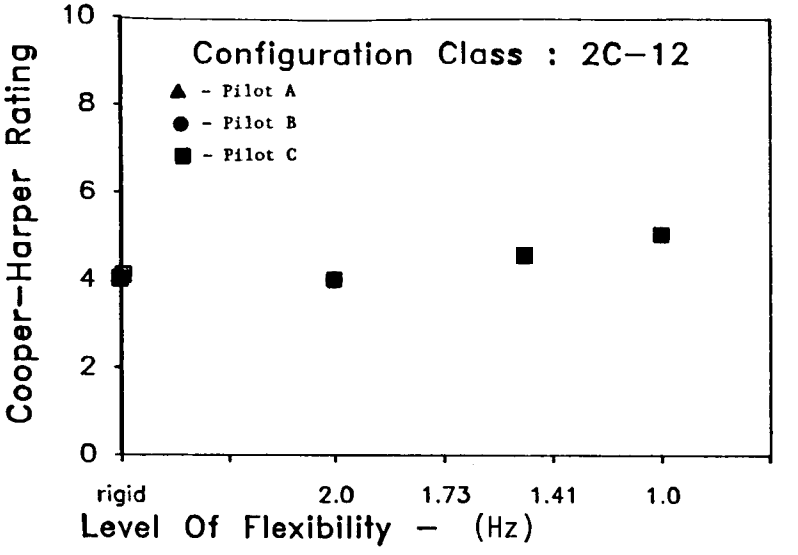

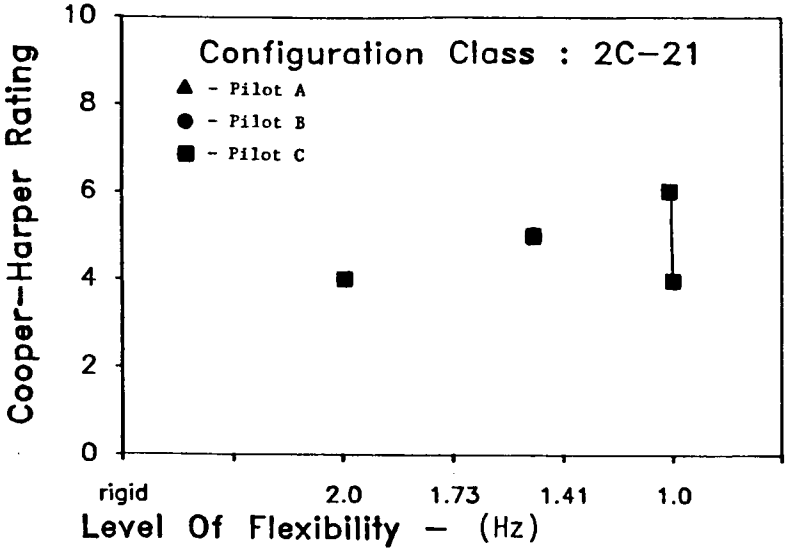

Symmetric Mode Frequency - varied Antisymmetric Mode Frequency - 2.0 Hz

Figure 18 - Cooper-Harper Rating : 2C-11, 2C-12 and 2C-21

The ratings are based on the Cooper-Harper scale, and each of the three evaluation pilots is indicated with a unique symbol. It should be noted that none of the pilots evaluated every configuration. Pilot B was able to evaluate most of the configurations, but pilots A and C only evaluated a portion of the possible configurations. Note that multiple data points with the same pilot ratings are indicated by multiple rating symbols. Note also that there are many runs in which no pilot ratings are available, this is due to the fact that the pilot was only requested to rate a given configuration when he felt proficient in the task. However, other data was collected for non-rated runs.

Figures 19 through 26 present the plots of the RMS values for the experimental responses described above. Figure 19 presents all the available pitch and flight-path tracking errors. Similarly, figures 20 through 26 present the available results for the other responses. The RMS pitch (or flight-path) and roll (or heading) errors correspond to the total tracking errors (in degrees) and are calculated from the responses P_ε and R_ε defined in Table 18. The RMS longitudinal and lateral stick displacements correspond to the linear displacements (in inches) of the control stick in the appropriate directions and are calculated from the responses δ_{long} and δ_{lat} defined in Table 18. Similarly, the RMS longitudinal and lateral stick rates correspond to the linear displacement rates (in inches/second) of the control stick and are calculated from the responses $\dot{\delta}_{long}$ and $\dot{\delta}_{lat}$. Finally, the RMS normal and lateral accelerations correspond to the accelerations (in g's) at the cockpit of the vehicle model (i.e. the accelerations that result from the numerical integration of the vehicle equations of motion, *not* the accelerations actually experienced by the pilot which are attenuated due to the washout logic and motion-base hardware). These RMS values are calculated from the responses $a_{n_{cp}}$ and $a_{y_{cp}}$ defined in Table 18.

Note that the RMS values for pitch (or flight-path) error, roll (or heading) error, longitudinal stick displacement, lateral stick displacement, longitudinal stick rate, and lateral stick rate are plotted for every configuration class for which response data was available. The normal accelerations, however, are only presented for variations in symmetric mode frequency and the lateral accelerations are presented for variations in antisymmetric mode frequency. The letters adjacent to each data point correspond to the pilot identifiers defined in Table 16. The asterisk that appears next to some of the letters indicates that the corresponding simulation run was given a subjective pilot rating and should be weighted accordingly.

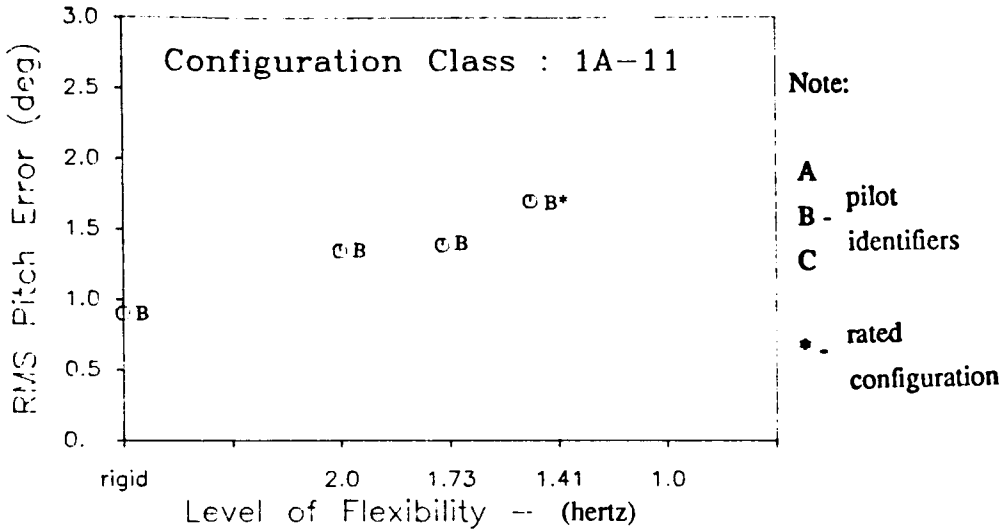

Note:

A
B - pilot identifiers
C

* - rated configuration

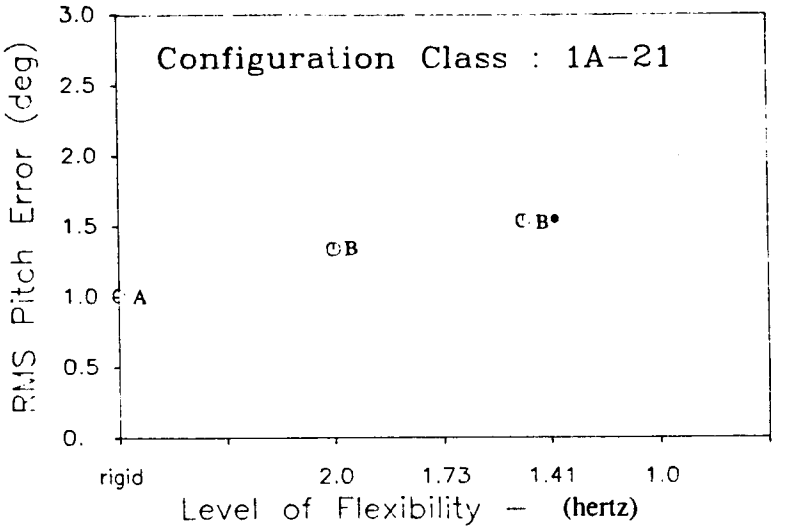

Symmetric Mode Frequency - varied

Antisymmetric Mode Frequency - 2.0 Hz

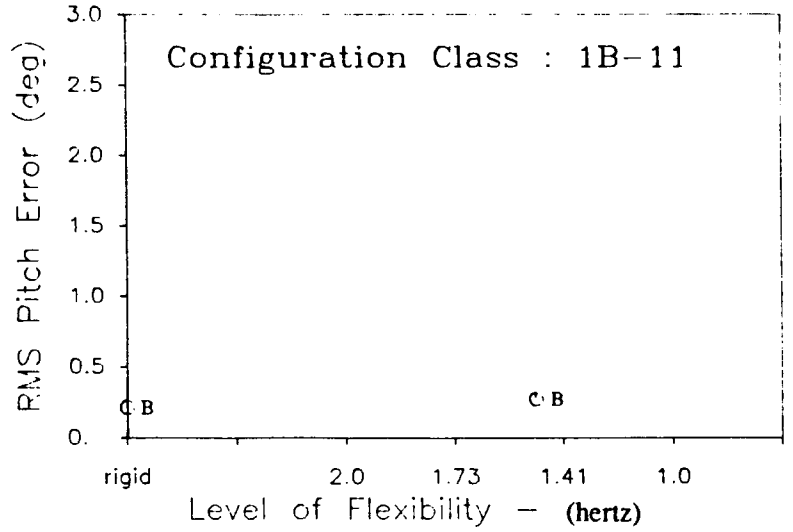

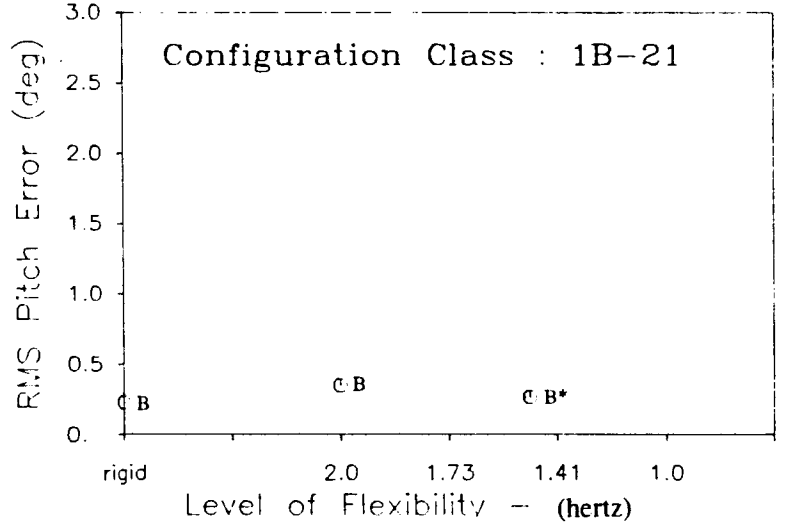

Symmetric Mode Frequency - 2.0 Hz

Antisymmetric Mode Frequency - varied

Figure 19a - RMS Pitch and Flight-path Tracking Errors (degrees)

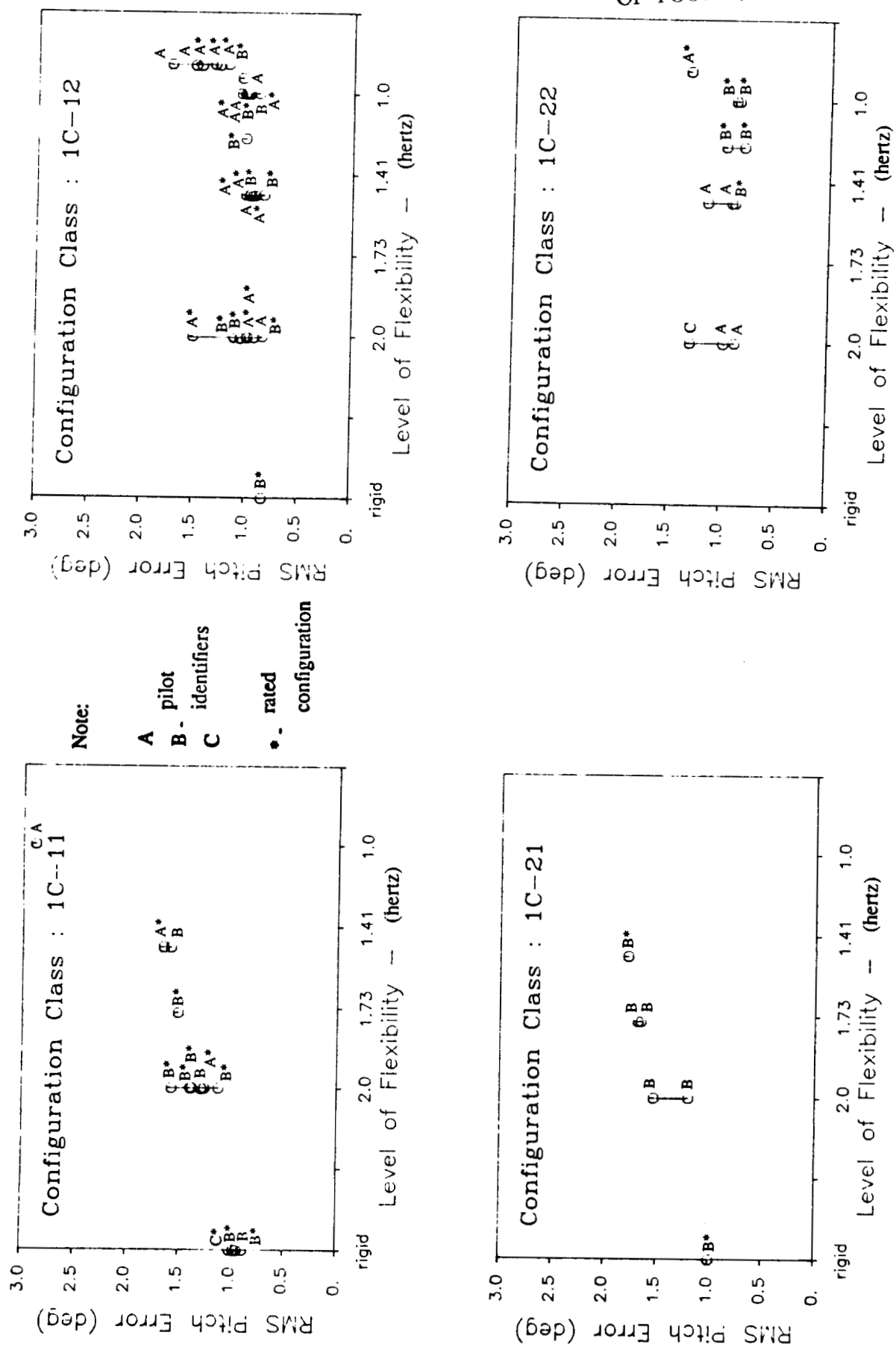

Symmetric Mode Frequency - varied Antisymmetric Mode Frequency - 2.0 Hz

Figure 19b - RMS Pitch and Flight-path Tracking Errors (degrees)

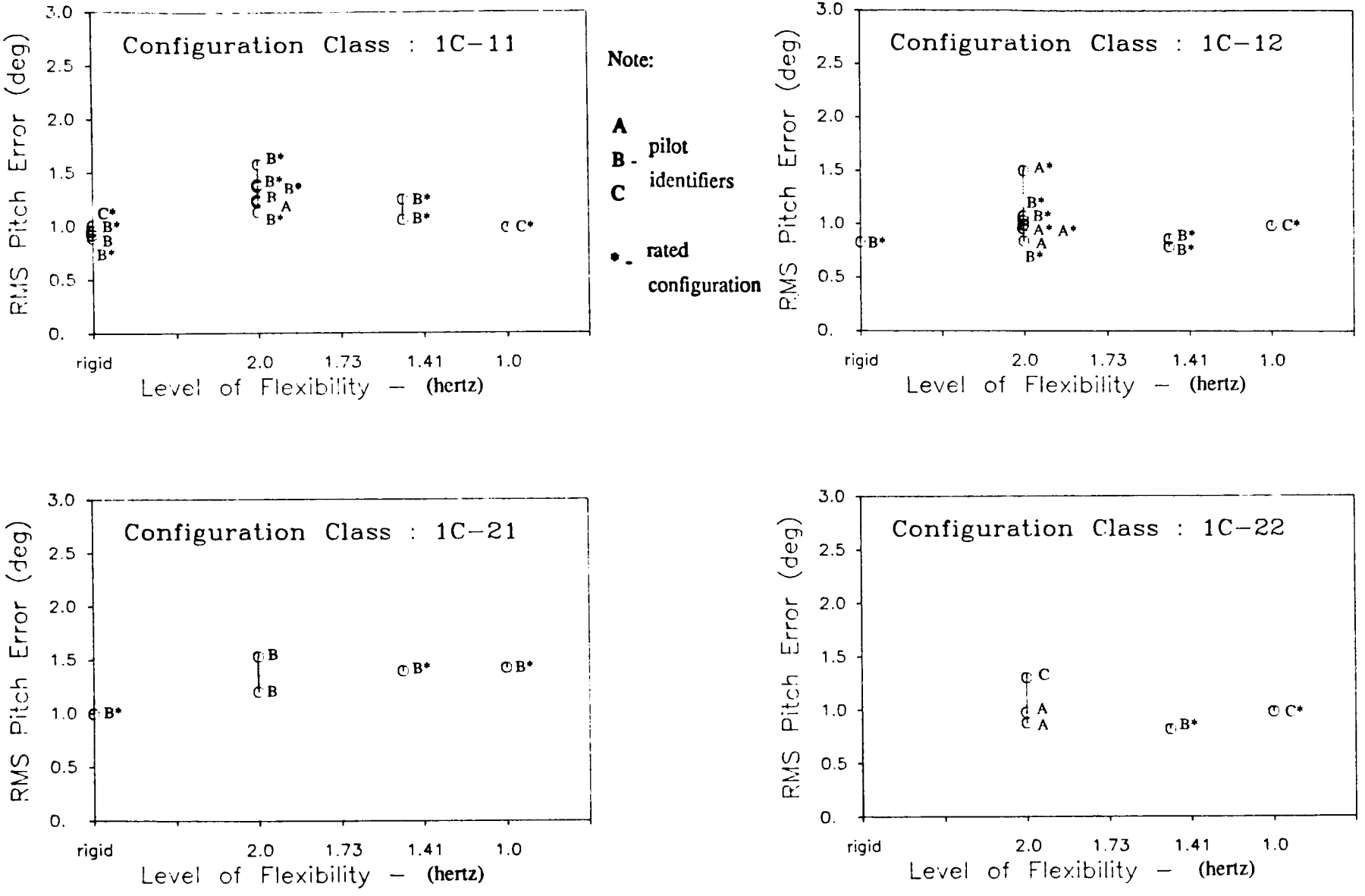

Symmetric Mode Frequency - 2.0 Hz Antisymmetric Mode Frequency - varied

Figure 19c - RMS Pitch and Flight-path Tracking Errors (degrees)

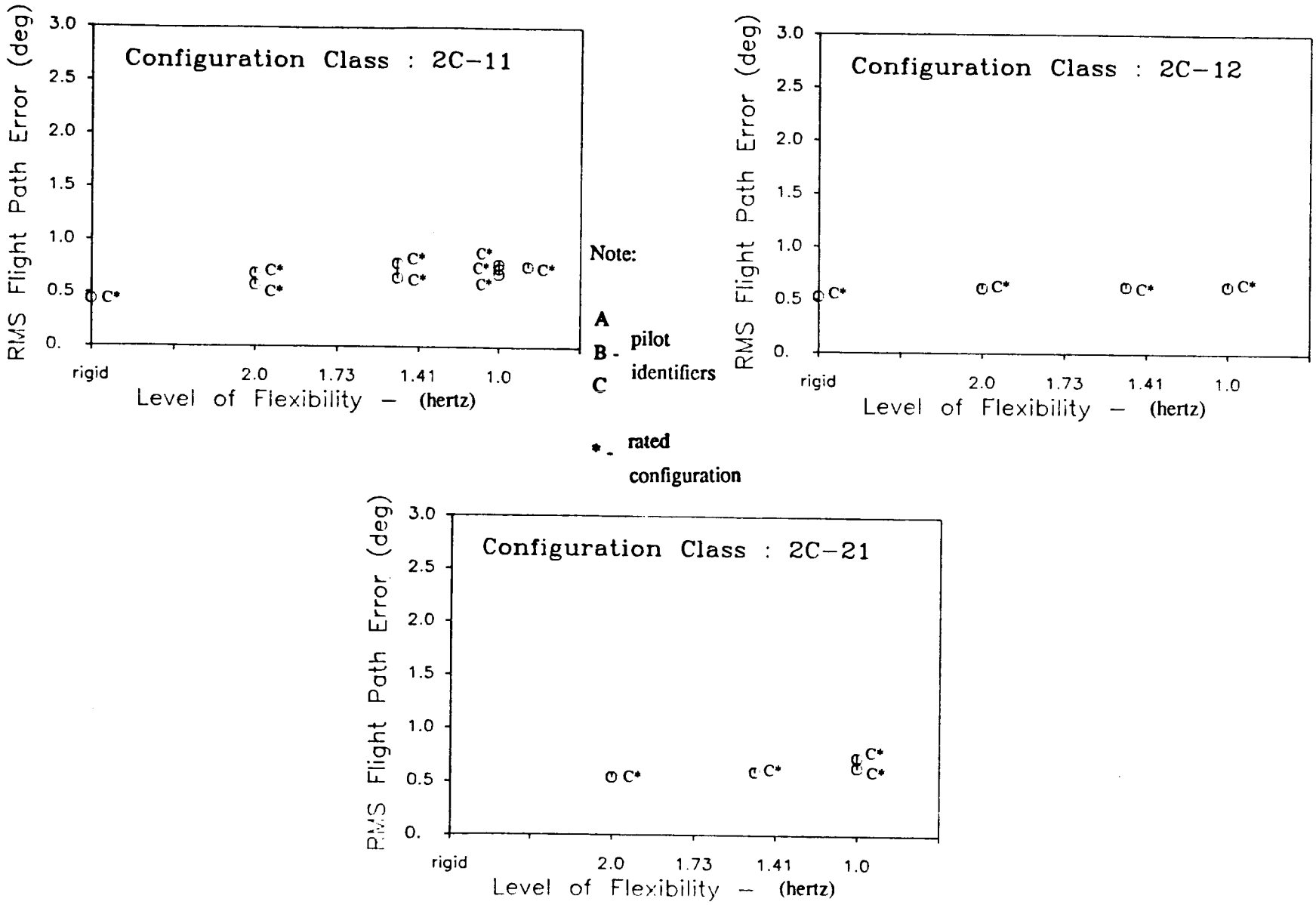

Symmetric Mode Frequency - varied Antisymmetric Mode Frequency - 2.0 Hz

Figure 19d - RMS Pitch and Flight-path Tracking Errors (degrees)

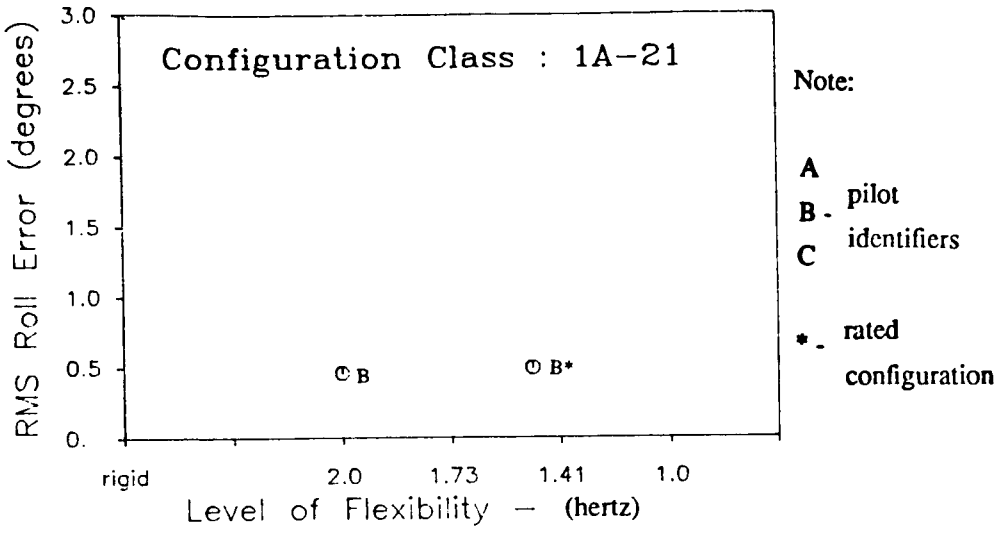

Note:

A
B - pilot identifiers
C

* - rated configuration

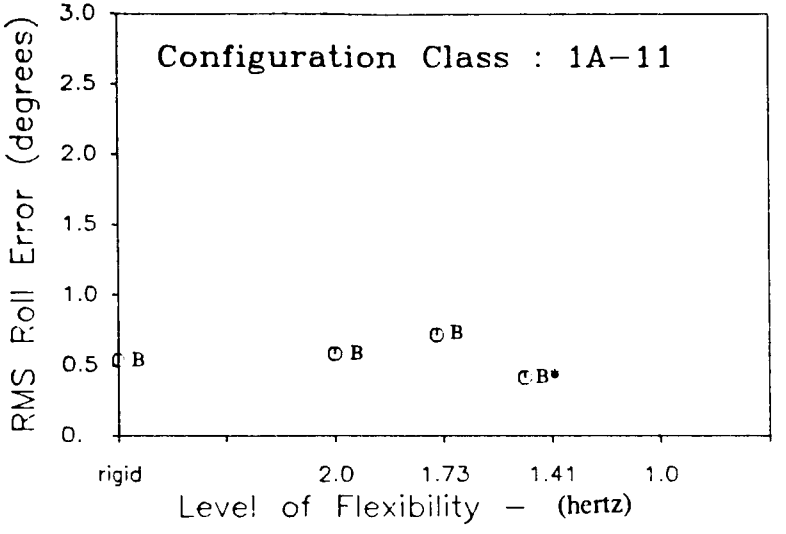

Symmetric Mode Frequency - varied

Antisymmetric Mode Frequency - 2.0 Hz

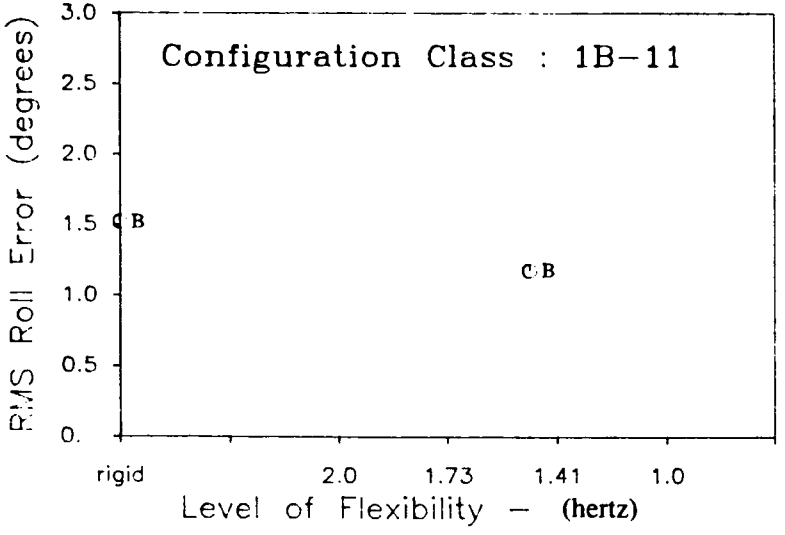

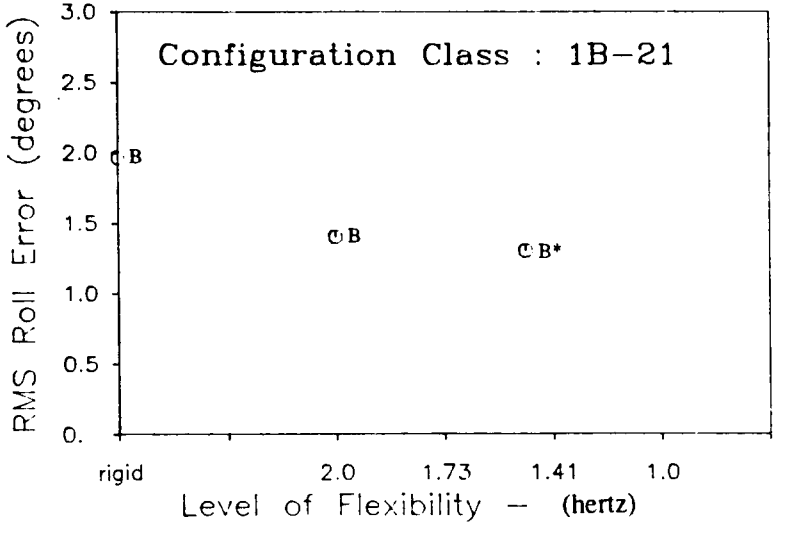

Symmetric Mode Frequency - 2.0 Hz

Antisymmetric Mode Frequency - varied

Figure 20a - RMS Roll and Heading Tracking Errors (degrees)

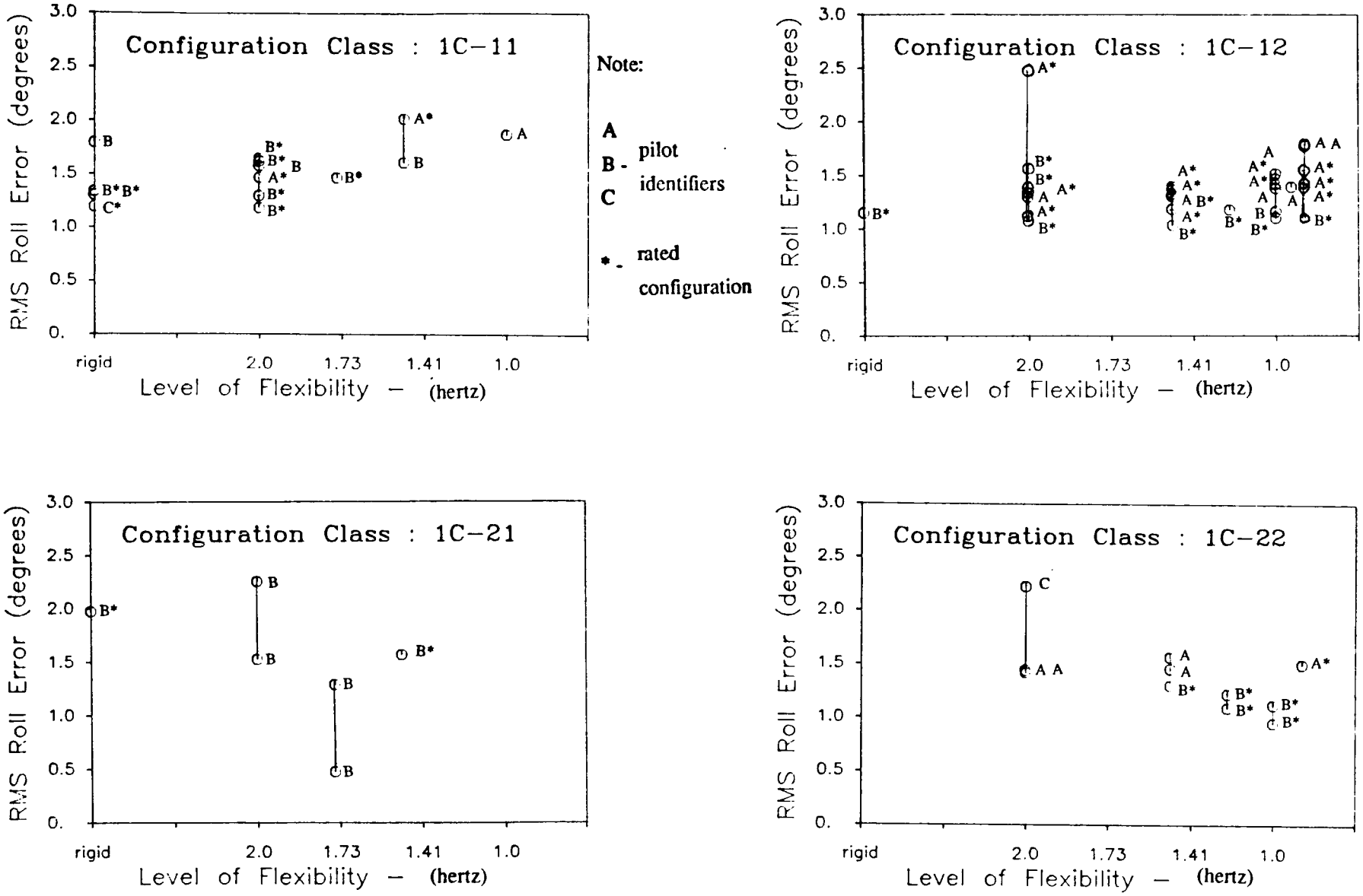

Symmetric Mode Frequency - varied Antisymmetric Mode Frequency - 2.0 Hz

Figure 20b - RMS Roll and Heading Tracking Errors (degrees)

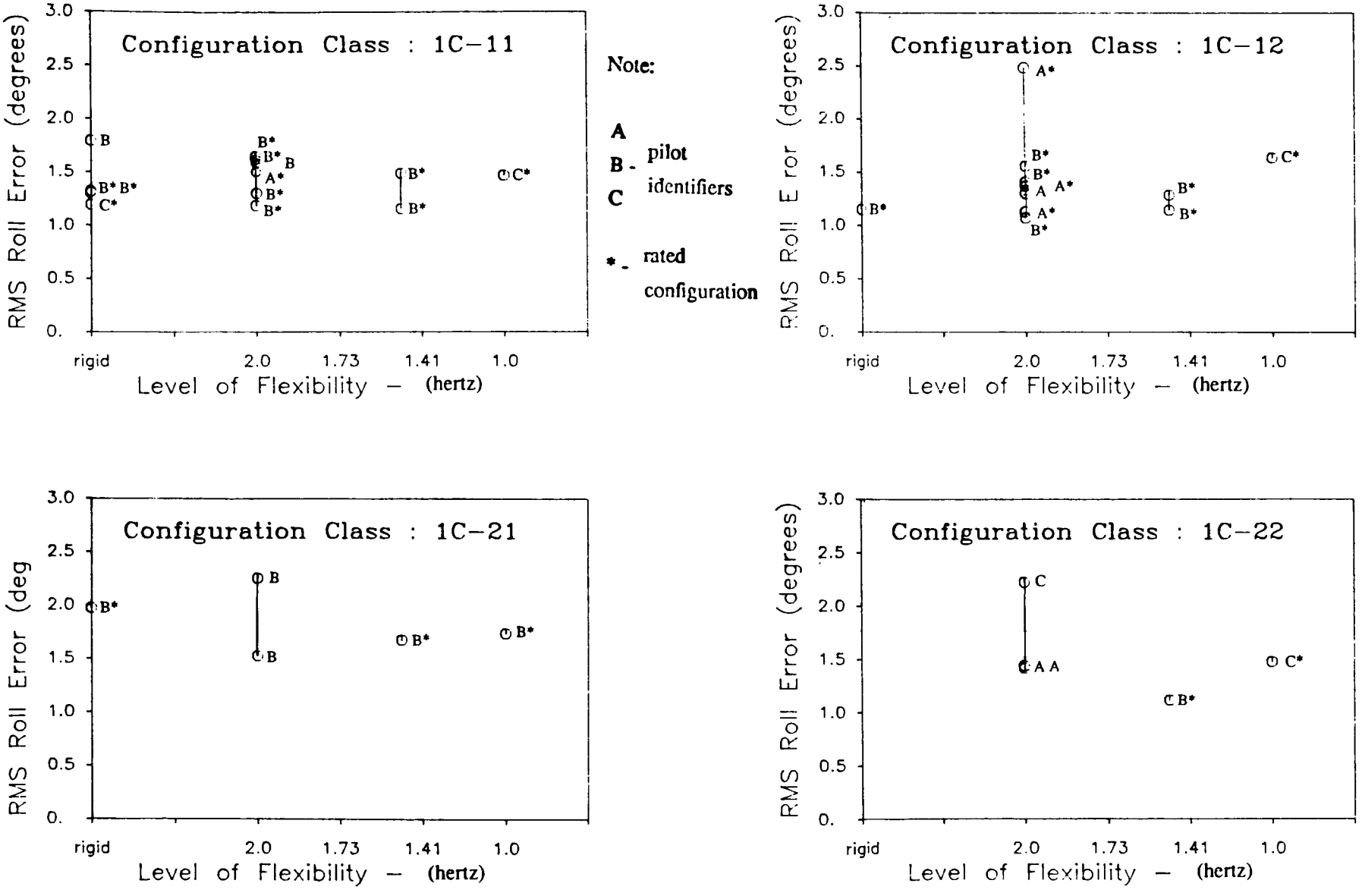

Symmetric Mode Frequency - 2.0 Hz Antisymmetric Mode Frequency - varied

Figure 20c - RMS Roll and Heading Tracking Errors (degrees)

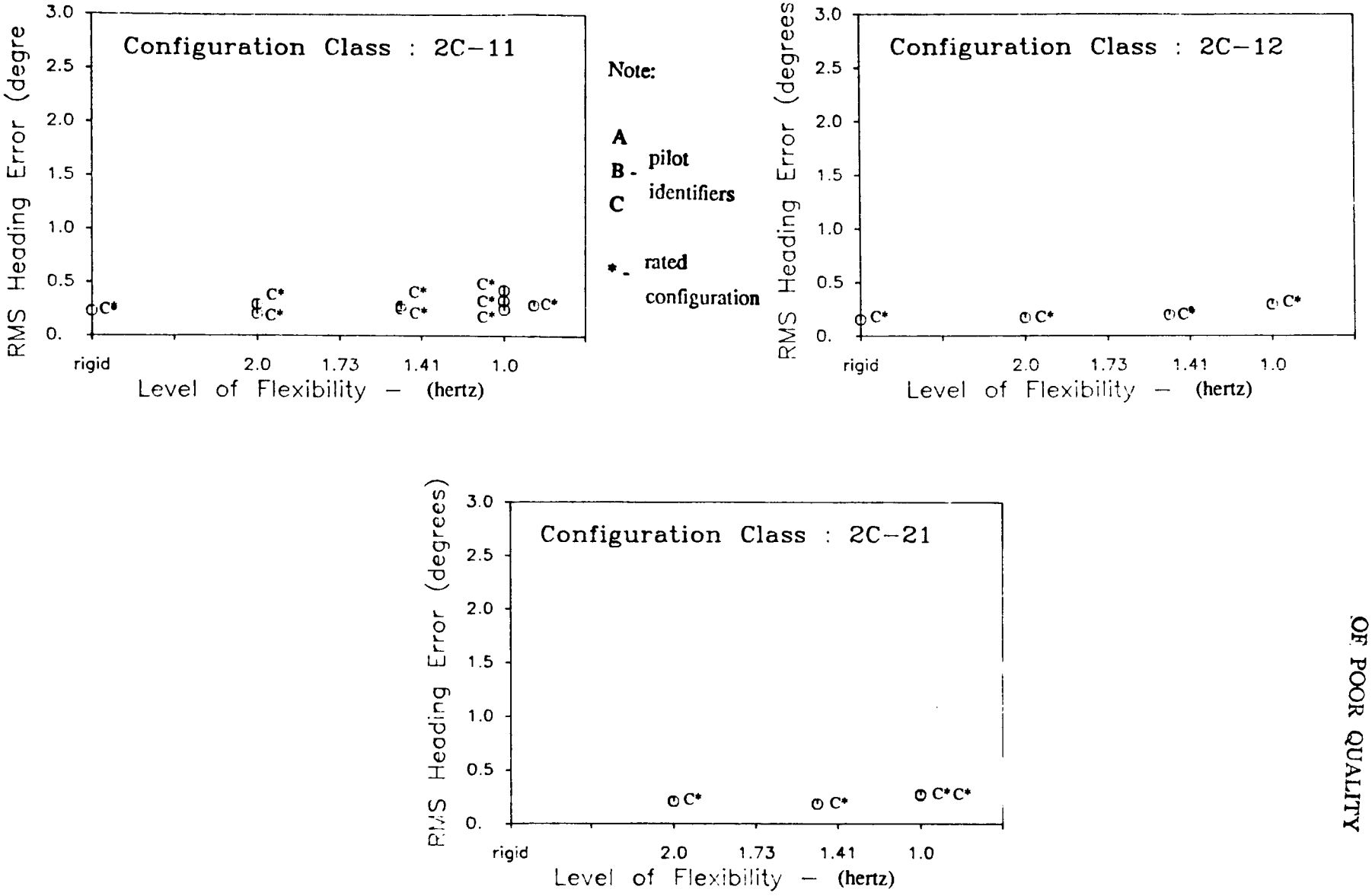

Symmetric Mode Frequency - varied Antisymmetric Mode Frequency - 2.0 Hz

Figure 20d - RMS Roll and Heading Tracking Errors (degrees)

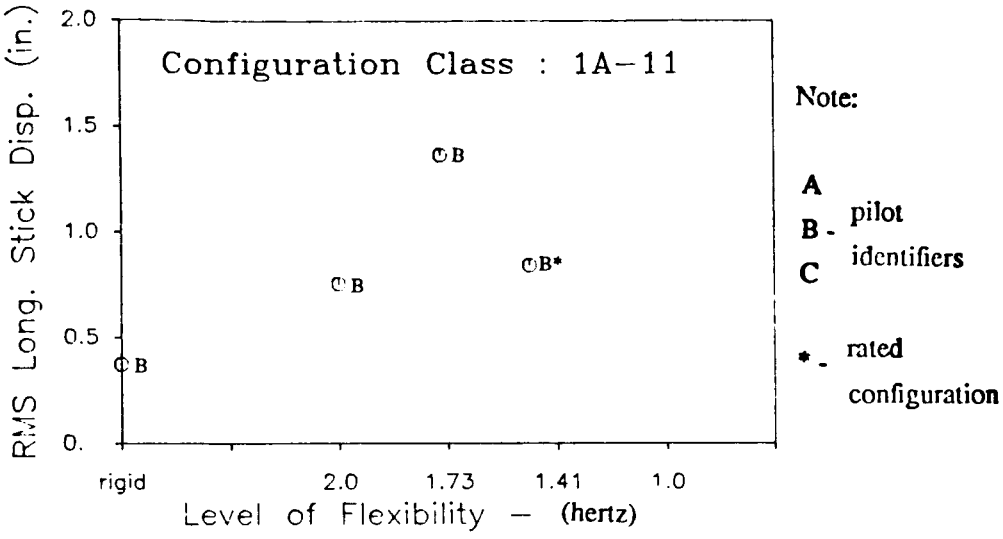

Note:

A
B - pilot identifiers
C

* - rated configuration

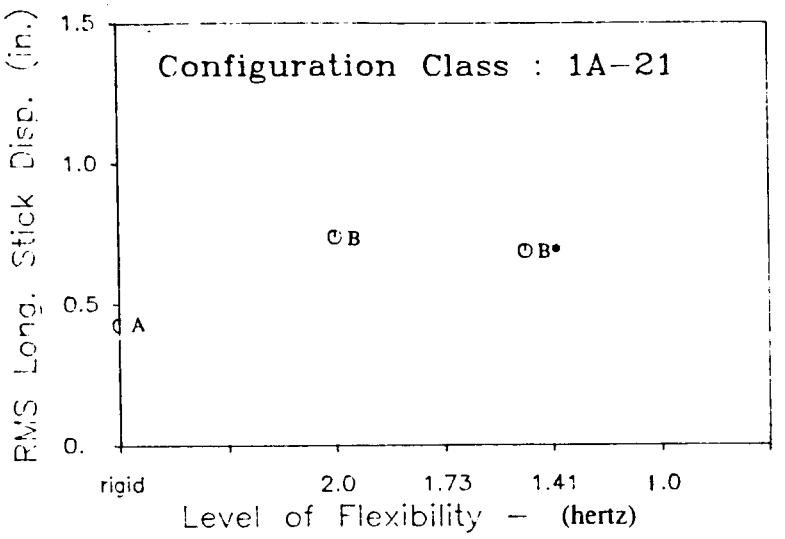

Symmetric Mode Frequency - varied

Antisymmetric Mode Frequency - 2.0 Hz

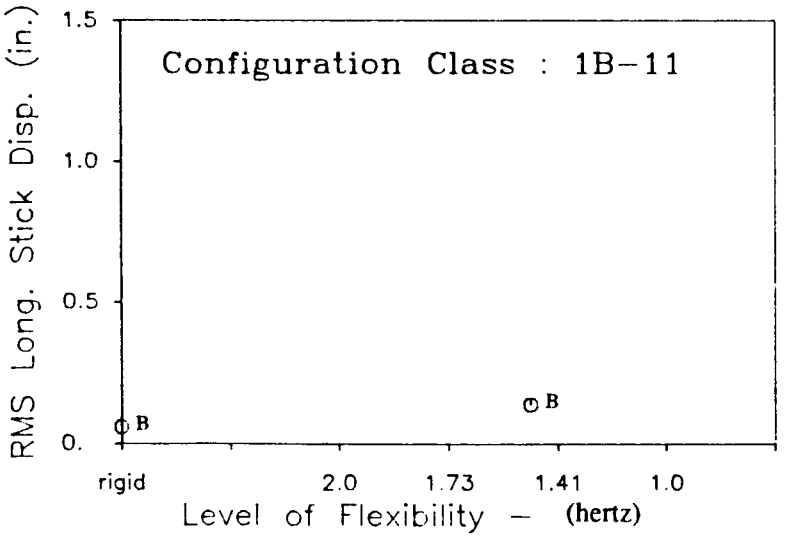

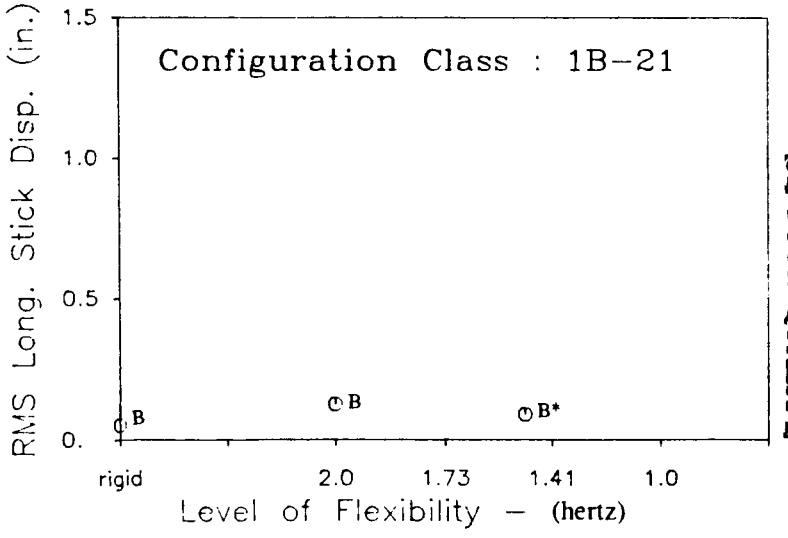

Symmetric Mode Frequency - 2.0 Hz

Antisymmetric Mode Frequency - varied

Figure 21a - Longitudinal Stick Displacements (inches)

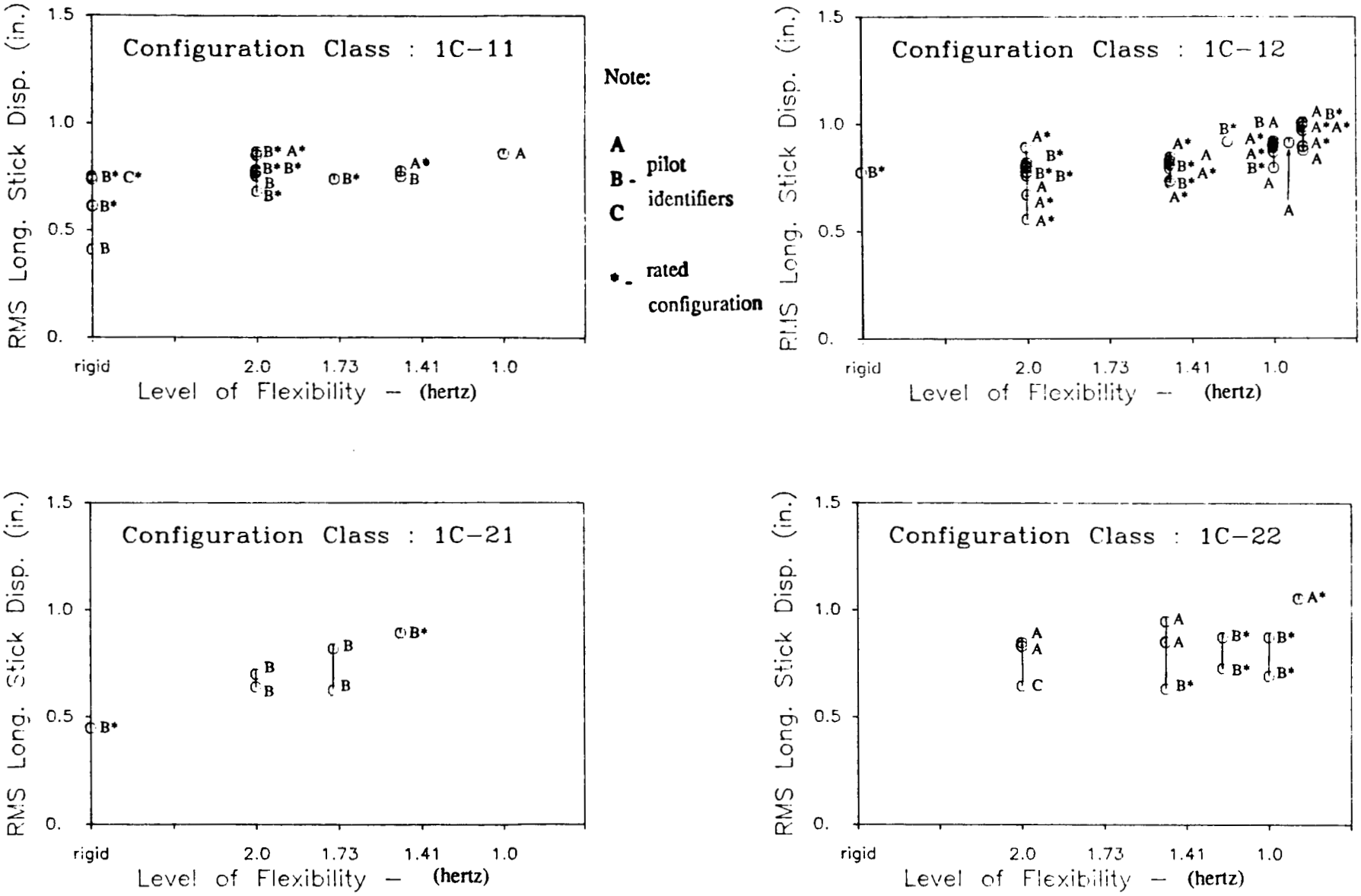

Symmetric Mode Frequency - varied Antisymmetric Mode Frequency - 2.0 Hz

Figure 21b - Longitudinal Stick Displacements (inches)

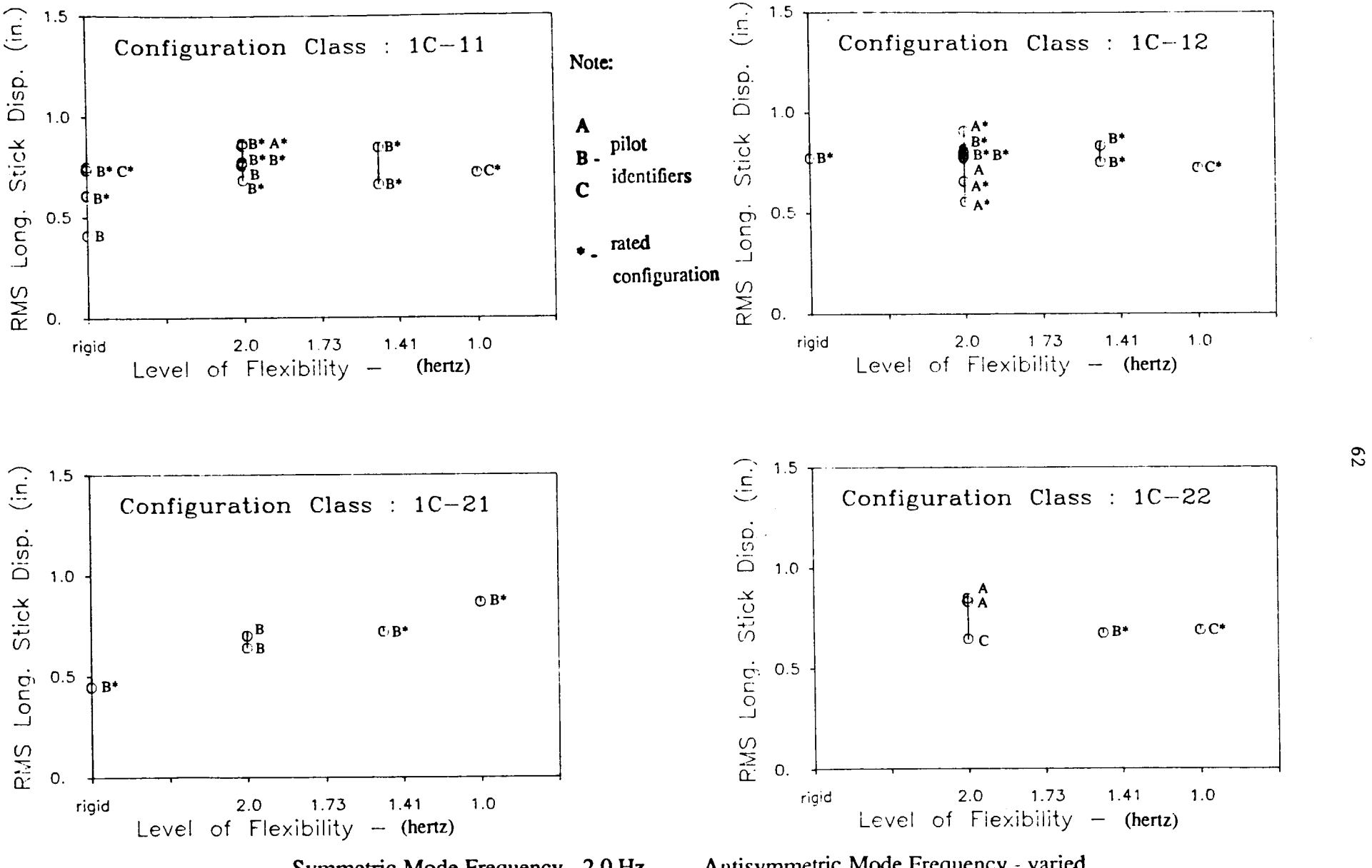

Symmetric Mode Frequency - 2.0 Hz Antisymmetric Mode Frequency - varied

Figure 21c - Longitudinal Stick Displacements (inches)

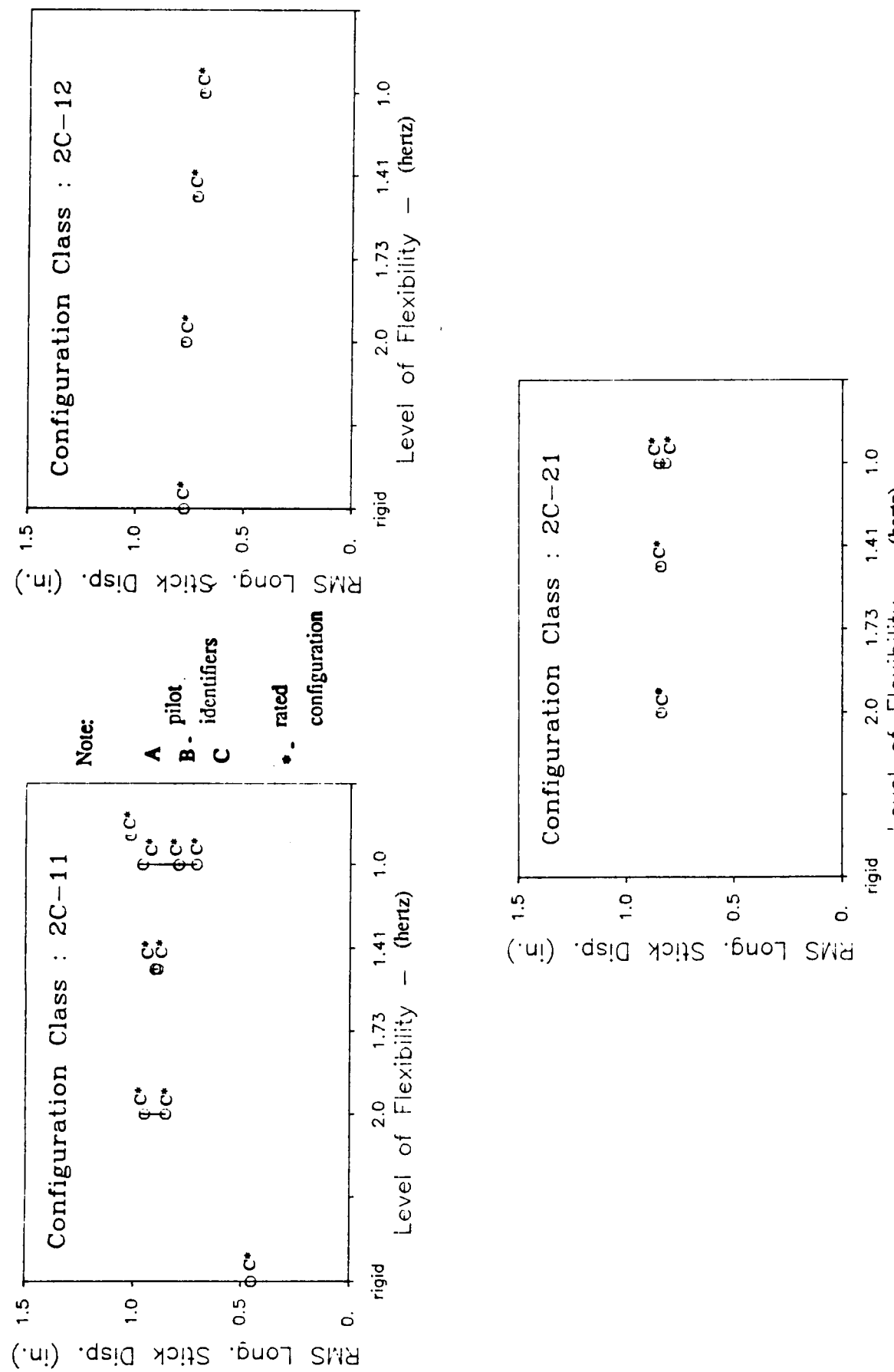

Symmetric Mode Frequency - varied Antisymmetric Mode Frequency - 2.0 Hz

Figure 21d - Longitudinal Stick Displacements (inches)

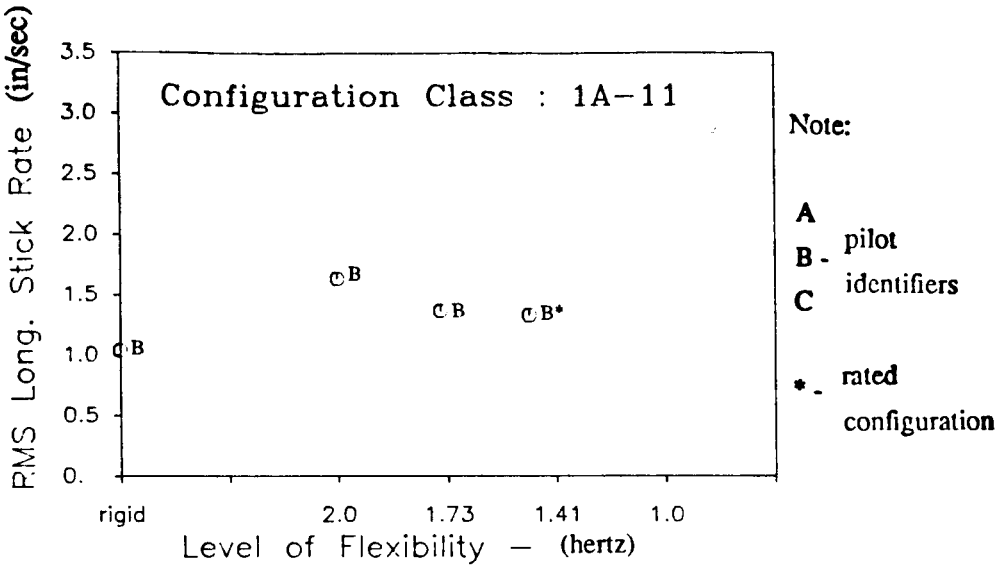

Note:

A
B - pilot identifiers
C

* - rated configuration

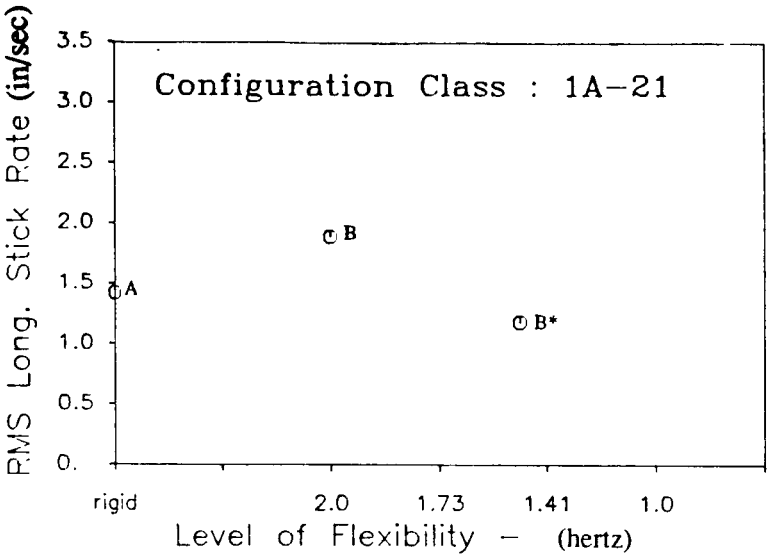

Symmetric Mode Frequency - varied

Antisymmetric Mode Frequency - 2.0 Hz

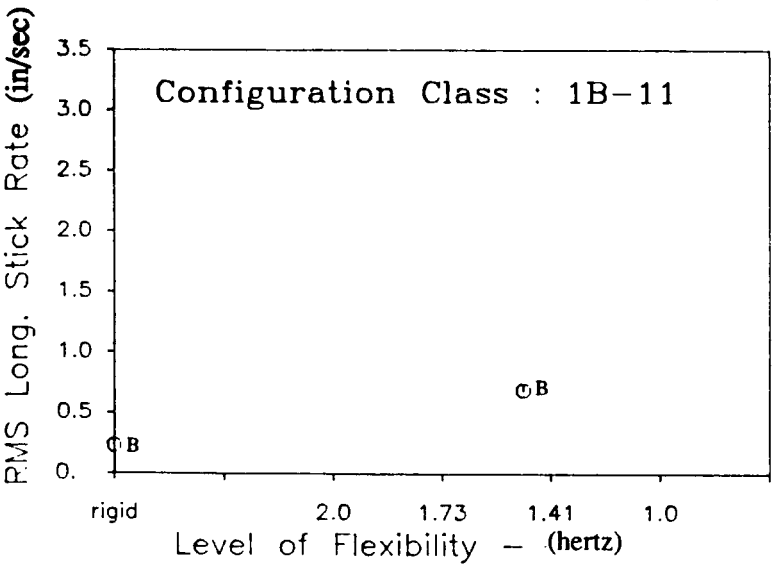

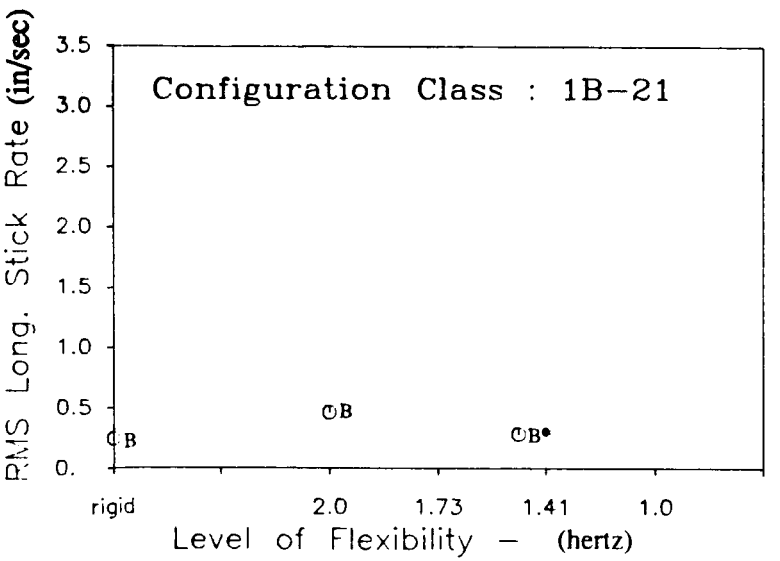

Symmetric Mode Frequency - 2.0 Hz

Antisymmetric Mode Frequency - varied

Figure 22a - RMS Longitudinal Stick Rates (inches/second)

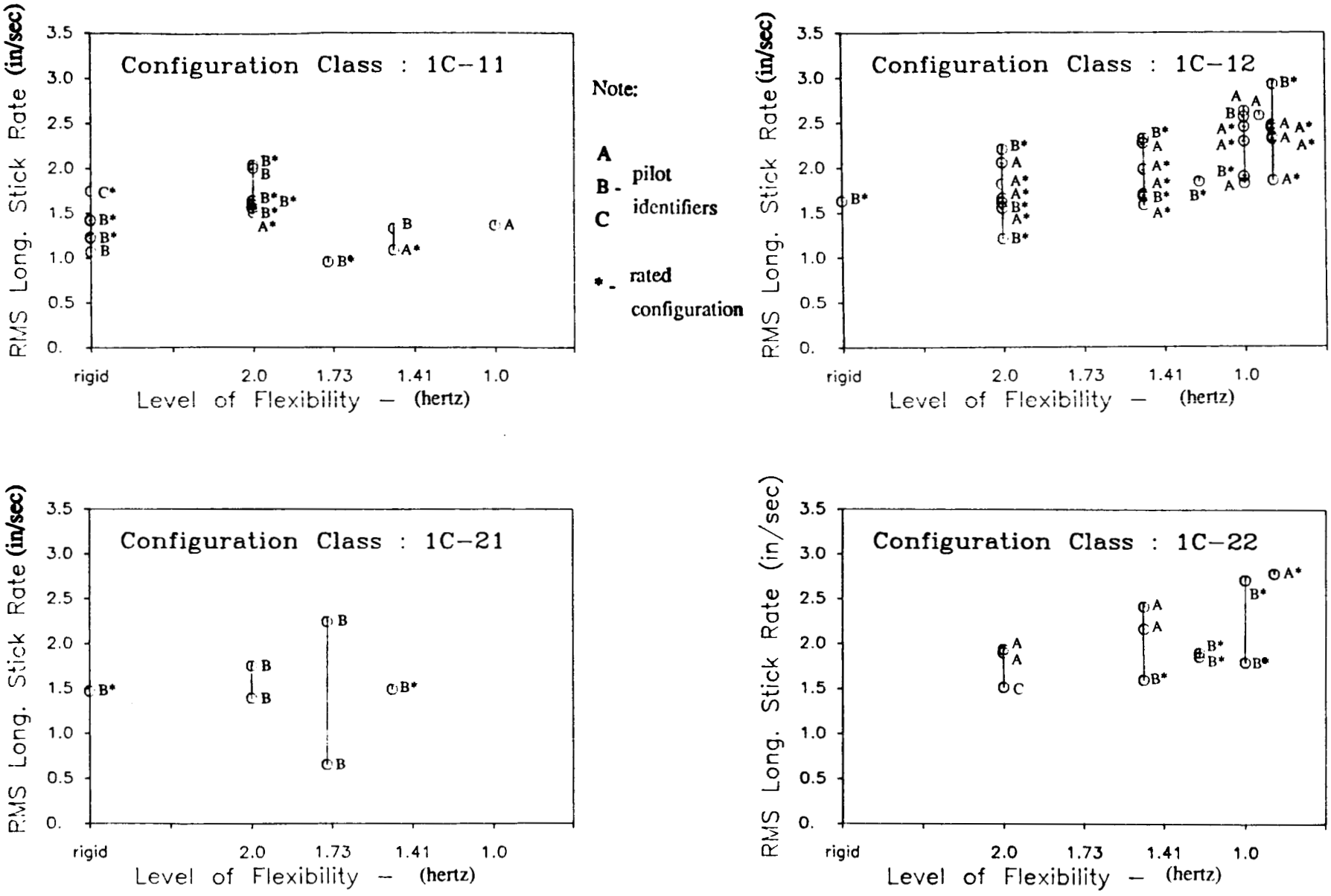

Symmetric Mode Frequency - varied Antisymmetric Mode Frequency - 2.0 Hz

Figure 22b - RMS Longitudinal Stick Rates (inches/second)

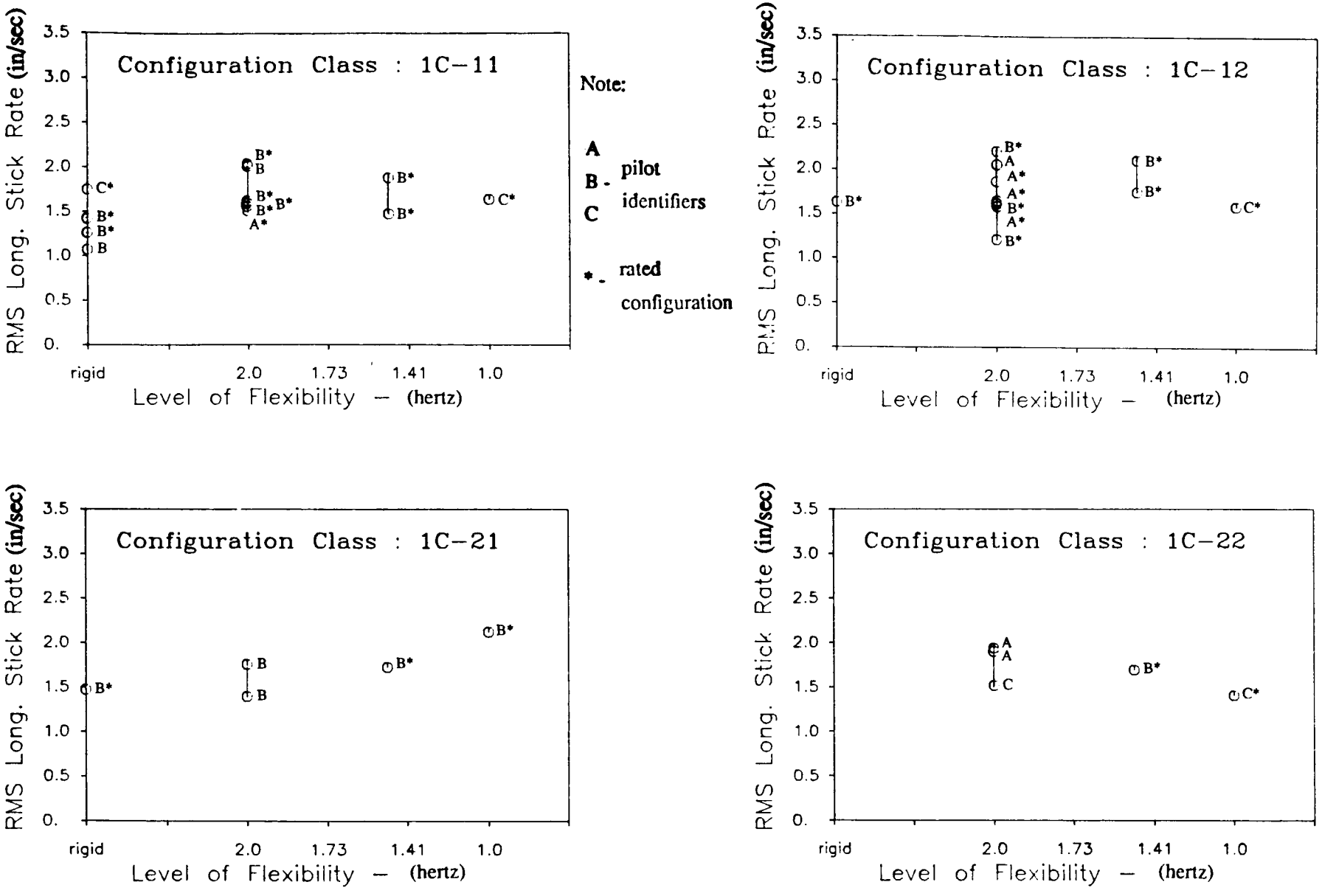

Symmetric Mode Frequency - 2.0 Hz Antisymmetric Mode Frequency - varied

Figure 22c - RMS Longitudinal Stick Rates (inches/second)

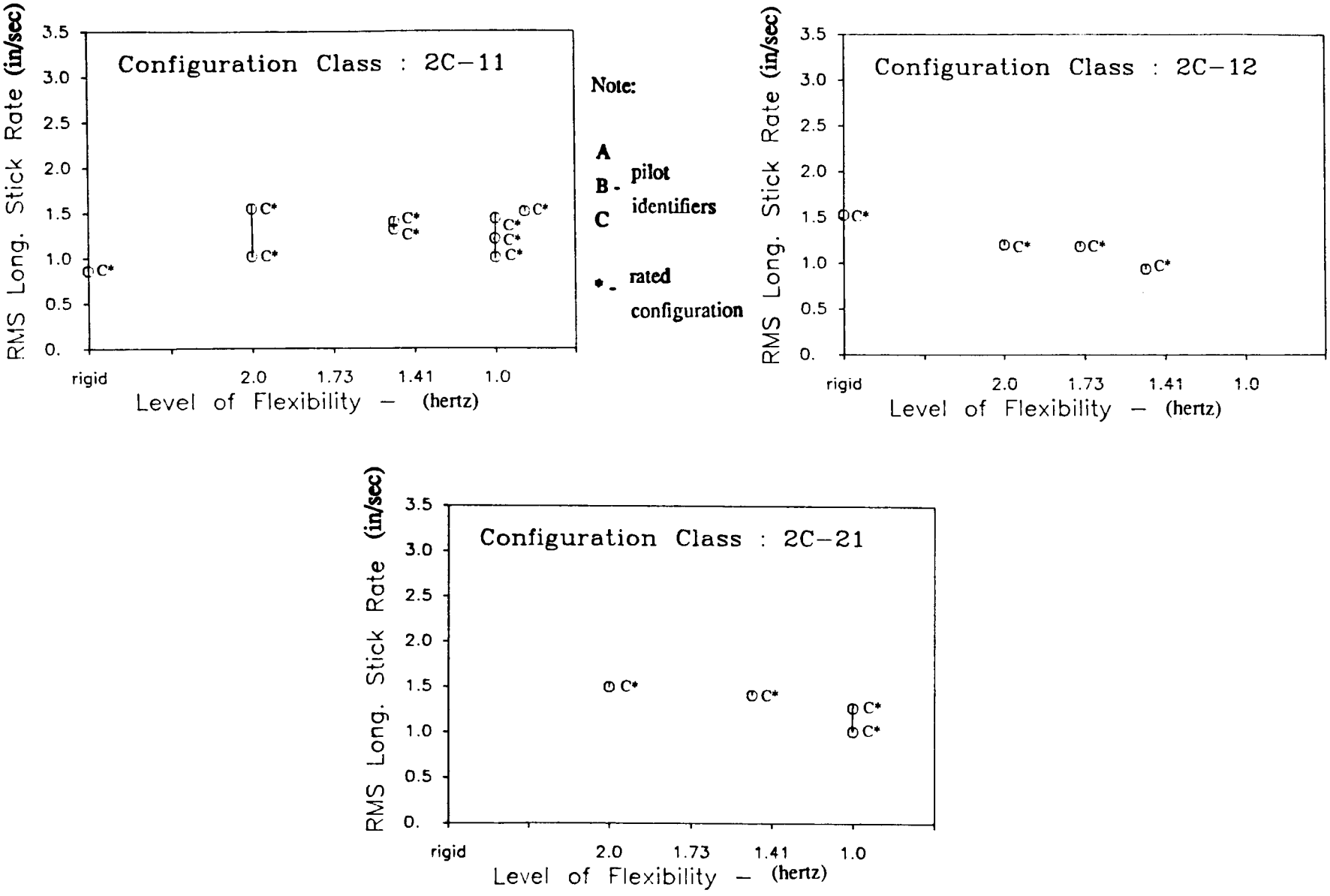

Symmetric Mode Frequency - varied Antisymmetric Mode Frequency - 2.0 Hz

Figure 22d - RMS Longitudinal Stick Rates (inches/second)

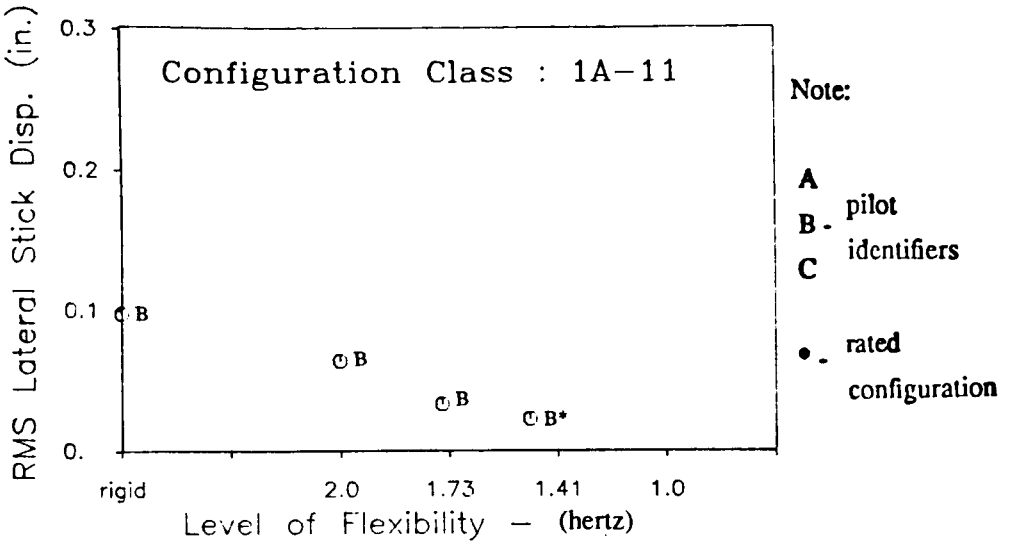

Note:

A
B - pilot identifiers
C

• - rated configuration

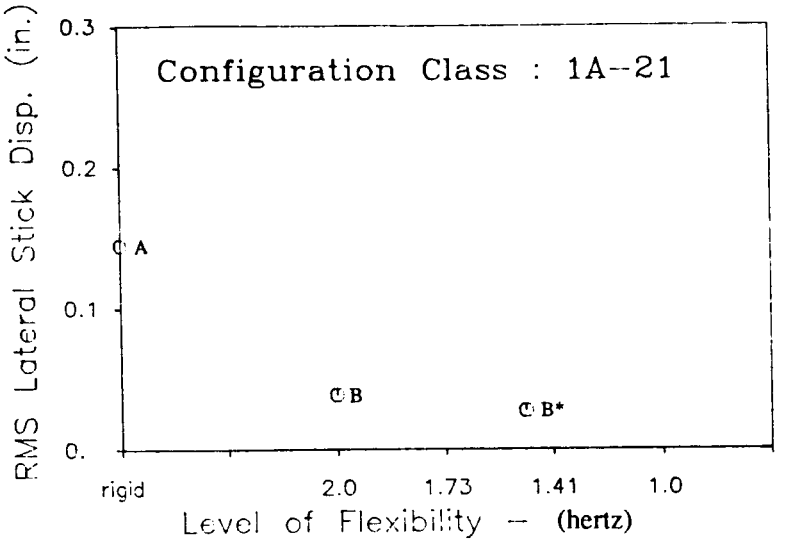

Symmetric Mode Frequency - varied Antisymmetric Mode Frequency - 2.0 Hz

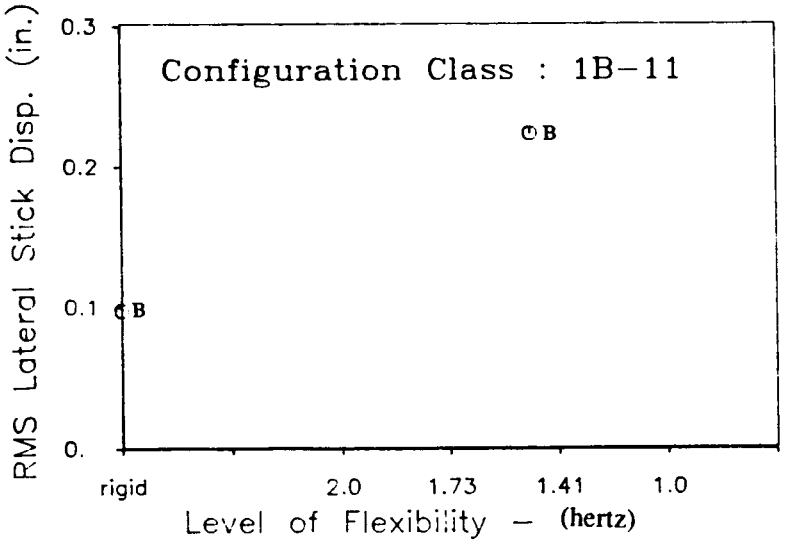

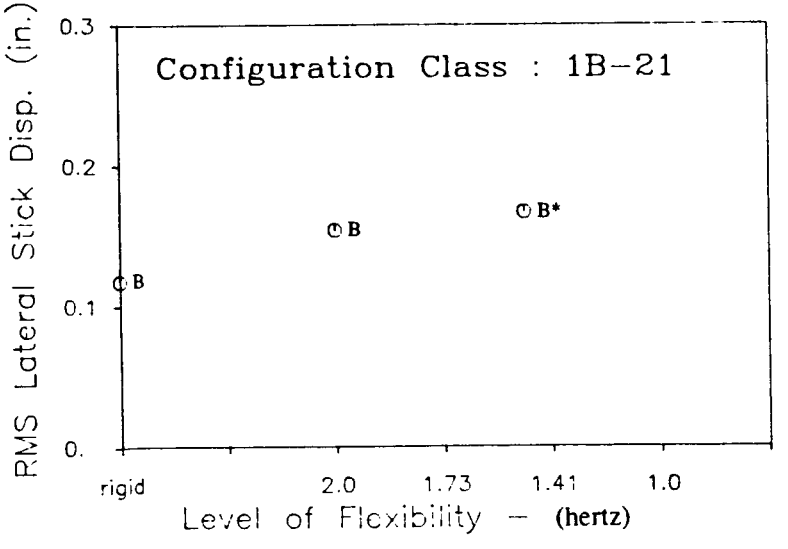

Symmetric Mode Frequency - 2.0 Hz Antisymmetric Mode Frequency - varied

Figure 23a - RMS Lateral Stick Displacements (inches)

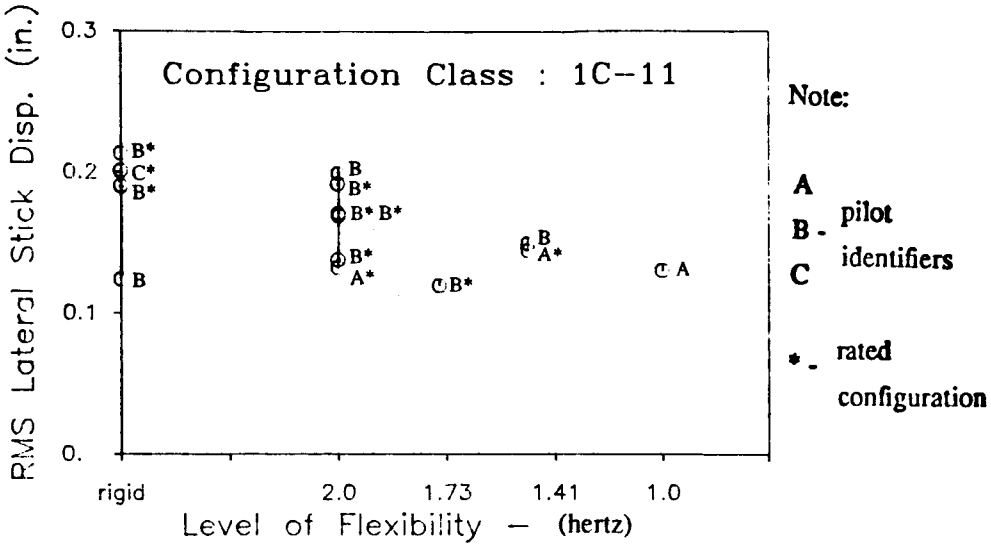

Note:

A
B - pilot
C identifiers

* - rated configuration

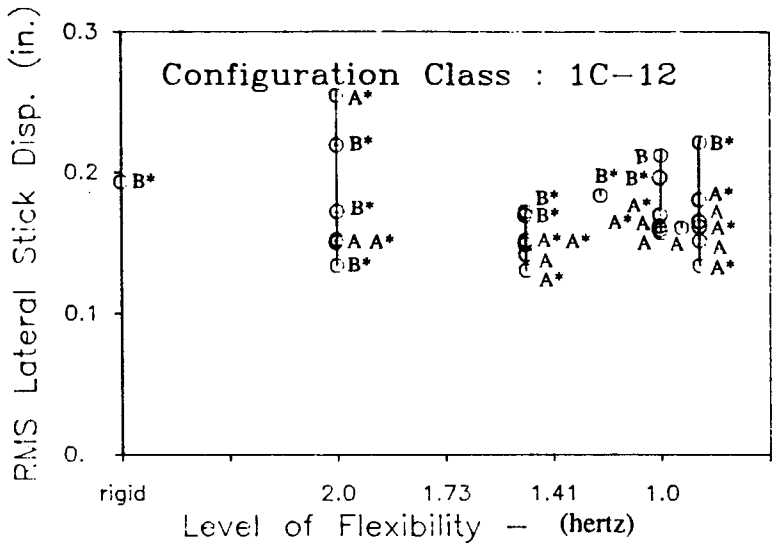

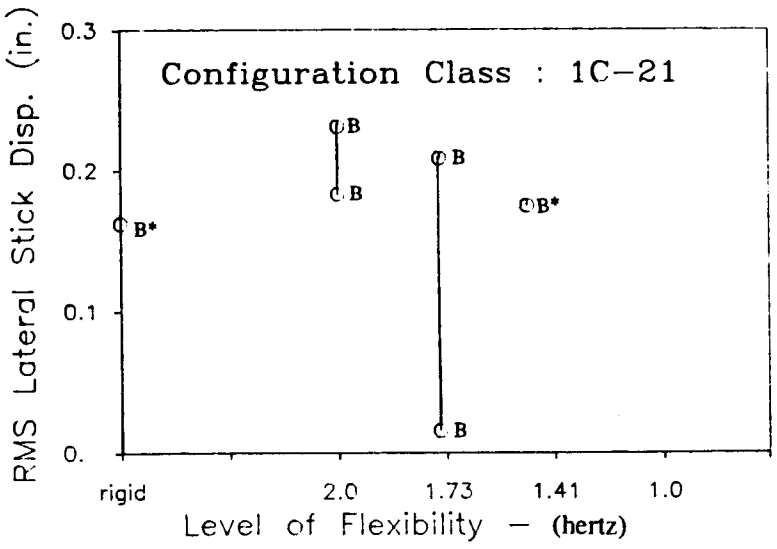

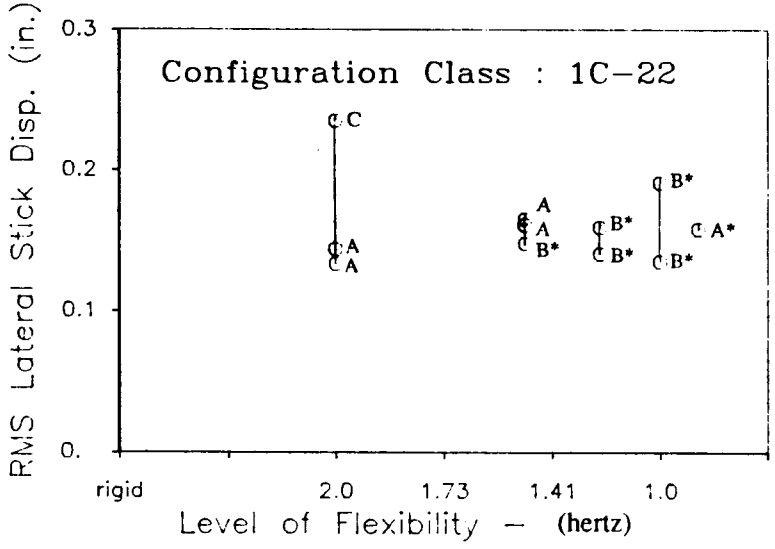

Symmetric Mode Frequency - varied Antisymmetric Mode Frequency - 2.0 Hz

Figure 23b - RMS Lateral Stick Displacements (inches)

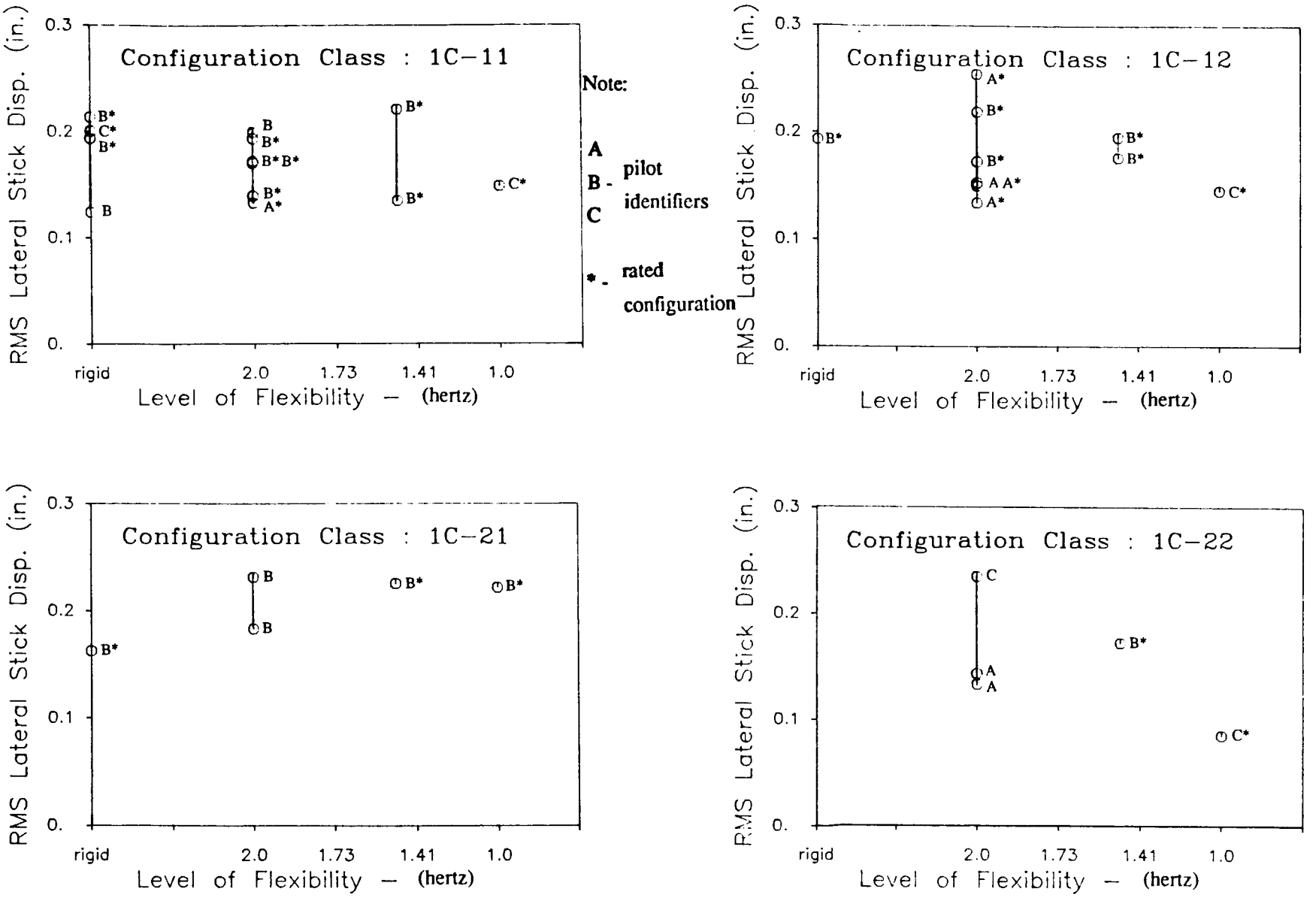

Symmetric Mode Frequency - 2.0 Hz Antisymmetric Mode Frequency - varied

Figure 23c - RMS Lateral Stick Displacements (inches)

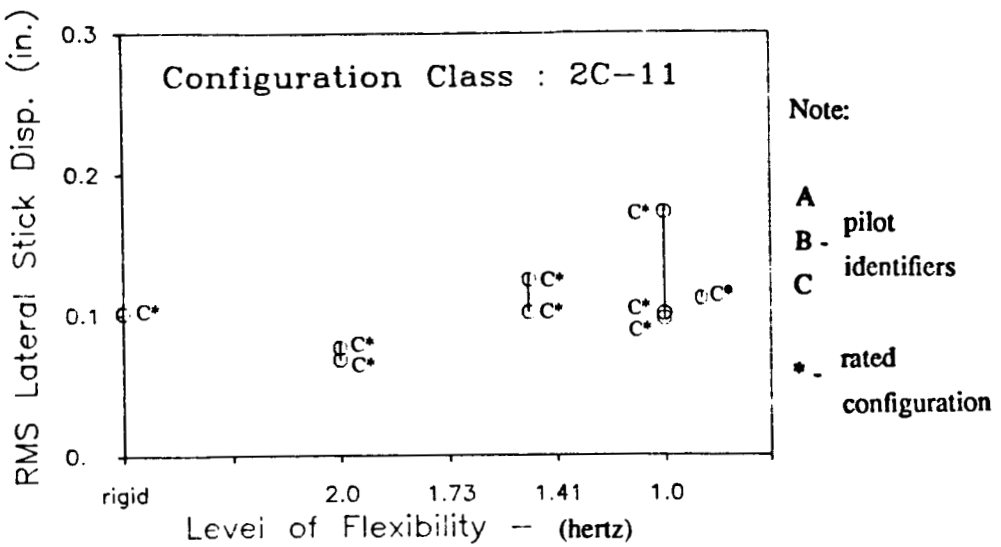

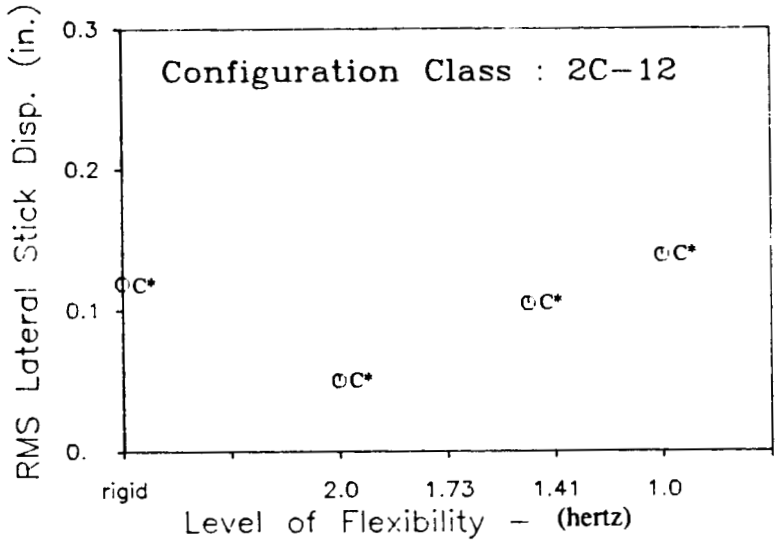

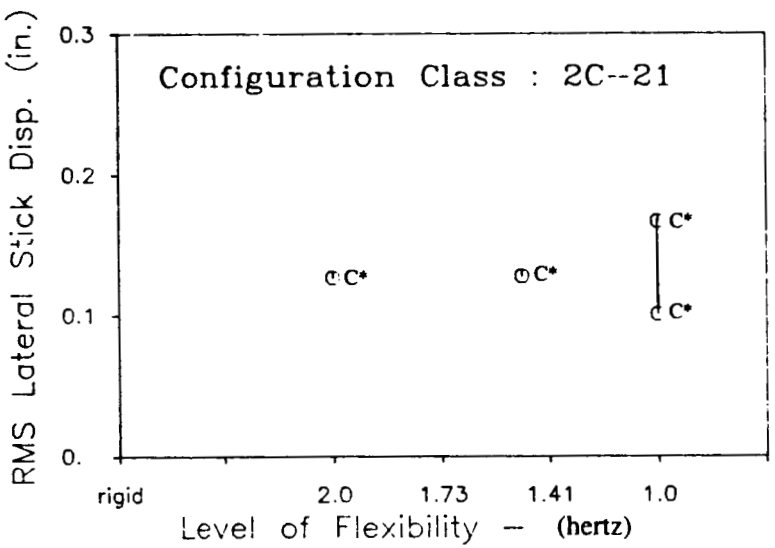

Symmetric Mode Frequency - varied Antisymmetric Mode Frequency - 2.0 Hz

Figure 23d - RMS Lateral Stick Displacements (inches)

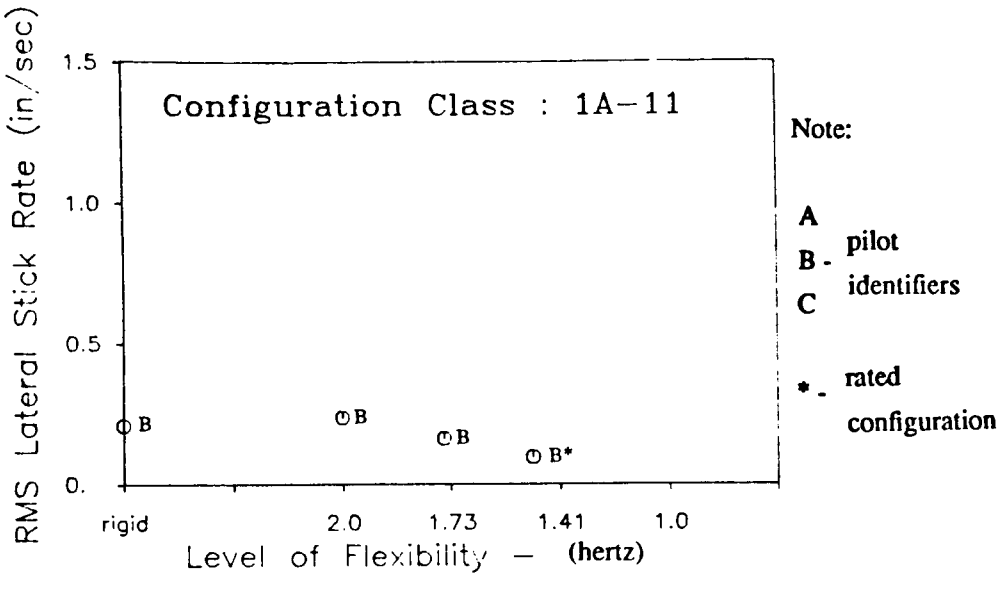

Note:

A
B - pilot identifiers
C

* - rated configuration

Symmetric Mode Frequency - varied

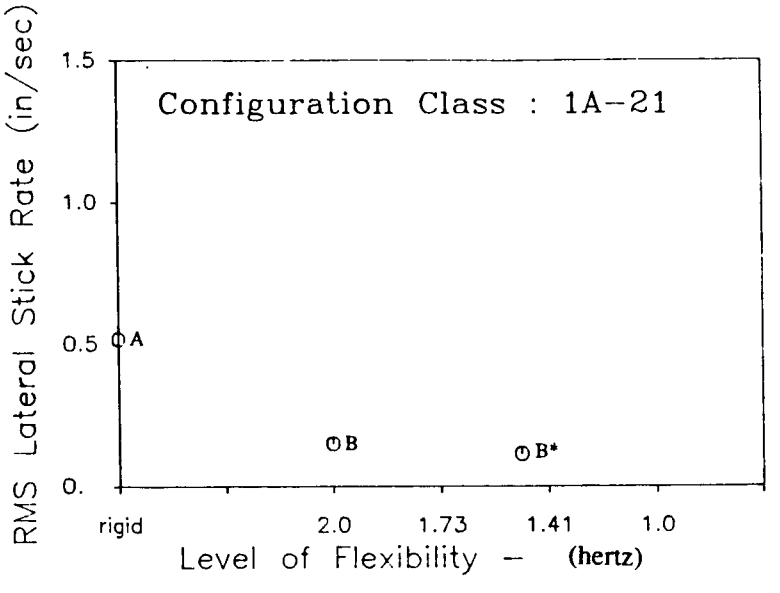

Antisymmetric Mode Frequency - 2.0 Hz

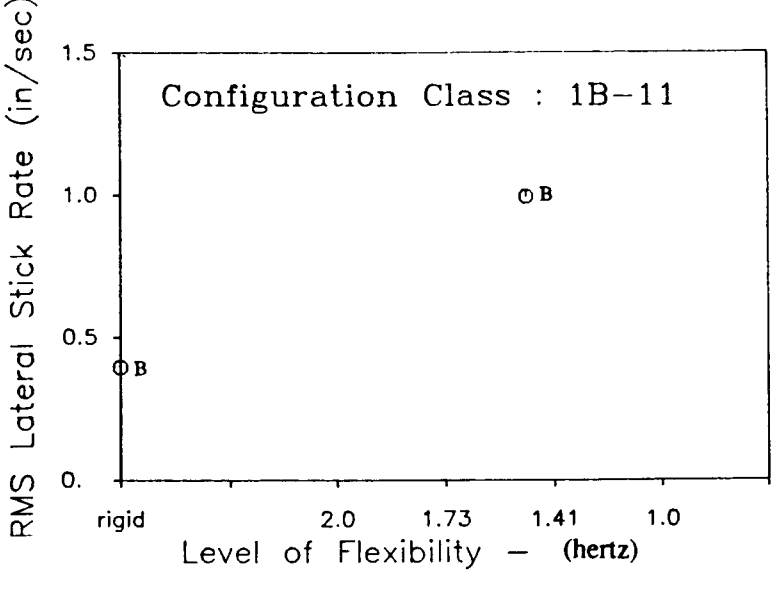

Symmetric Mode Frequency - 2.0 Hz

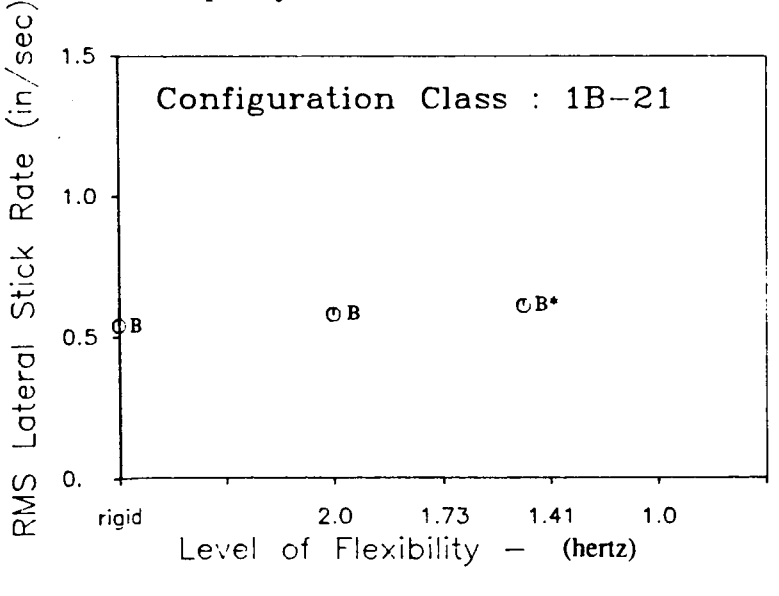

Antisymmetric Mode Frequency - varied

Figure 24a - RMS Lateral Stick Rates (inches/second)

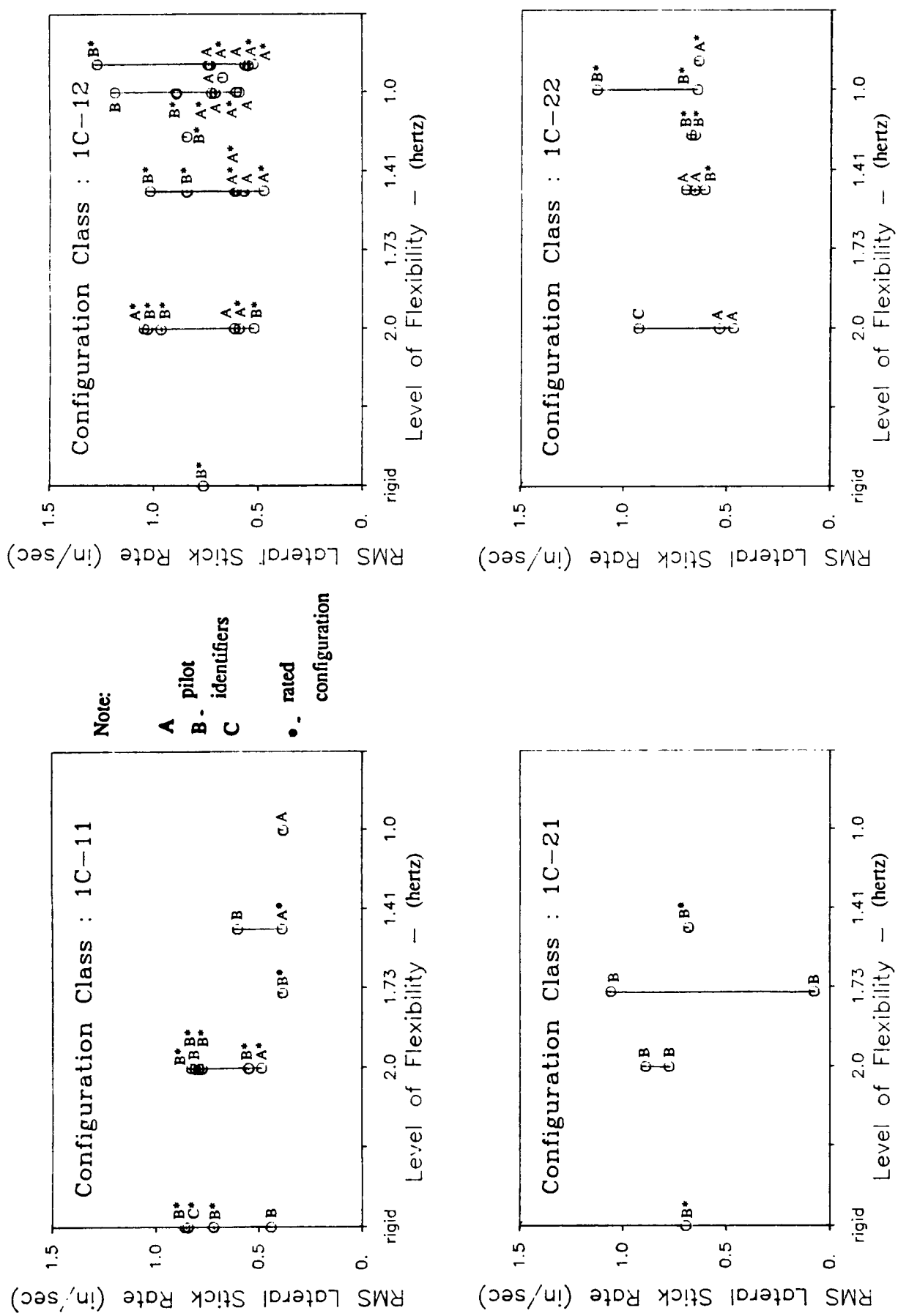

Figure 24b - RMS Lateral Stick Rates (inches/second)

Symmetric Mode Frequency - varied Antisymmetric Mode Frequency - 2.0 Hz

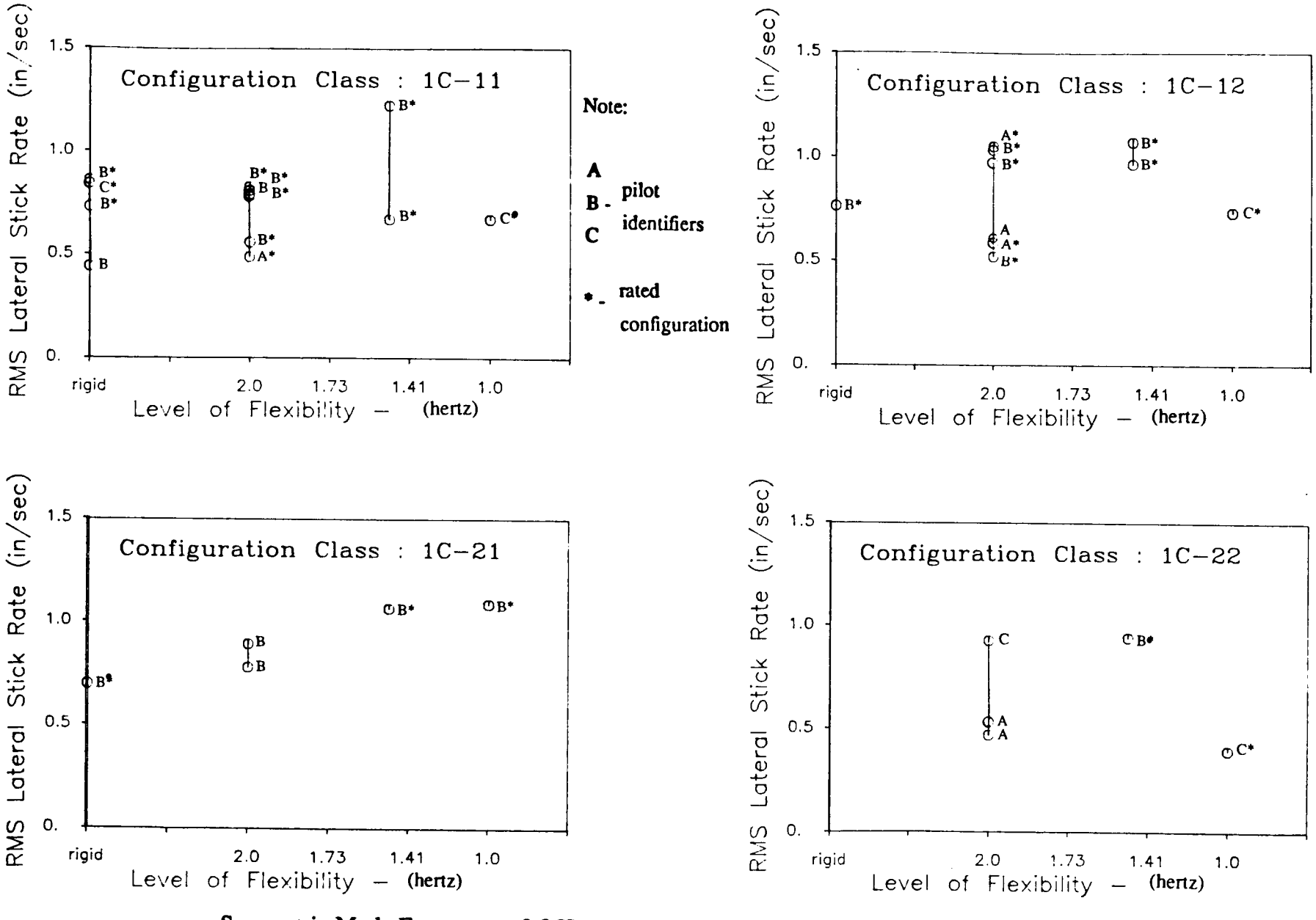

Symmetric Mode Frequency - 2.0 Hz Antisymmetric Mode Frequency - varied

Figure 24c - RMS Lateral Stick Rates (inches/second)

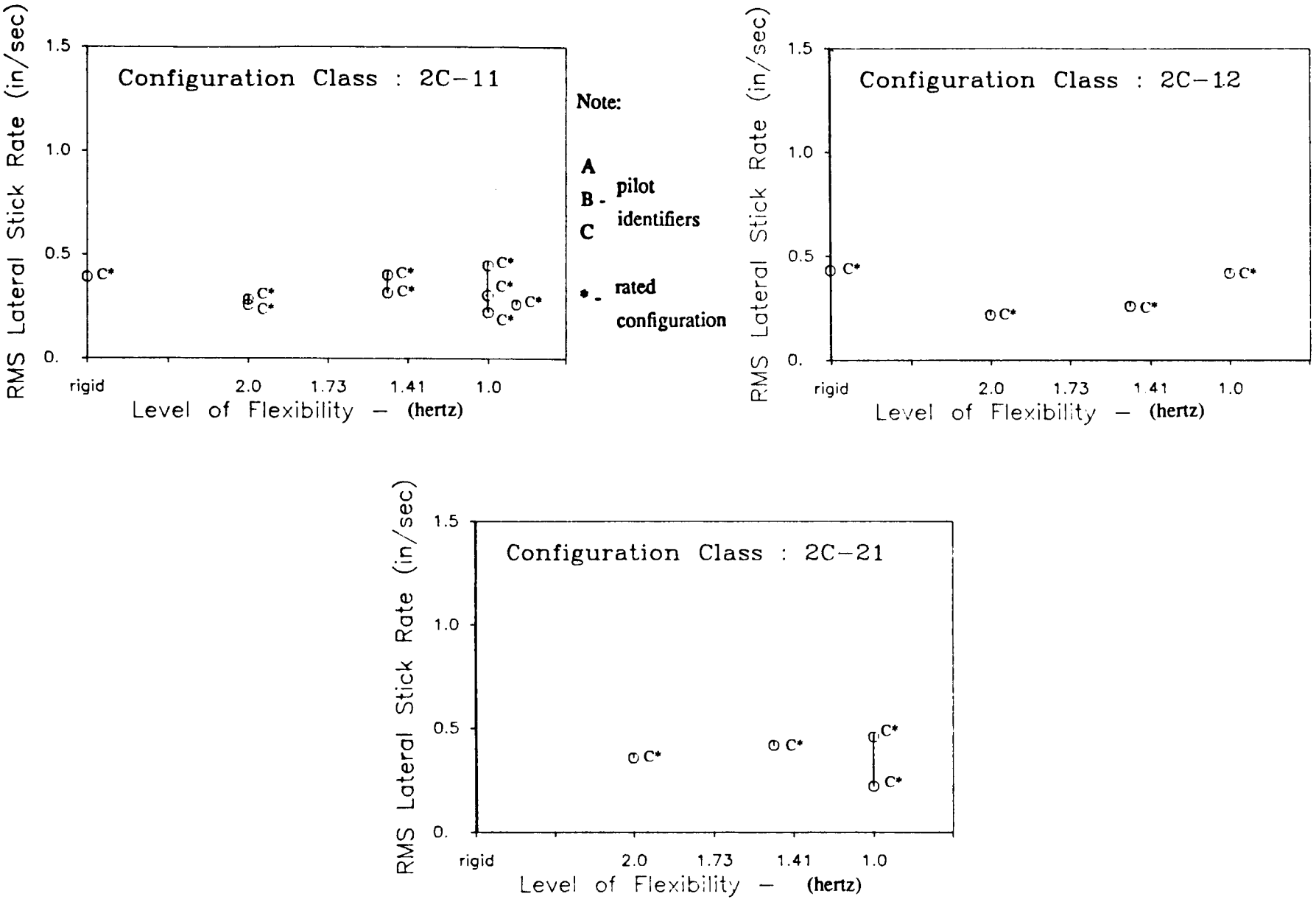

Symmetric Mode Frequency - varied Antisymmetric Mode Frequency - 2.0 Hz

Figure 24d - RMS Lateral Stick Rates (inches/second)

Note:

A
B - pilot
C identifiers

• - rated configuration

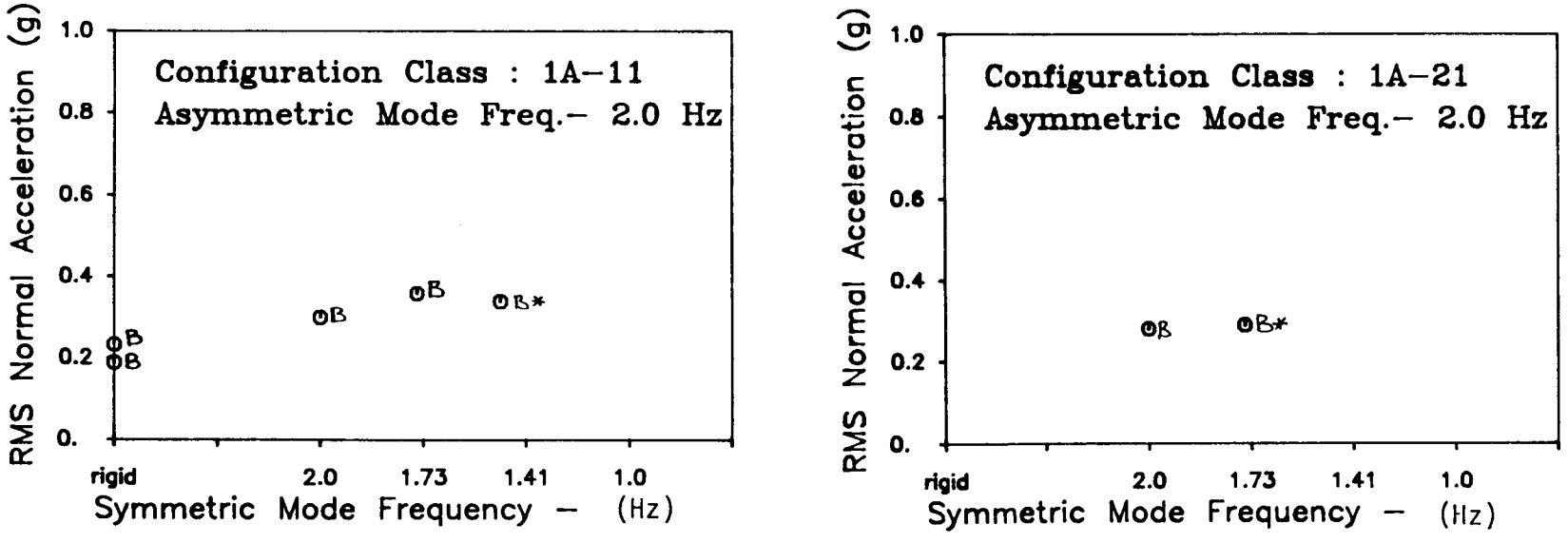

Figure 25a - RMS Normal Accelerations (g's)

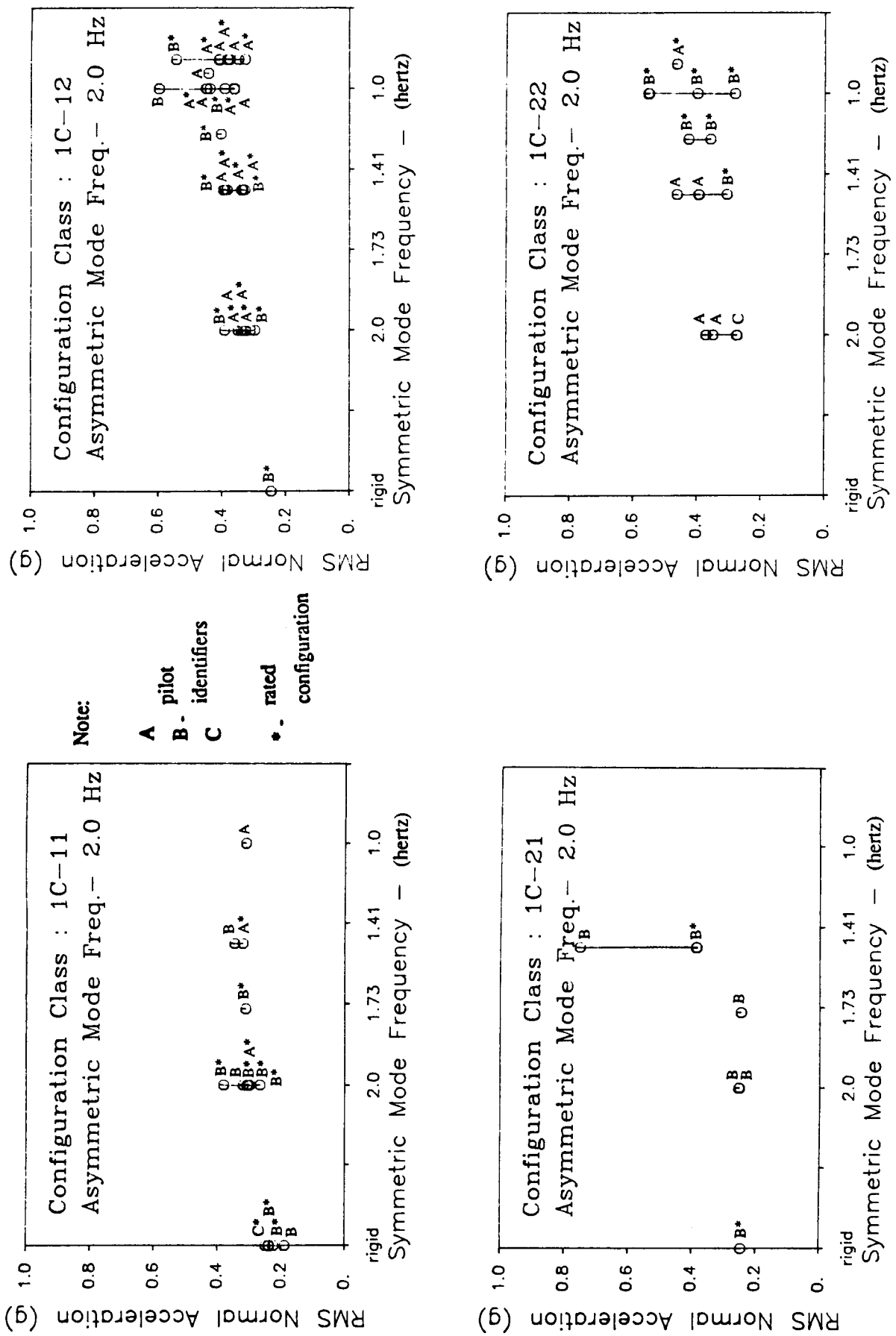

Figure 25b - RMS Normal Accelerations (g's)

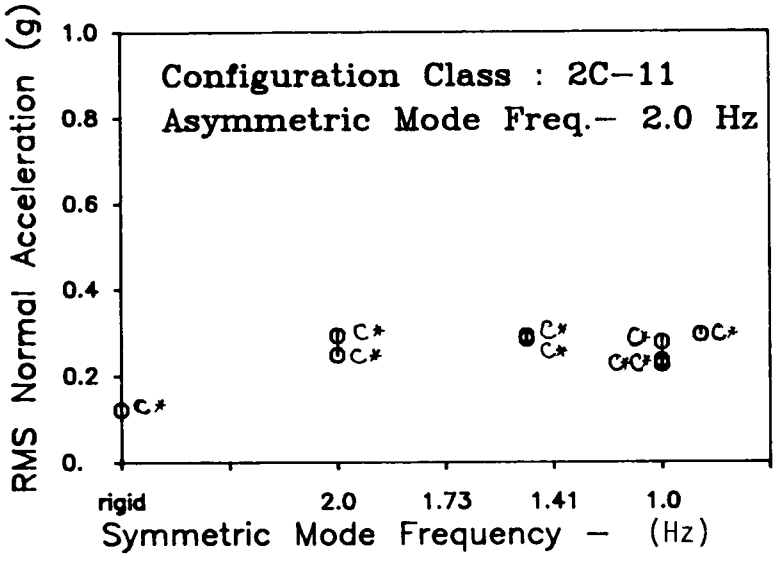

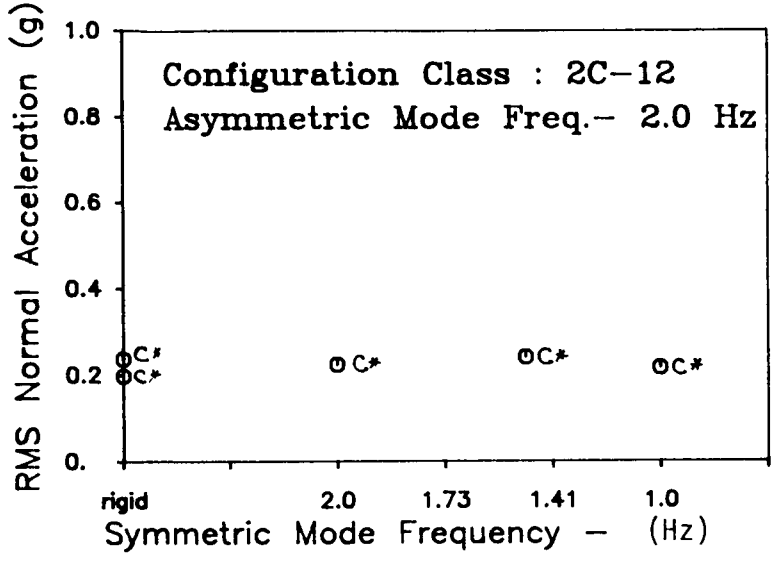

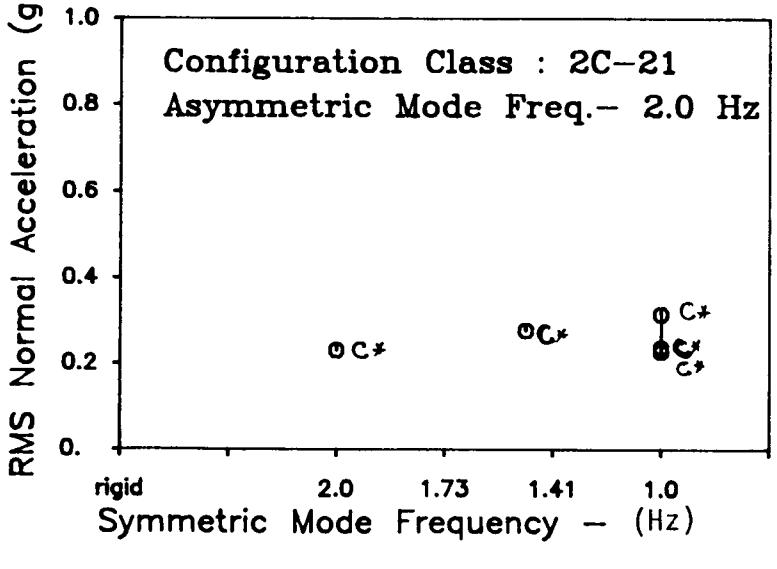

Note:

A
B - pilot
C identifiers

* - rated configuration

Figure 25c - RMS Normal Accelerations (g's)

Note:

A
B - pilot
C identifiers

* - rated configuration

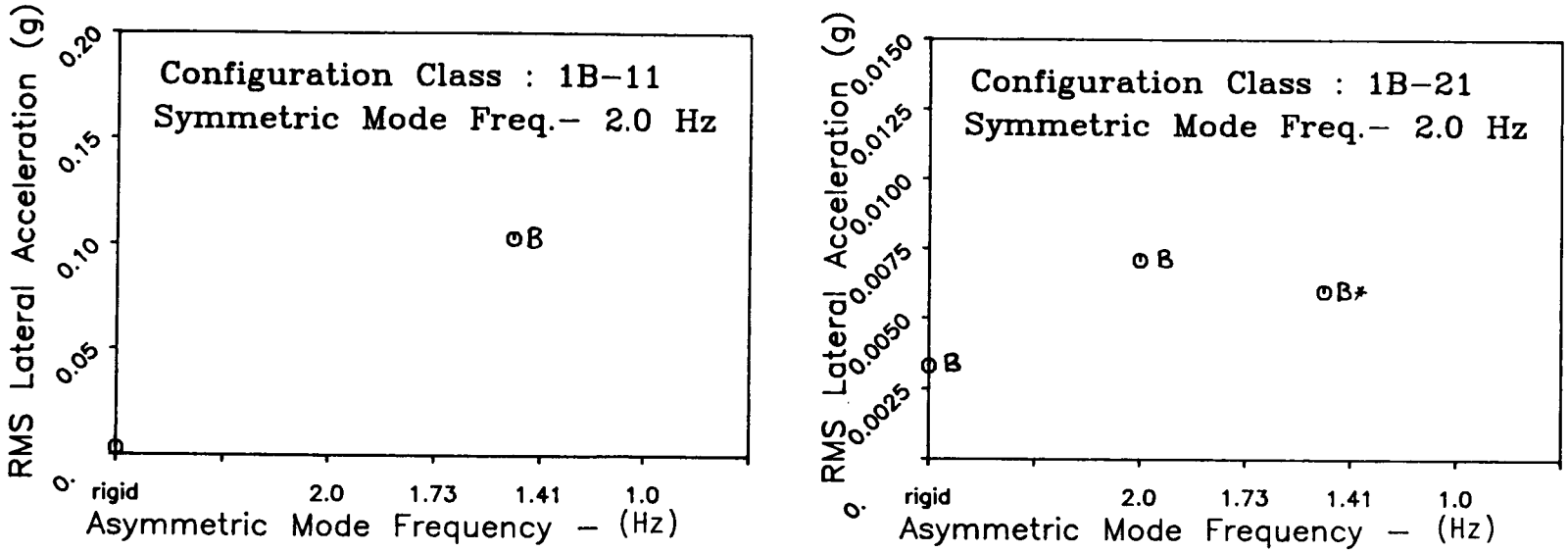

Figure 26a - RMS Lateral Accelerations (g's)

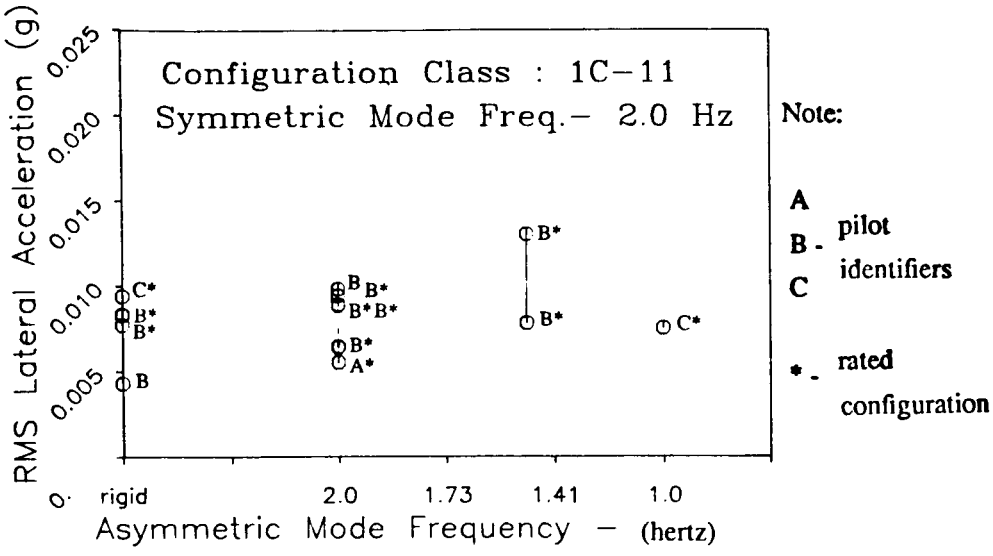

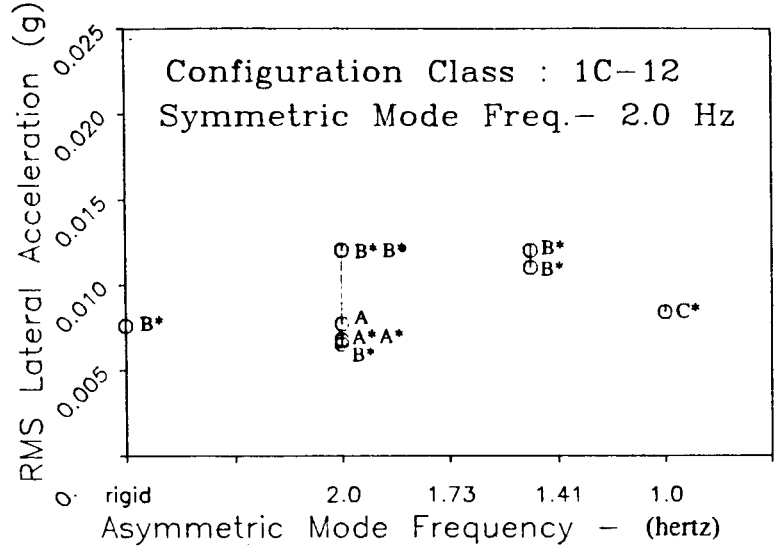

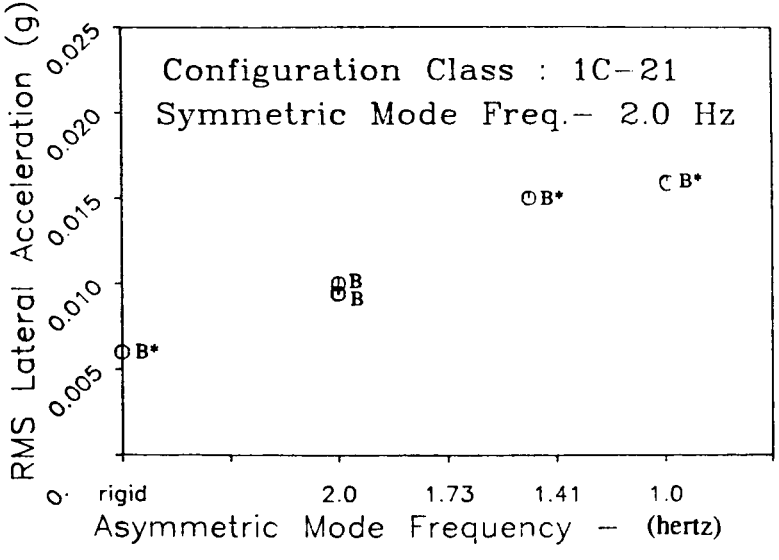

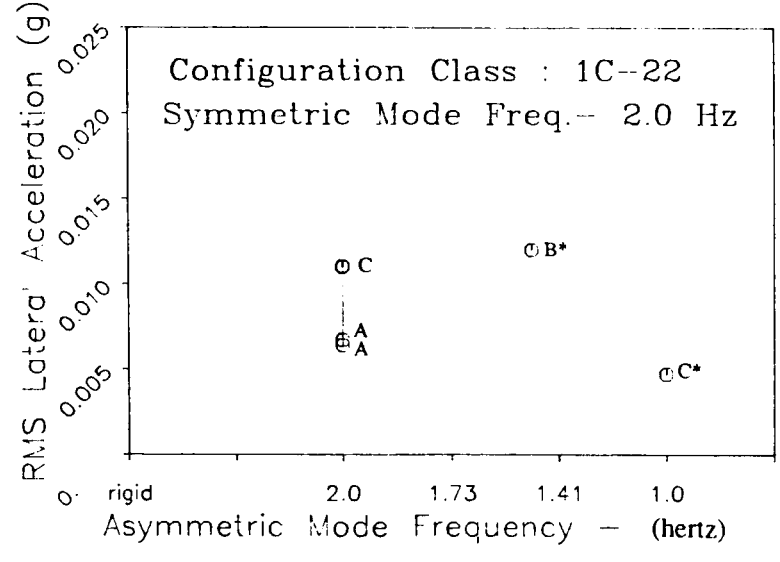

Figure 26b - RMS Lateral Accelerations (g's)

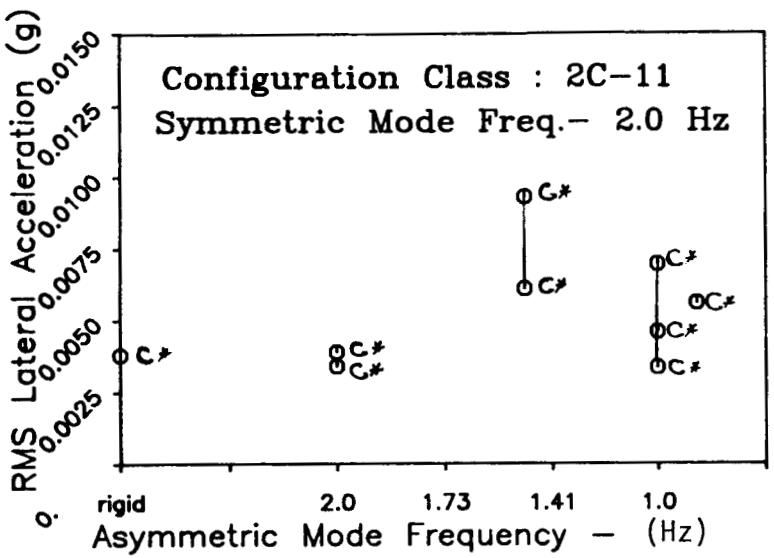

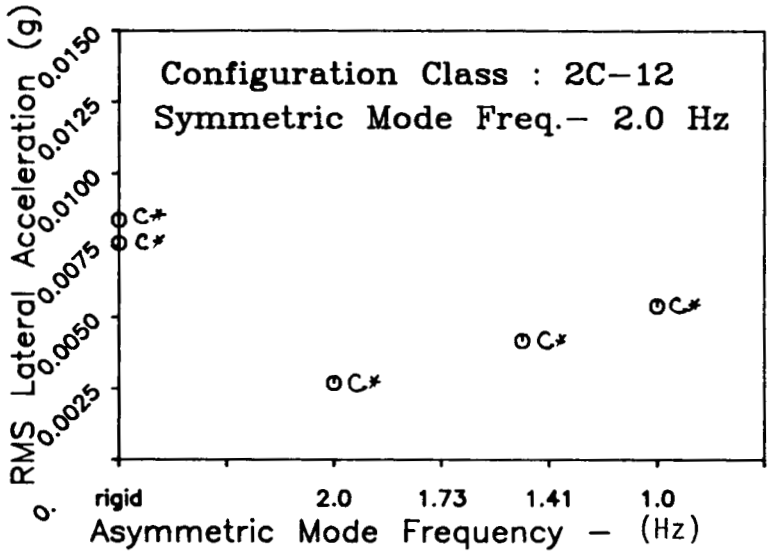

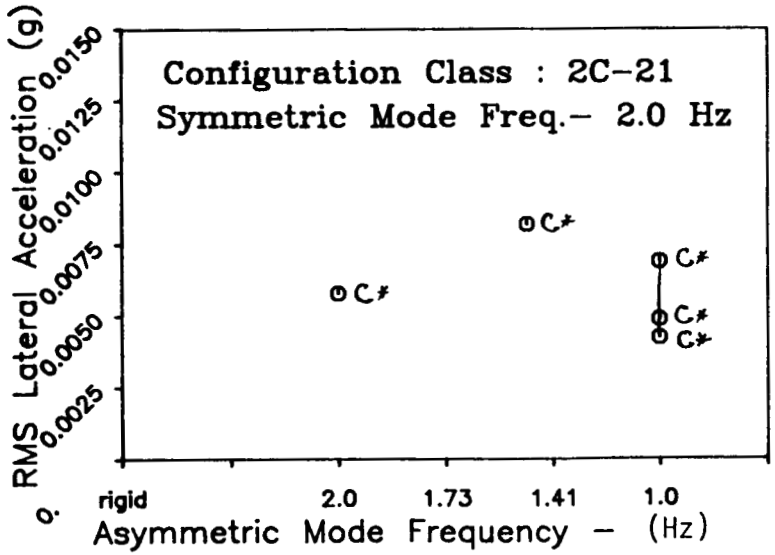

Note:

A
B - pilot
C identifiers

* - rated configuration

Figure 26c - RMS Lateral Accelerations (g's)

Discussion of Results

Some comparisons of the graphical results for pilot ratings and RMS responses will be considered now. In particular, the results which correspond to the configuration classes associated with the dual-axis pitch/roll pursuit tracking task in which the symmetric mode is changed to represent variations in structural flexibility will be reviewed. The case number designations associated with these configuration classes are 1C-11, 1C-12, 1C-21, and 1C-22. Class 1C-11 corresponds to motion enabled with flexible display dynamics, class 1C-12 corresponds to motion enabled but with rigid display dynamics, configuration class 1C-21 corresponds to motion disabled with flexible display dynamics, and class 1C-22 corresponds to motion disabled with rigid display dynamics.

Figure 16 depicts the pilot rating results for the specified configuration classes. First look at the variations in pilot rating for changes in structural flexibility. A clear trend toward increased Cooper-Harper pilot rating (degraded handling qualities) with increased flexibility is evident for configuration classes 1C-11 and 1C-21, those classes with the flexible display dynamics. However, the configuration classes which utilize the rigid display (1C-12 and 1C-22), do not exhibit this behavior. In fact, the data for classes 1C-12 and 1C-22 seem to indicate a minimum (best) handling qualities rating for an intermediate level of flexibility ($\omega \approx$ 1.4 Hertz). These trends are indicated regardless of whether motion was used or not. So motion appears to have little effect on these pilot ratings, while display dynamics significantly altered the pilot's opinion of the handling qualities.

Now consider Figure 19b which depicts the RMS pitch tracking errors. The variations in tracking errors with changes in structural flexibility indicate the same trends as the pilot ratings. Also, these trends are reflected in the roll tracking errors shown in Figure 20b. The fact that motion seems to have an insignificant effect on tracking performance is believed to be attributable (in part) to the attenuation of the motion commands by the motion logic (discussed later).

Figure 21b depicts the RMS longitudinal stick displacements for the same configuration classes (1C-11, 1C-12, 1C-21, and 1C-22). There appears to be a slight increase in stick

displacements with decreased stiffness for all classes. Also, there appears to be little difference between flexible and rigid display (1C-X1 versus 1C-X2), or between motion and no motion (1C-1X versus 1C-2X).

Figure 22b depicts the RMS longitudinal stick rates for the specified configuration classes. The slight trend toward increased stick rate activity with reduced stiffness is noted with rigid display dynamics, (i.e. in configuration classes 1C-12 and 1C-22). On average, the more flexible configurations (i.e. with symmetric mode frequency below 1.7 Hertz) have RMS stick rates for the rigid display configurations which are clearly higher than those for the flexible display configurations. The filtered rigid display may allow the pilot to be more aggressive and achieve better performance. There is, however, no apparent effect of motion status on longitudinal stick rate.

Figures 23b and 24b depict the RMS lateral stick displacements and displacement rates for the same four configuration classes. Except for a slight reduction in rate with increased flexibility for class 1C-11, these responses do not indicate any significant trend between the amount of lateral stick activity and the degree of structural flexibility, the presence of motion, or the type of display dynamics. Note, however, that structural stiffness for these results is characterized by variations in the symmetric mode frequency which should affect the longitudinal axis more than the lateral axis.

A limited spectral analysis of the pilot stick inputs was also performed. The frequency spectra, or more specifically the power spectral density (PSD) was calculated from the time series data using the Weiner-Khinchine Theorem described in reference 13. Two sets of data will be considered. The first set of vehicle configurations serve to address the changes in the frequency spectra of pilot inputs due to the effects of motion and display dynamics. The second set of vehicle configurations serve to address some relationships between the frequency spectra of pilot inputs and pilot ratings, pilot comments and task performance and the effects of flexibility.

First consider some consequences of motion and display dynamics on pilot inputs. For this purpose four representative vehicle configurations are compared, each with the same dynamics and differing only in motion and display status. Configurations 1C-11-5, 1C-12-3, 1C-21-5, and 1C-22-2 each have the same dynamics; (pitch/roll) tracking task, symmetric mode frequency of 1.5 Hertz, antisymmetric mode frequency of 2.0 Hertz, pitch SCAS pitch-

C-2

rate gain of 2.0, and phugoid augmentation engaged. They differ however in that 1C-11-5 has motion enabled and utilizes the flexible display, 1C-12-3 has motion enabled but utilizes the rigid display, configuration 1C-21-5 has the motion disabled and utilizes the flexible display, and 1C-22-2 has the motion disabled and uses the rigid display dynamics. The simulation runs for each configuration that were used to calculate the PSD's were performed on the same day in consecutive evaluations by the same pilot.

Figure 27 presents the PSD of the longitudinal stick rate for each of the four configurations. Note that for configurations 1C-11-5 (motion) and 1C-21-5 (no motion), those configurations that utilize the flexible display dynamics, spectral peaks occur near the vibration frequency of the symmetric mode (which is approximately the frequency of the associated aeroelastic mode). The other two configurations, with the rigid display dynamics, exhibit no peaks of this type. The pilot ratings and tracking performance for the first two configurations (flexible display) which demonstrate the spectral peaks had noticeably worse dynamic properties.

The second set of experimental configurations were chosen to help further address relationships between the frequency spectra of pilot inputs and pilot ratings, pilot comments, and task performance. The configurations used for this analysis include 1C-11-1, 1C-11-2, and 1C-11-3. Each configuration corresponds to the pitch/roll pursuit tracking task. Configuration 1C-11-1 corresponds to a rigid vehicle where the pitch SCAS pitch-rate gain, K_Q, is 2.0 and the phugoid augmentation is disengaged. Configuration 1C-11-2 corresponds to a flexible vehicle where both structural mode vibration frequencies are 2.0 Hertz, the pitch SCAS pitch-rate gain is 2.0 and the phugoid augmentation is disengaged. Configuration 1C-11-3 is identical to configuration 1C-11-2 with the exception that the phugoid augmentation is engaged. Because of their similarity, configurations 1C-11-2 and 1C-11-3 will both be referred to as the "flexible configuration" in the subsequent discussion. Configuration 1C-11-1 will of course be referred to as the "rigid configuration."

Three runs for the two configuration types are considered. Figure 28 presents the PSD of the longitudinal stick displacement for each of the three runs for the rigid and flexible configurations. This figure also includes the pilot identifier, pilot rating, and RMS pitch tracking error for each run. Note that even though the data was obtained from runs that were performed on different days, and in one instance by a different pilot, the characteristic shapes of the PSD curves are consistent. The rigid configuration has PSD's which exhibit fairly

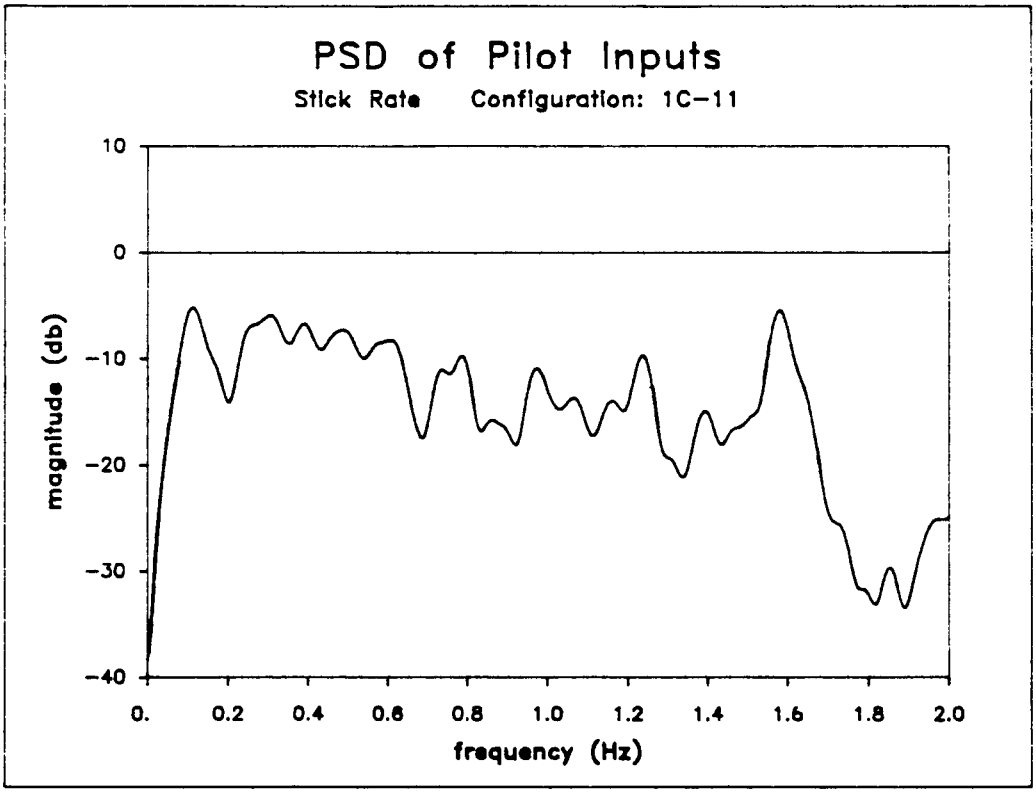

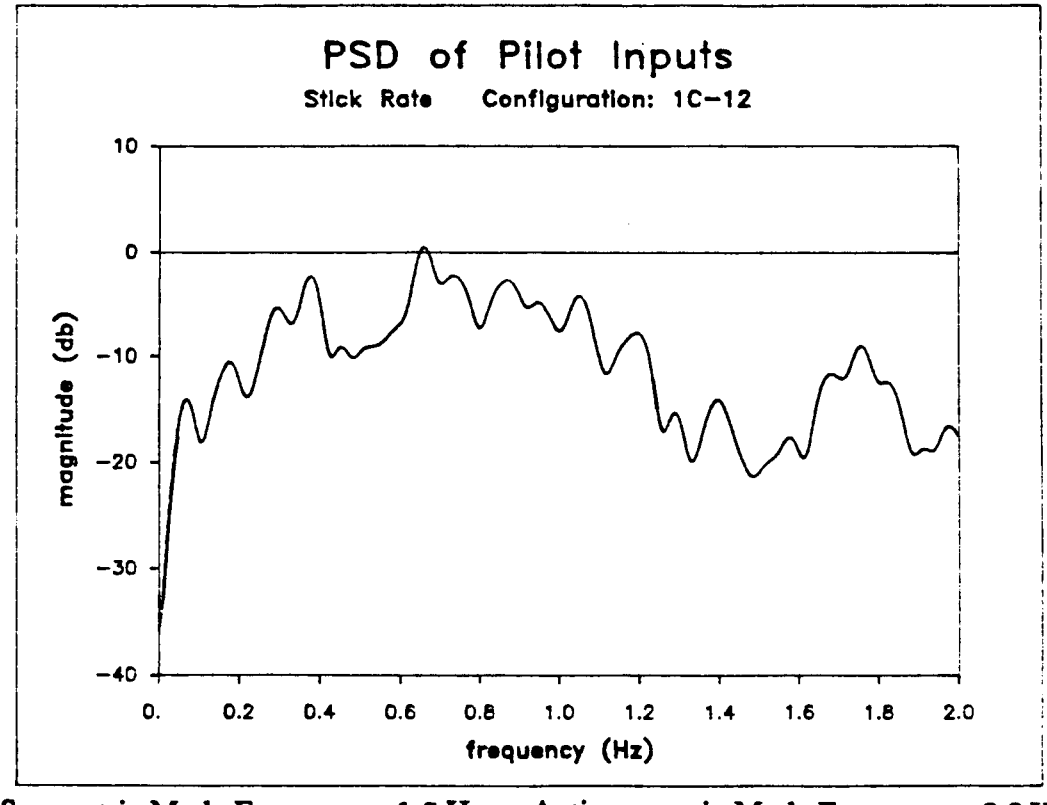

Symmetric Mode Frequency - 1.5 Hz Antisymmetric Mode Frequency - 2.0 Hz

Figure 27 - PSD of Longitudinal Stick Rates - Motion and Display Effects

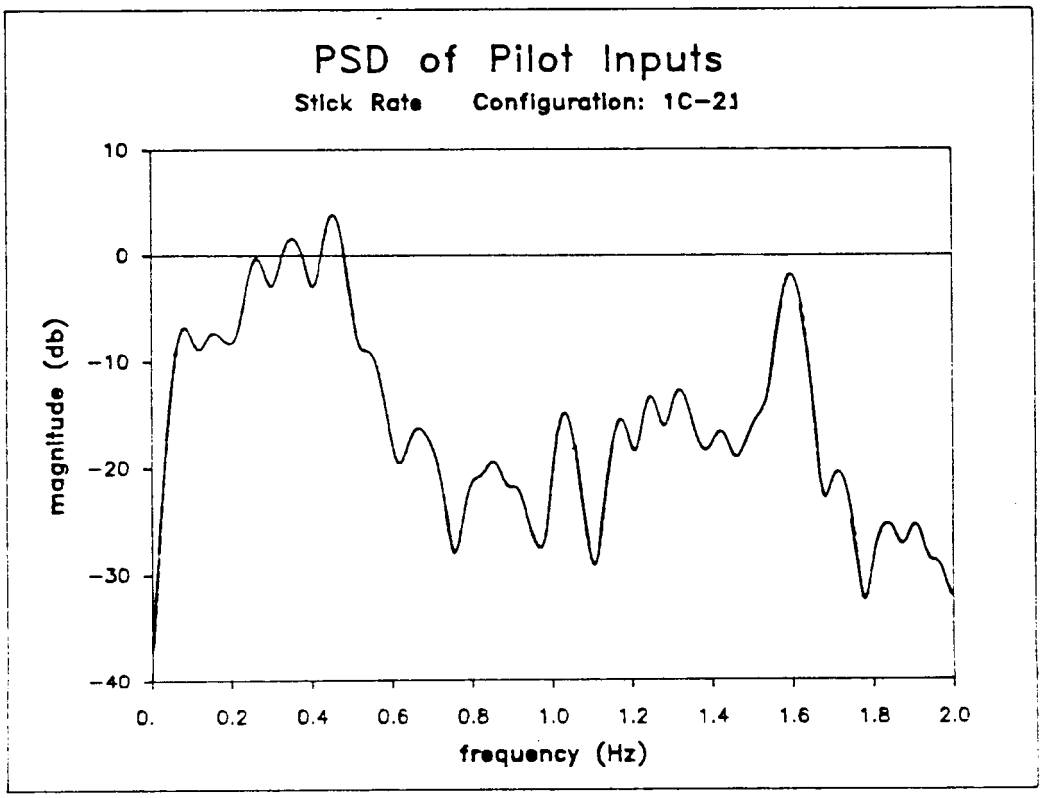

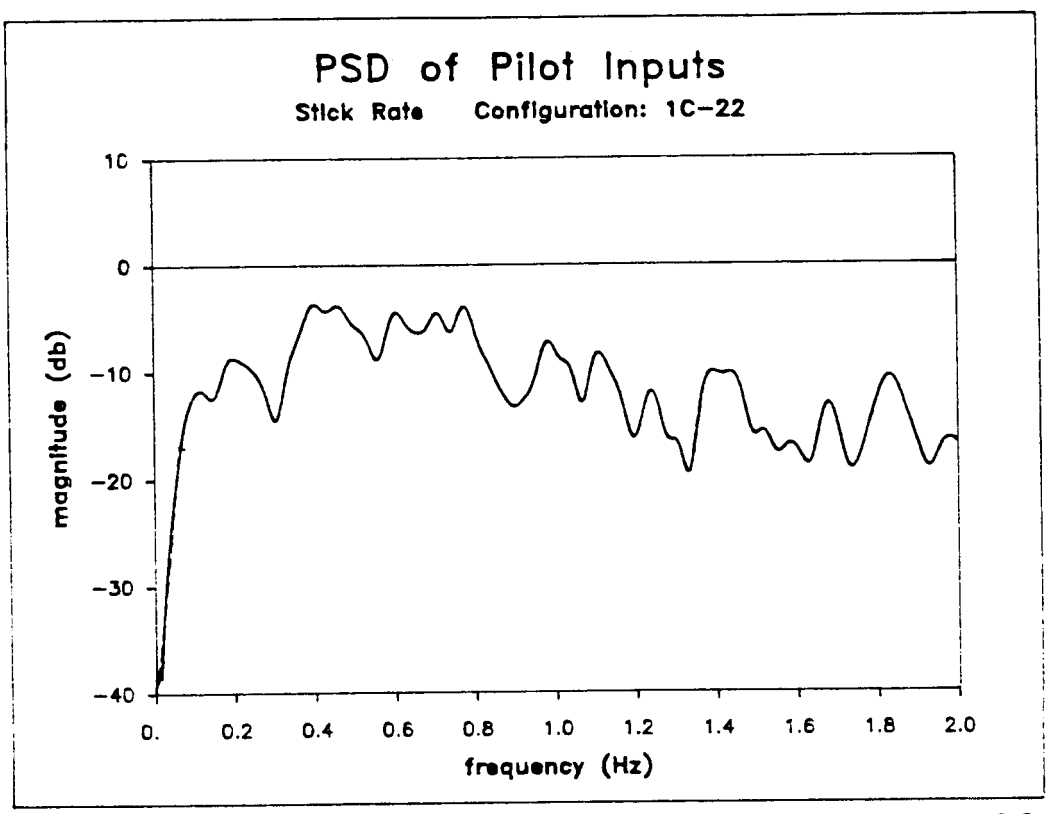

Symmetric Mode Frequency - **1.5 Hz** Antisymmetric Mode Frequency - **2.0 Hz**

Figure 27 - PSD of Longitudinal Stick Rates - Motion and Display Effects concluded

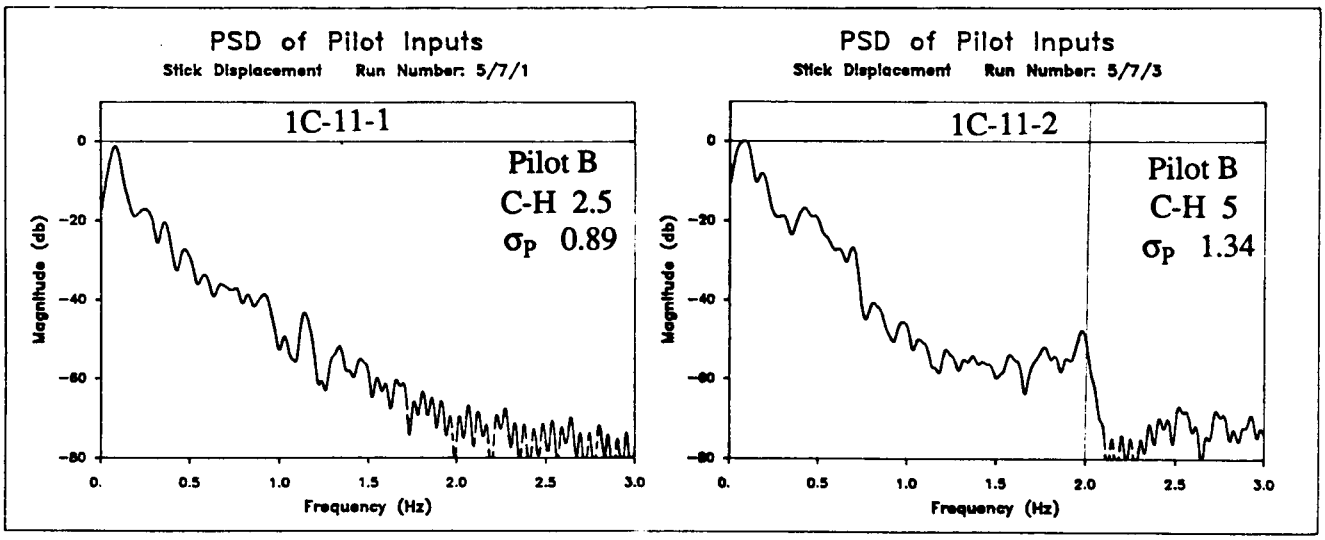

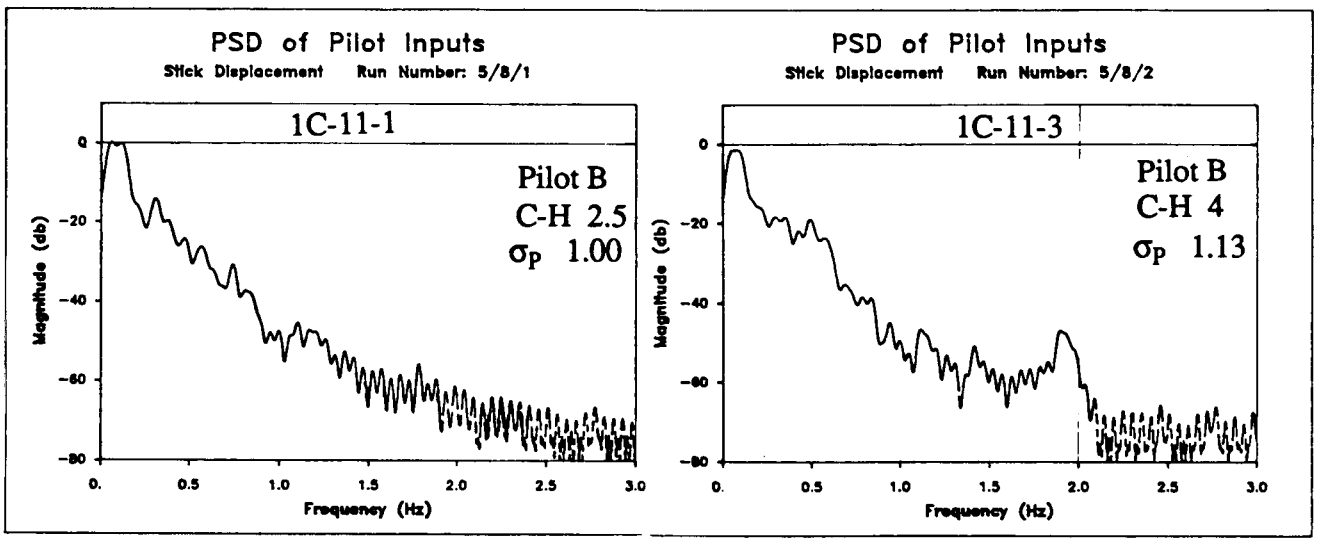

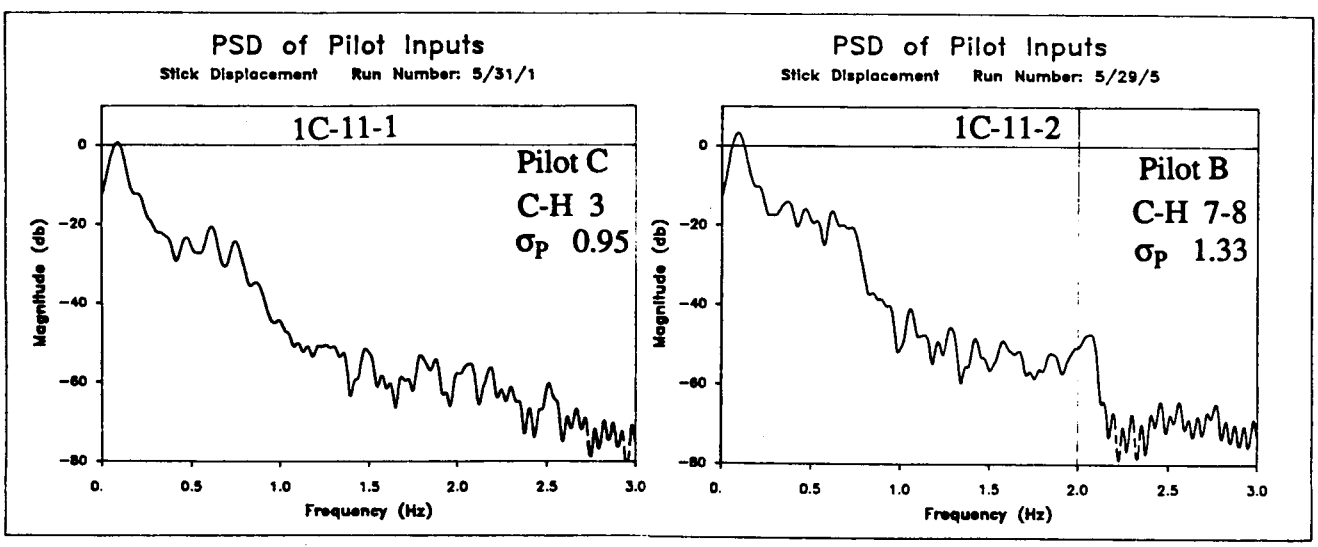

rigid configurations elastic configurations

Figure 28 - PSD of Longitudinal Stick Displacements - Rigid and Flexible Configurations

smooth, gradual reduction in magnitude as frequency increases. The flexible configuration has PSD's which exhibit higher power below the frequency of the symmetric mode, and a marked reduction beyond that point.

Figure 29 presents the PSD of the longitudinal stick rate for the same simulation runs. The pilot identifier, pilot rating, and RMS pitch tracking error are also included here. The characteristic shape of the PSD curves are consistent for these responses as well. The rigid configuration has power spectra which are fairly constant in magnitude out to a frequency of about one Hertz and then drop gradually as frequency increases. The elastic configuration exhibits similar behavior but near the symmetric mode frequency (2.0 Hertz) an obvious peak occurs which is then followed by a sudden drop in magnitude.

Now consider the pilot comments and ratings for these configurations in the context of the previous discussion. Table 19 presents the pilot comments, subjective ratings and RMS pitch tracking errors associated with each of the simulation runs described above. These comments indicate that the rigid configuration presented no difficulty in completing the required task, consistent with the pilot ratings and tracking errors. However, the flexible configuration required the pilot to carefully alter his technique to perform the task successfully. Comments such as,

"let oscillations die out, but could be aggressive,"

"flying aggressively but smoothly ..."

"applied learned technique ..."

and

"... considerable compensation required"

indicate that he had to provide fairly complicated compensation to perform the task. The comments also tend to imply that the pilot was trying to intentionally avoid exciting the structural mode, that is, act like a notch filter. The frequency spectra seem to support this by the characteristic shapes of the curves.

The generally higher pilot ratings that the flexible configuration received (compared to those of the rigid configuration) imply that the flexible configuration was significantly harder to fly in the specified task. In addition, the variations in pilot rating among the three flexible configuration runs (i.e. from Cooper-Harper 4 to 8) indicate that the vehicle is sensitive to the

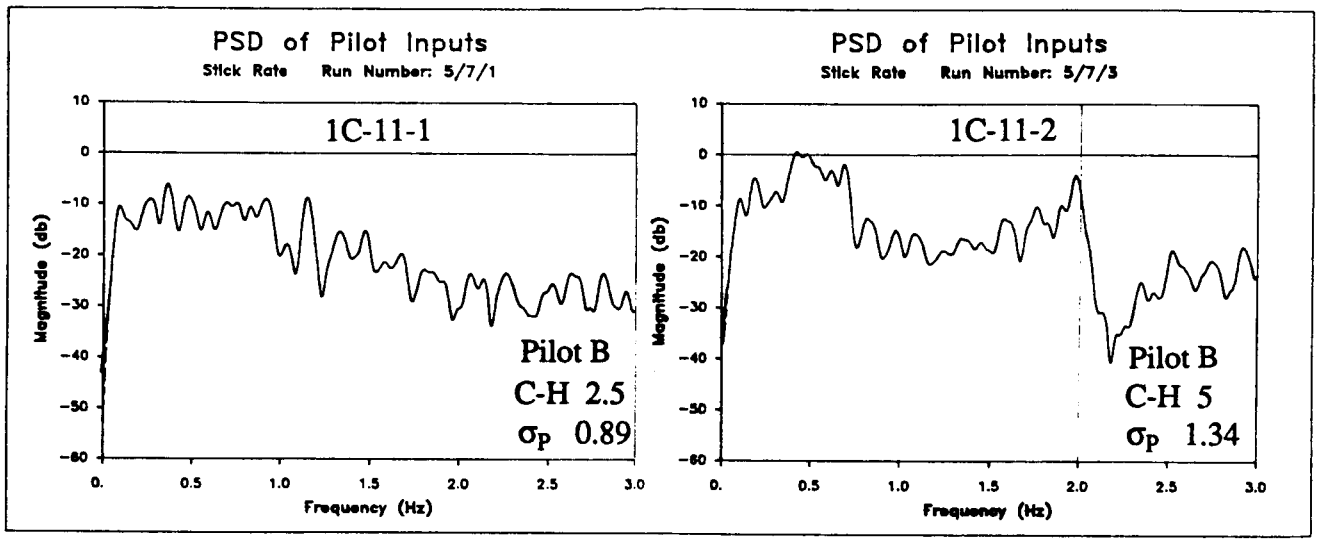

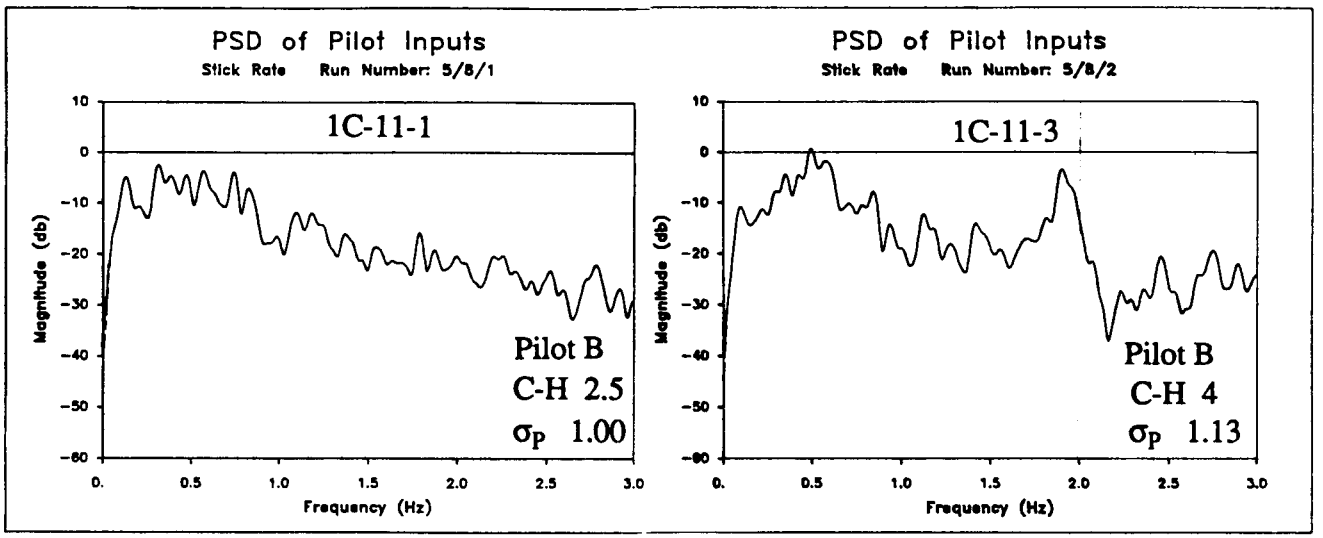

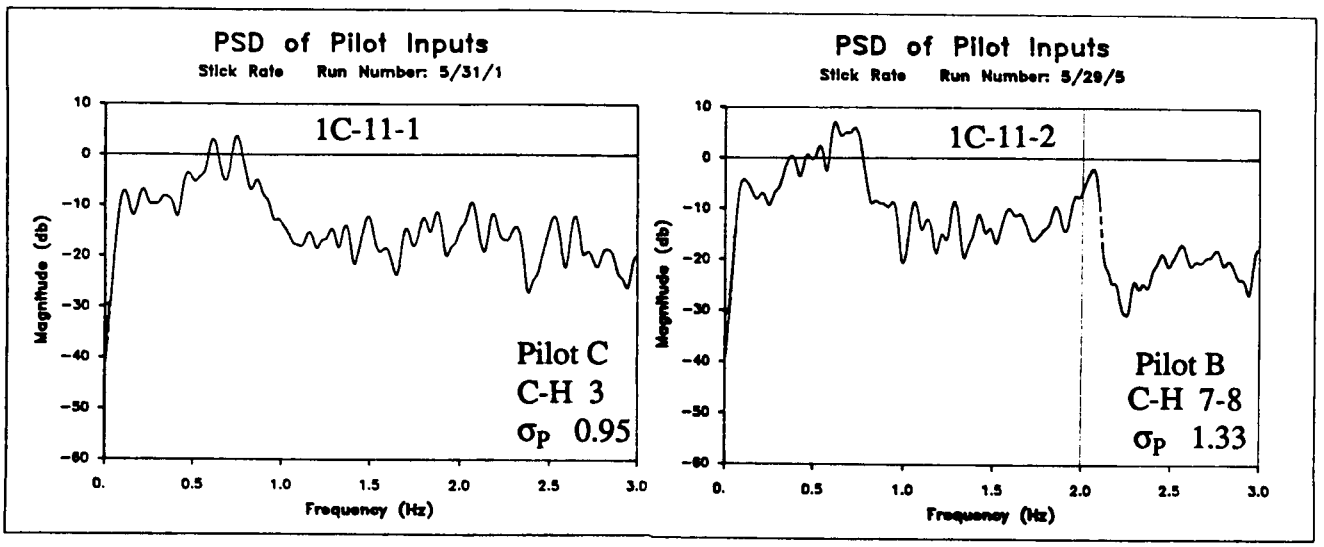

rigid configurations elastic configurations

Figure 29 - PSD of Longitudinal Stick Rates - Rigid and Flexible Configurations

Table 19 - Pilot Comments, Ratings and Tracking Performance

CONFIG.	RUN	PILOT	COMMENT	C-H RATING	RMS PITCH ERRO
1C-11-1	5/7/1	B	- slight tendency to bobble in pitch and roll	2.5	0.89
	5/8/1	B	- could perform task easily - tried to be more aggressive, led to diminishing returns, possibly in worse longitudinal tracking scores	2.5	1.00
	5/31/1	C	- had to work a little -noticed pitch sensitivity	3	0.95
1C-11-2	5/7/3	B	- have to rest right arm on right leg for precise inputs - let oscillations die out, but could be aggressive	5	1.34
	5/29/5	B	- not putting smooth inputs in - really aggressive (noticably more aggressive inputs) - acquisition easy; fine tracking hard - hard to control this display - not as "tuned up" today, referring to piloting technique	7-8	1.33
1C-11-3	5/8/2	B	- applied learned technique, part of his compensation - flying aggressively but smoothly, did not let dot completely vibrate freely by "smoothing" - the performance was as good as previous run but considerable compensation required	4	1.13

pilot's technique in the specified task. The comments associated with the run which received a rating of 8 imply that the pilot's compensation was inappropriate, that is he was not "tuned up" properly. On the other hand, the comments for the run which received a rating of 4 imply that the pilot's compensation, though complicated, was well chosen for the task.

The above discussion indicates that the differences in the vehicle dynamics and in the experimental conditions can noticeably alter the properties of the inputs that the pilot produces. In addition, even though the RMS values for longitudinal stick inputs showed little variation due to the changes in the level of flexibility and the display dynamics that were used, the frequency characteristics of those inputs differ considerably.

Simulator Dynamics

To assure that the motion cues which are produced in such a simulation are improving the realism and not corrupting it, some knowledge of the simulator capabilities and experimental validity are needed. Frequency response data for the simulator was obtained to more completely document the simulation facility and address these points. This data was used, for example, to investigate the degree to which motion cues are attenuated by hardware limitations and signal filtering, thus affecting the validity of the simulation. Though simulation validity was not a specific objective of this study, the data that was collected could be used in subsequent analyses to address this issue.

Figure 30 depicts a functional block diagram of the simulator. Frequency response data was collected at the locations identified by the letters A through E. The responses measured at these points are given in Table 20. The units and sign conventions for these responses are given in Table 21. The measurements were made for eight frequencies for the longitudinal responses (viz. ω = 0.25, 0.5, 0.75, 1.0, 1.25, 1.5, 1.75, and 2.0 Hertz) and at three frequencies for the lateral responses (viz. ω = 0.25, 0.5, and 0.75 Hertz). The amplitude of the force inputs was twenty pounds.

The vehicle model that was used corresponds exactly to the model that was used in the simulation study. This includes the equations of motion, control system and control loader parameters. The frequencies of the two modeled structural modes were varied to address the effects of reduced stiffness on motion capability. Frequency response plots for the transfer

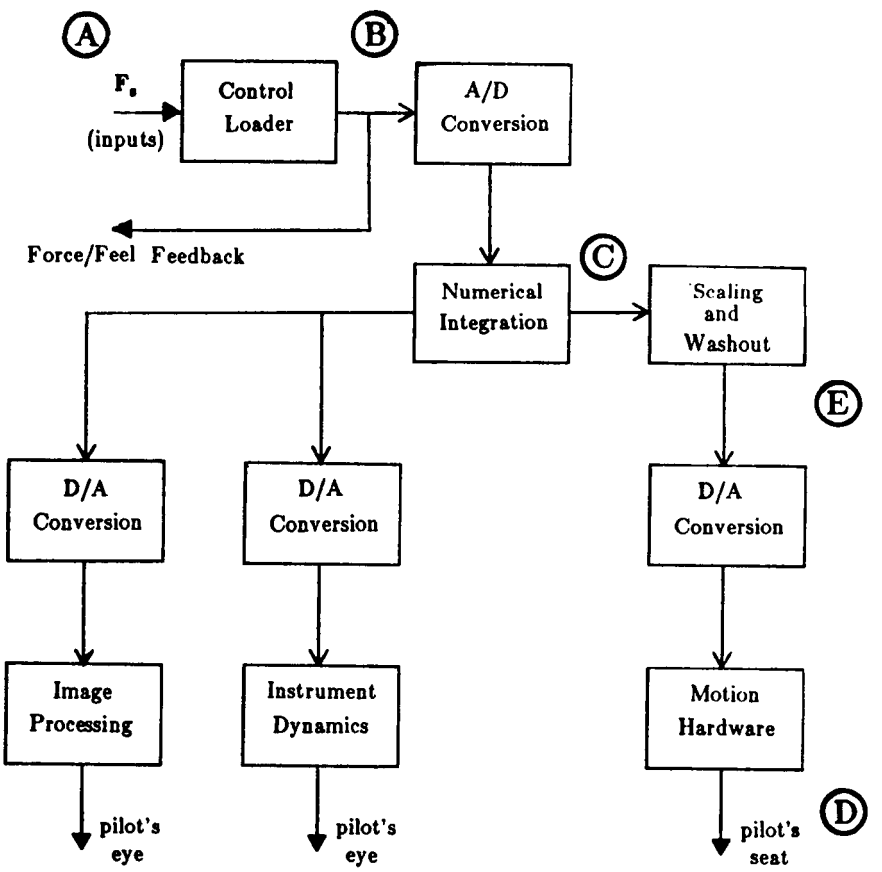

Figure 30 - Simulator Functional Block Diagram

Table 20 - Frequency Response Inputs and Outputs

Data Sets									
A to B		B to C		C to D		A to D		A to E	
Input	Output	Input	Output	Input	Output	Input	Output	Input	Output
F_{pitch}	δ_{pitch}	δ_{pitch}	$n_{z_{cp}}$ $\dot{\theta}$	$n_{z_{cp}}$ $\dot{\theta}$	$\hat{n}_{z_{cp}}$ $\hat{\dot{q}}$	F_{Pitch}	$\hat{n}_{z_{cp}}$ $\hat{\dot{q}}$	F_{pitch}	$\hat{n}_{z_{com}}$ $\hat{\dot{q}}_{com}$
F_{roll}	δ_{roll}	δ_{roll}	$n_{y_{cp}}$ p	$n_{y_{cp}}$ p	$\hat{n}_{y_{cp}}$ $\hat{\dot{p}}$	F_{roll}	$\hat{n}_{y_{cp}}$ $\hat{\dot{p}}$	F_{roll}	$\hat{n}_{y_{com}}$ $\hat{\dot{p}}_{com}$

Table 21 - Scale Factors and Units

Parameter	Units	Sign Conventions
F_{pitch}, F_{roll}	lbs	F_{pitch} - positive aft F_{roll} - positive right
δ_{pitch}, δ_{roll}	inches	$\dot{\theta}$ - positive up
$\dot{\theta}$, p	$\frac{rad}{sec}$	p - positive right
$\dot{\hat{q}}$	$\frac{rad}{sec^2}$	$\dot{\hat{q}}$ - positive up
$\dot{\hat{p}}$	$\frac{rad}{sec^2}$	$\dot{\hat{p}}$ - positive right
$n_{z_{cp}}$, $\hat{n}_{z_{com}}$	g's	$n_{z_{cp}}$, $\hat{n}_{z_{com}}$ - positive down
$n_{y_{cp}}$, $\hat{n}_{y_{com}}$	g's	$n_{y_{cp}}$, $\hat{n}_{y_{com}}$ - positive right
$\hat{n}_{z_{cp}}$, $\hat{n}_{y_{cp}}$	g's	$\hat{n}_{z_{cp}}$ - positive down $\hat{n}_{y_{cp}}$ - positive right

functions described in Table 20 are shown in Figures 31 through 35. These responses correspond to the baseline vehicle (i.e. $\omega_y = \omega_z = 2.0$ Hertz). Complete frequency response data for the vehicle model with several different vibration frequencies is presented in Appendix 6.

As the structural stiffness is reduced, the responses associated with the vehicle dynamics (i.e. the responses between A or B and C, D or E) change. Note also that the data includes the time delays associated with numerical integration and conversion from digital to analog signals and vice versa. In addition, the washout filters and motion hardware are nonlinear, and so the frequency responses of the simulator are input amplitude dependent, in general.

The result that the presence (or lack) of motion cues did not seem to significantly affect the simulated vehicle responses or the task performance, discussed previously was surprising. One would think that motion cues could be beneficial in providing additional information that the pilot can use in performing the required task. However, the pilot would also be inclined to limit his inputs in order to improve the ride quality and accept reduced performance when motion was present while becoming more aggressive and trying to improve performance when motion was not present. More aggressive behavior would result in larger inputs and lead to higher normal accelerations. But the RMS normal accelerations (shown in Figure 25) are not strongly dependent on motion status.

This may have been due to several factors relating to the motion system of the simulator. Due to the limited travel of the motion base, washout is needed to avoid constantly hitting the displacement, rate or acceleration limits. As shown in Figure 40, the washout filters severly attenuate the motion cues, especially acceleration cues, thus reducing the amount of motion that the pilot feels. In addition, any bandwidth limitations of the motion system could make the accuracy of simulating the effects of structural vibration questionable, due to attenuation of higher-frequency motion and phase shifts which can cause the motion cues to be out of phase with the visual cues. This was in fact also indicated, for example, in Figure 40, especially in pitch acceleration.

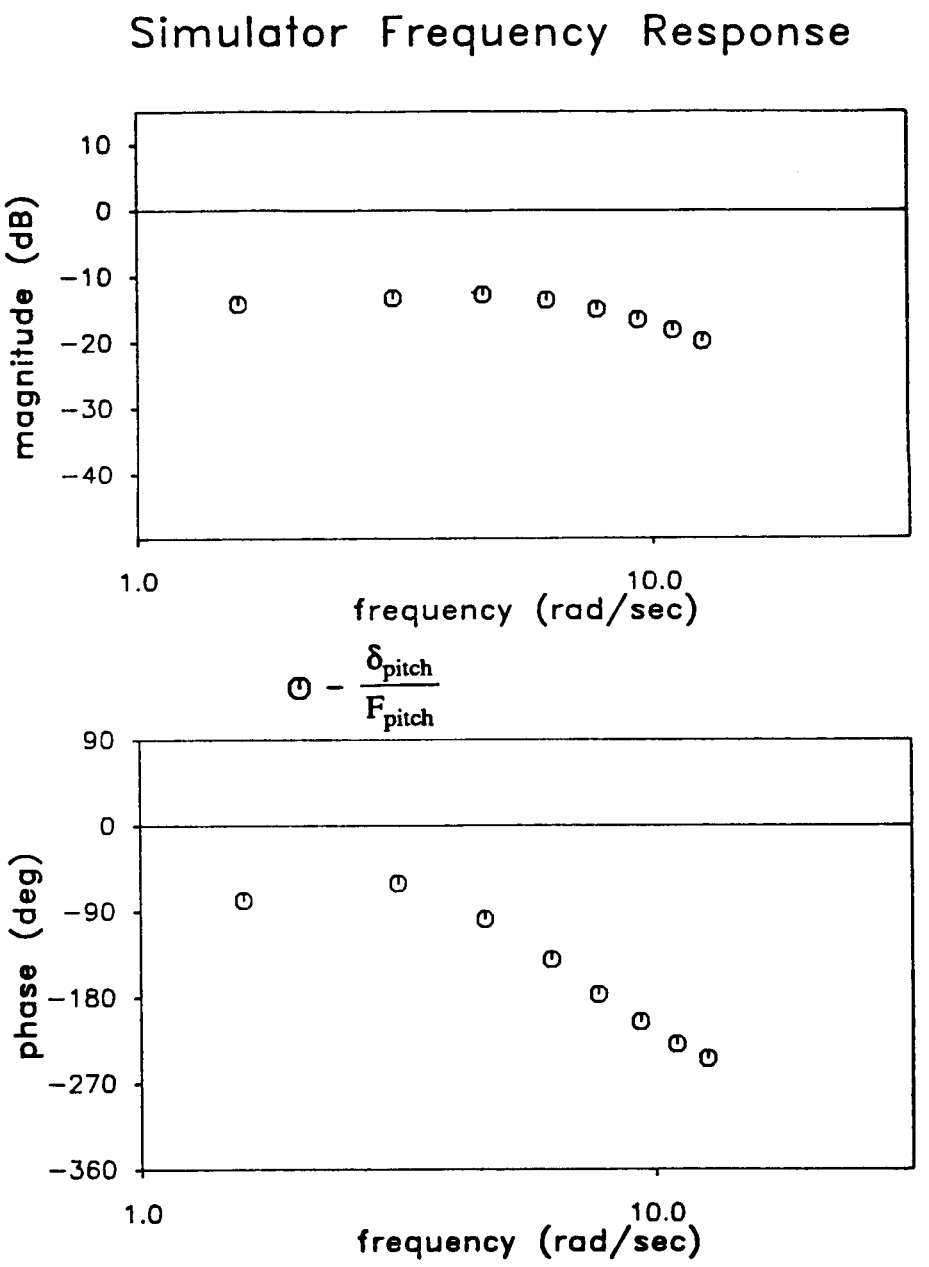

Figure 31 - Simulator Frequency Response : $\frac{\delta_{pitch}}{F_{pitch}}$

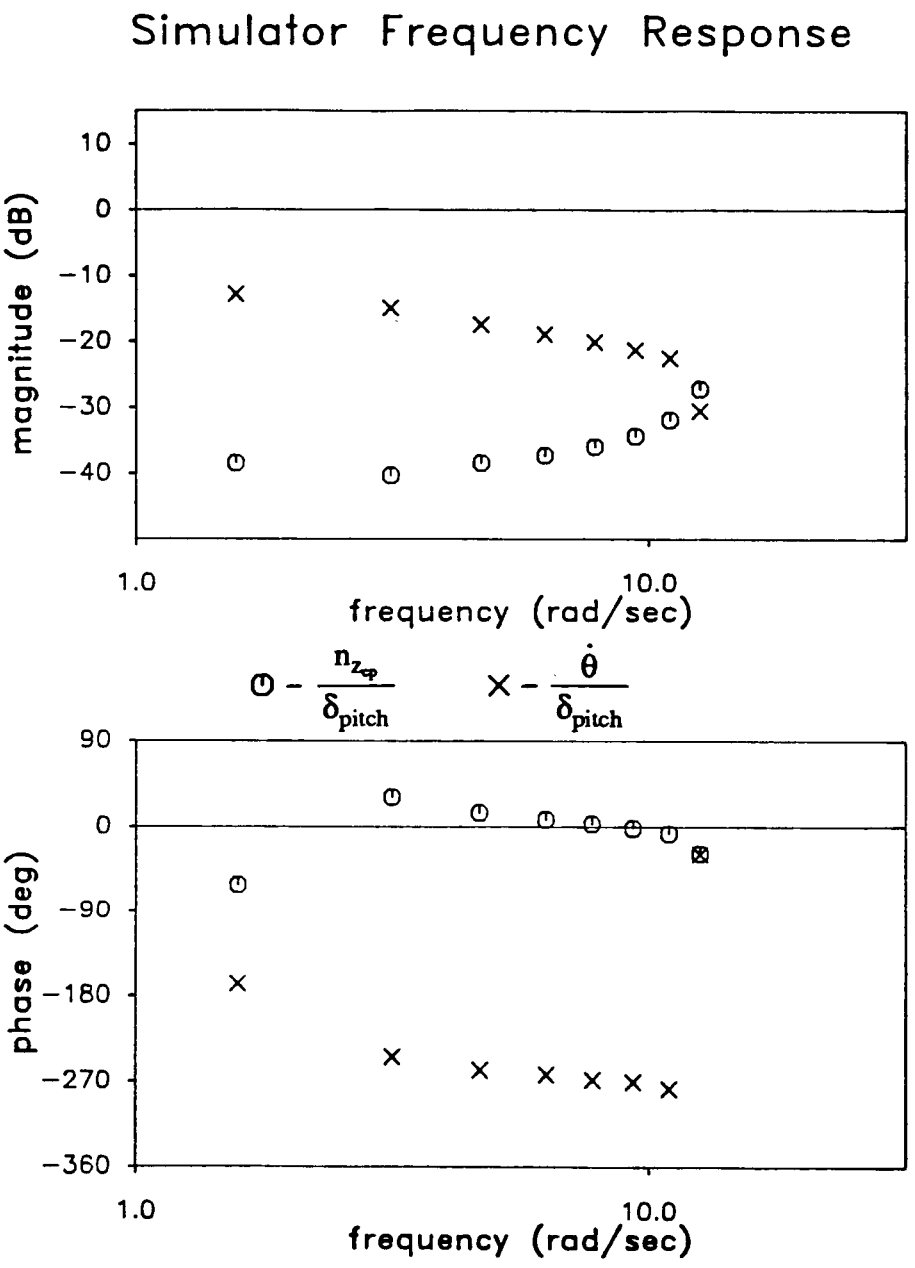

Figure 32 - Simulator Frequency Response : $\frac{n_{z_{cp}}}{\delta_{pitch}}$, $\frac{\dot{\theta}}{\delta_{pitch}}$

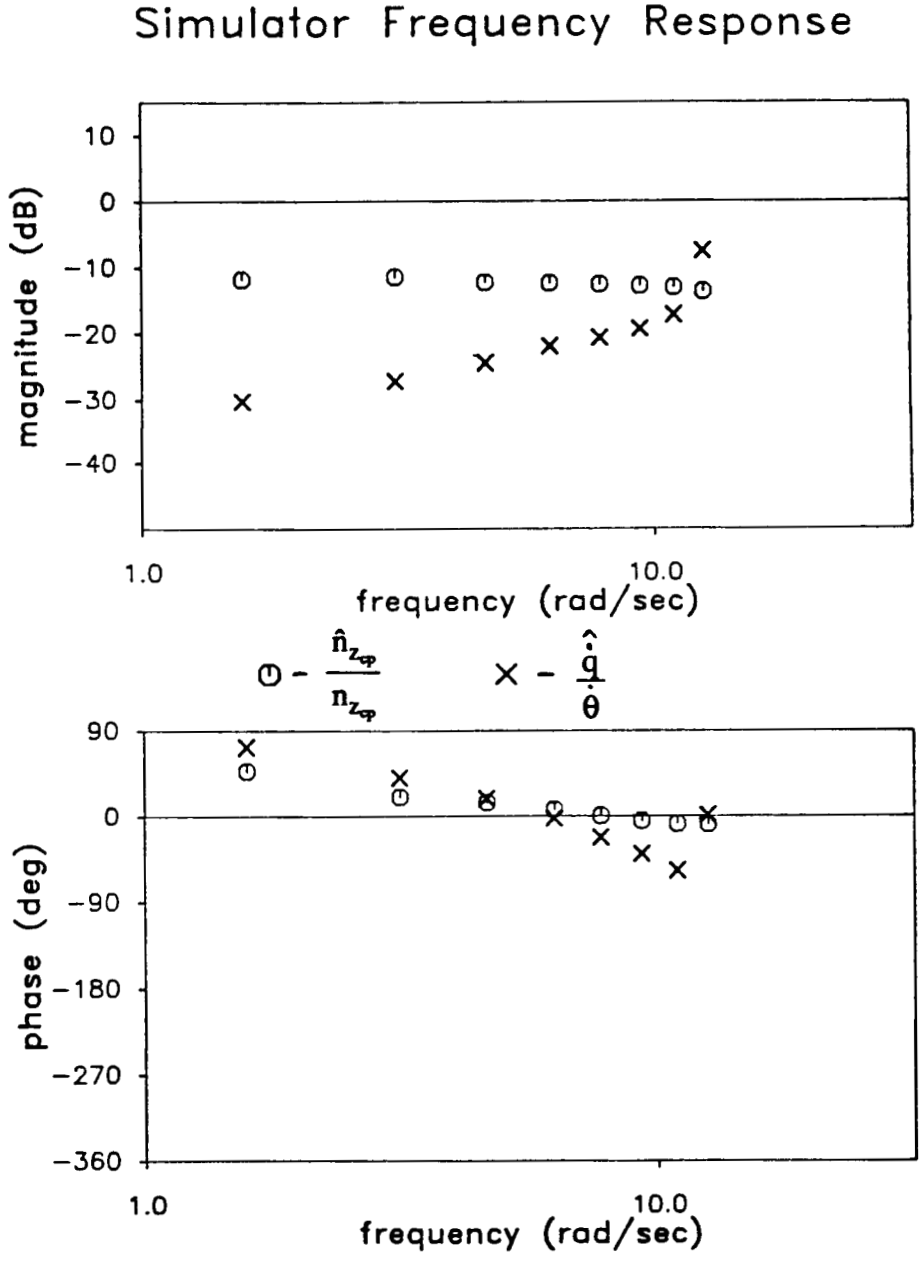

Figure 33 - Simuator Frequency Response : $\frac{\hat{n}_{z_{cp}}}{n_{z_{cp}}}$, $\frac{\hat{\dot{q}}}{\dot{\theta}}$

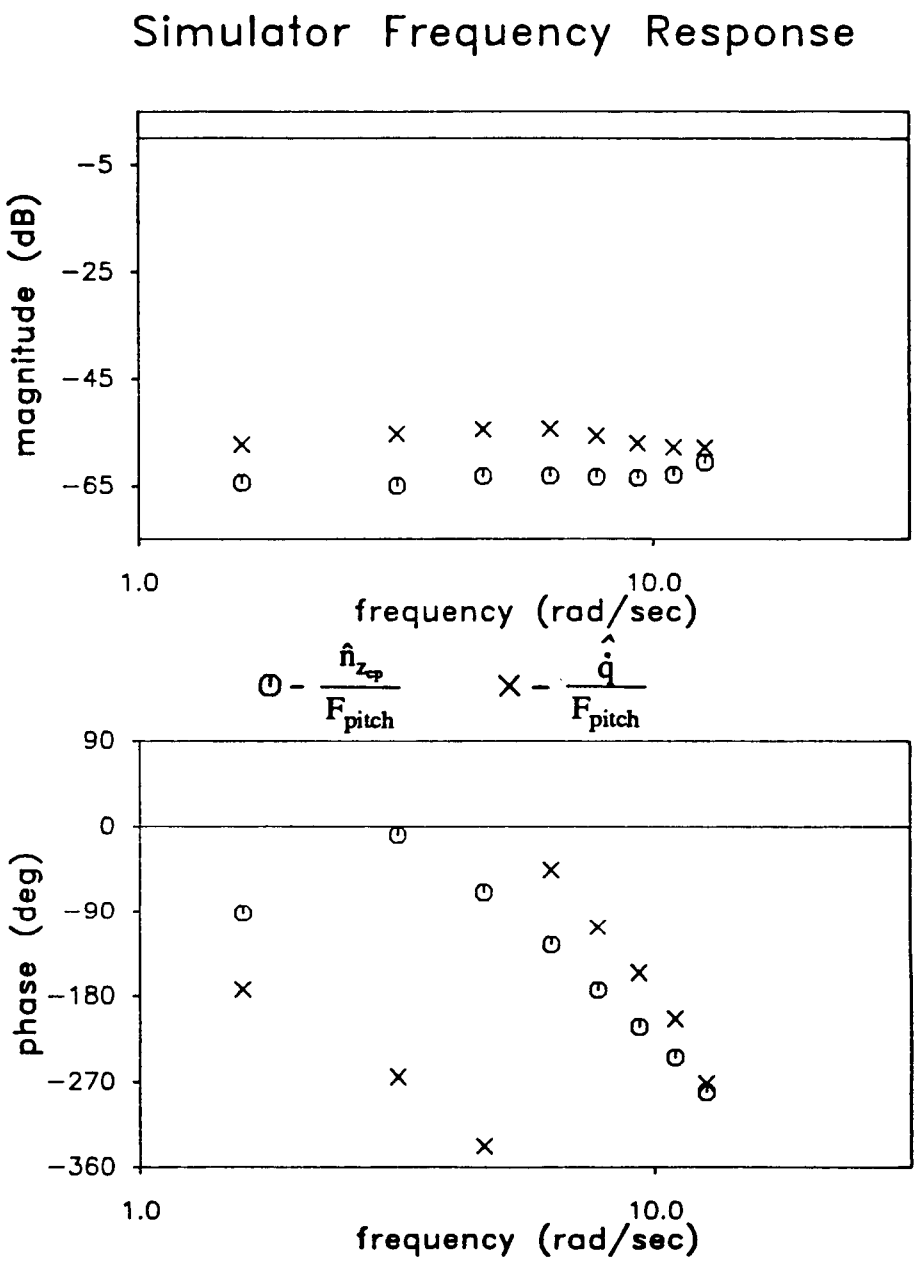

Figure 34 - Simuator Frequency Response : $\frac{\hat{n}_{z_{cp}}}{F_{pitch}}$, $\frac{\hat{\dot{q}}}{F_{pitch}}$

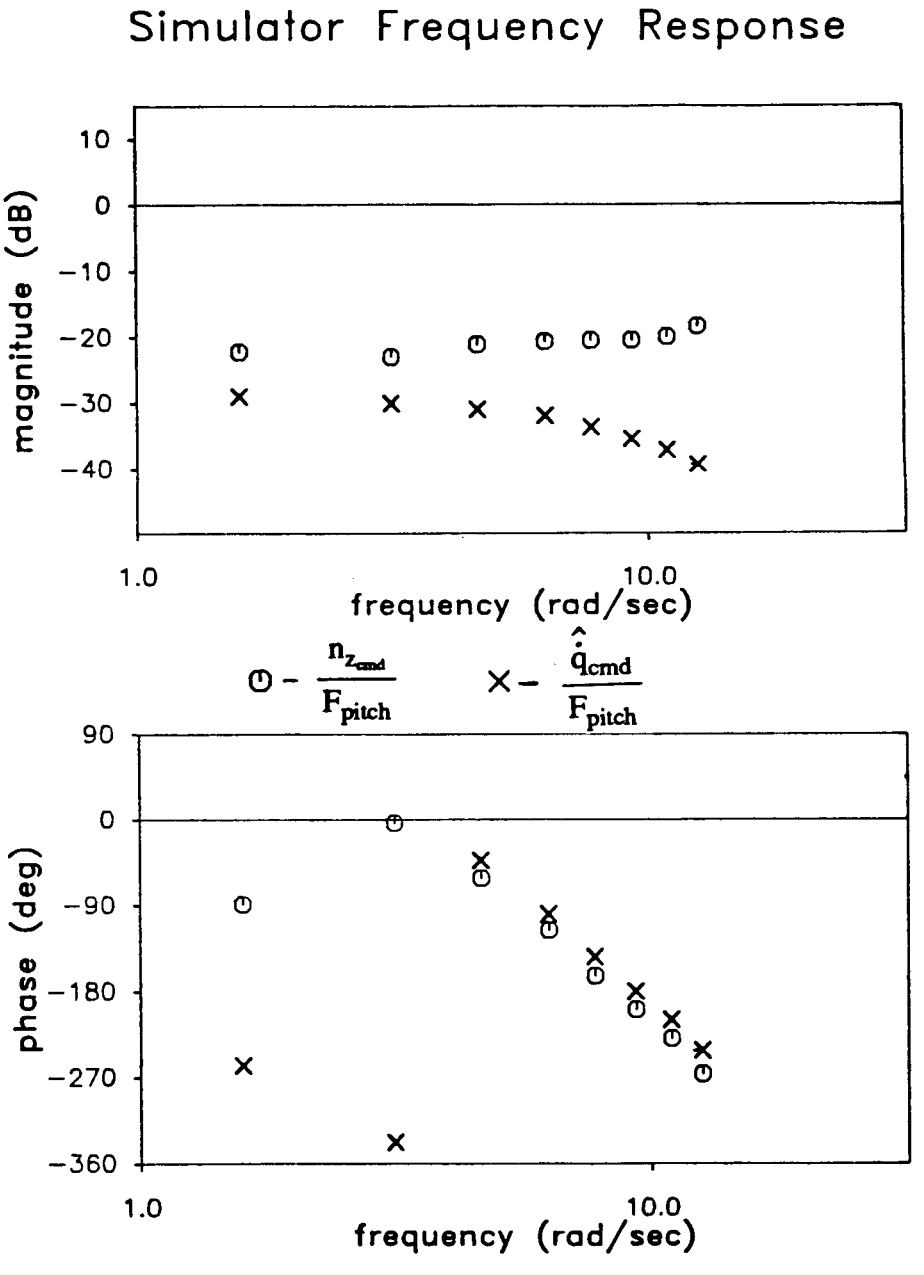

Figure 35 - Simuator Frequency Response : $\frac{\hat{n}_{z_{cmd}}}{F_{pitch}}$, $\frac{\hat{\dot{q}}_{cmd}}{F_{pitch}}$

CHAPTER 4
SUMMARY AND CONCLUSION

The goal of this study was to develop an elastic aircraft model and conduct a simulation experiment to address the effects of aeroelastic dynamics on aircraft responses. This goal was accomplished with the vehicle model developed to describe the general motions of a representative large elastic aircraft and the simulation experiment documented in this report. This report included a discussion of all major aspects of the vehicle, including the equations of motion, aerodynamic data, geometry and structural data, control system dynamics, control loader data, and engine dynamics. In addition, all the information needed to implement the vehicle model on the Langley Visual/Motion Simulator was presented.

A description of the experimental set-up and procedure, and a presentation of the experimental results were also included in this report. The task definitions, display dynamics and symbology, and configuration definitions were discussed. The results included pilot comments and subjective ratings, and important vehicle-response statistics and stick spectra. Frequency response data for the simulator were also included.

A review and analysis of some of the pilot rating data and vehicle-response time-series data is also included. The results indicate that there are fundamental differences between the dynamics of rigid aircraft and elastic aircraft and that these differences can manifest themselves in increased tracking errors, degraded handling qualities, and changes in the frequency content of the pilot inputs. The results also confirm that handling qualities and tracking performance can significantly degrade as the level of flexibility is increased. The results also indicate the importance of the display dynamics. The definition of the displayed variables, or visual cues, have been shown to significantly affect results.

Clearly, the reduction of structural stiffness combined with flexible display dynamics (those that incorporate the effects of structural deformation) lead to considerable degradations in handling qualities. The utilization of "rigid" display dynamics, which ideally filter out the effects of structural deformation, however, lead to little degradation in tracking performance regardless of the level of flexibility. That is, with the rigid display, results are less sensitive to variations in the level of structural stiffness than for the flexible display. This can be interpreted in terms of the pitch-rate-to-stick-deflection transfer functions listed in Chapter 2,

Table 7. For the rigid display, the effective pole-zero cancellation in the pitch-rate transfer function is noted, while in the flexible display case similar pole-zero cancellations do not occur.

CHAPTER 5
RECOMMENDATIONS

The general nature of this experiment and the variety of recorded response data that is available allows many issues which affect pilot/vehicle interactions for elastic aircraft to be addressed. The experiment was specifically designed to help study, evaluate, and develop predictive tools for pilot/vehicle performance, and to identify the degree and manner in which the simulator itself contributes to the pilot/vehicle interactions. The recorded time histories of all important pilot inputs and system responses are available for detailed statistical and time series analysis. In addition, the simulator model was developed to be readily altered and extended for use in future studies. Some specific applications of the experimental data and simulation model that could be performed in the future will be discussed.

The response data from the pilot and vehicle simulation can be used to help extend and validate pilot modeling methods. For example, models for human operators need to be extended to account for multiple loop closures in multiple-axes tasks, and the experimental data is available to validate these extensions. The data can also be used to determine pilot describing functions that could then be used to identify the effects of motion cues and display dynamics on pilot dynamics.

Frequency responses of the simulator were also collected. These can be used to further address the effects of simulator characteristics. For example, a model of the simulator could be developed and used in conjunction with the vehicle mathematical model and a pilot model (the OCM or crossover model) to quantify the effects of delays, lags, washout of motion cues, and other simulator dynamics on pilot/vehicle performance. Once these effects are identified, it may then be possible to better extrapolate results from experimental simulator studies to actual flight characteristics. In this way simulation could become a more valuable analysis and design tool.

The general, open structure of the elastic vehicle model that was used in the experiment has many applications for future research as well. Since it is a full multi-input, nonlinear, six degree of freedom model of a flexible aircraft and since it was developed to be easily altered and extended (for example, changing the level of stiffness, adding additional elastic degrees of freedom or implementing additional control systems) it can be used to study many aspects of advanced flight control development. Current flight control research is involved with multivariable control systems, robustness issues, functionally integrated control systems, etc. All of these areas could be studied experimentally using the elastic aircraft model developed for this study.

References

[1] Schmidt, D.K., "A Modal Analysis of Flexible Aircraft Dynamics with Handling Qualities Implications," *Journal of Guidance Control and Dynamics,* Vol. 8, No. 2, March-April, 1985.

[2] Schmidt, D.K., "Pilot Modeling and Closed-Loop Analysis of Flexible Aircraft," *Journal of Guidance Control and Dynamics,* Vol. 8, No. 1, January-February, 1985.

[3] Waszak, M.R. and Schmidt, D.K., "Analysis of Flexible Aircraft Longitudinal Dynamics and Handling Qualities : Volumes I and II," NASA CR-177943, June 1985.

[4] Yen, W.Y., "Effects of Dynamic Aeroelasticity on Handling Qualities and Pilot Rating." Phd. Thesis, School of Aeronautical and Astronautical Engineering, Purdue University, 1977.

[5] Parrish, R.V., et. al., "Compensation Based On Linearized Analysis For A Six-Degree-Of-Freedom Motion Simulator," NASA TN D-7349, November 1973.

[6] Martin, D.J., "A Digital Program For Motion Washout On Langley's Six-Degree-Of-Freedom Motion Simulator," NASA CR-145219, July 1977.

[7] Rollins, J.D., "Description and Performance of the Langley Visual Landing Display System," NASA TM-78742, August 1978.

[8] Copeland, James L. (ed.), *Research through Simulation.* NASA Langley Research Center, Publication NF-125.

[9] Waszak, M.R. and Schmidt, D.K., "On The Flight Dynamics of Aeroelastic Vehicles," AIAA Paper 86-2077, Atmospheric Flight Mechanics Conference, Williamsburg, VA, August 1986 (*Journal of Aircraft*, Vol. 25, No. 3, March 1988).

[10] Etkin, Bernard. *Dynamics of Flight - Stability and Control.* John Wiley and Sons, NY, 1982.

[11] Davidson, J.B. and Schmidt, D.K., "Flight Control Synthesis for Flexible Aircraft Using Eigenspace Assignment," NASA CR-178164, June 1986.

[12] Anderson, M.R. and Schmidt, D.K., "Closed-Loop, Pilot Vehicle Analysis of the Approach and Landing Task," *Journal of Guidance, Control and Dynamics,* Volume 10, Number 2, March-April 1987, pp. 187-194.

[13] Bendat, J.S. and Piersol, A.G. *Random Data - Analysis and Measurement Procedures,* second edition. John Wiley and Sons, NY, 1986.

NASA
National Aeronautics and Space Administration

Report Documentation Page

1. Report No.	2. Government Accession No.	3. Recipient's Catalog No.
NASA CR-4102		

4. Title and Subtitle
A Simulation Study of the Flight Dynamics of Elastic Aircraft. Volume One - Experiment, Results and Analysis

5. Report Date
December 1987

6. Performing Organization Code

7. Author(s)
Martin R. Waszak, John B. Davidson, and David K. Schmidt

8. Performing Organization Report No.

9. Performing Organization Name and Address
Purdue University
School of Aeronautics and Astronautics
West Lafayette, IN 47907

10. Work Unit No.
505-66-01-02

11. Contract or Grant No.
NAG-1-254

12. Sponsoring Agency Name and Address
National Aeronautics and Space Administration
Langley Research Center
Hampton, VA 23665-5225

13. Type of Report and Period Covered
Contractor Report

14. Sponsoring Agency Code

15. Supplementary Notes
NASA Technical Monitors: William D. Grantham and Jarrell R. Elliott
Langley Research Center

Volume Two—Data

16. Abstract

The simulation experiment described herein addresses the effects of structural flexibility on the dynamic characteristics of a generic family of aircraft. The simulation was performed using the NASA Langley VMS simulation facility. The vehicle models were obtained as part of this research project. The simulation results include complete response data and subjective pilot ratings and comments and so allow a variety of analyses. The subjective ratings and analysis of the time histories indicate that increased flexibility can lead to increased tracking errors, degraded handling qualities, and changes in the frequency content of the pilot inputs. These results, furthermore, are significantly affected by the visual cues available to the pilot.

17. Key Words (Suggested by Authors(s))	18. Distribution Statement
Flexible Aircraft Flight Dynamics Flying Qualities Ground-Based Simulation	Unclassified - Unlimited Subject Category 08

19. Security Classif.(of this report)	20. Security Classif.(of this page)	21. No. of Pages	22. Price
Unclassified	Unclassified	110	A06

For sale by the National Technical Information Service, Springfield, Virginia 22161